THE UNIVERSITY OF READING

Department of Meteorology

RAINFALL ESTIMATION USING POLARIMETRIC WEATHER RADAR

ROBERT JOHN THOMPSON

A thesis submitted for the degree of Doctor of Philosophy

January 2007

DECLARATION

I confirm that this is my own work and the use of all material from other sources has been properly and fully acknowledged.

Robert John Thompson

ABSTRACT

Rainfall is a key observable of the weather, of importance to society. Rain gauges only provide point measurements; for areal rainfall information a radar may be used. Radars measuring just reflectivity (Z) may suffer large errors in derived rainrates due to drop size distribution (DSD) variations. The introduction of dual-polarisation radars to operational networks should lead to improvements in rainfall estimation, although these radars suffer high noise levels in polarisation parameters (~ 0.7 dB in differential reflectivity [Z_{DR}]).

This thesis examines rainfall characteristics, considering the effect of DSD changes on radar parameters. The difficulties caused by Z_{DR} noise are examined, showing problems for rainfall estimation. Rainfall statistics are studied, finding that relative rainrate changes are the same at all rainrates. Decorrelation of rainrate to 0.5 in the southern UK is shown to take 4.5 minutes, which mean sampling rainfall in "snapshots" only every 5 minutes generates a 20% error in hourly accumulations as shown in the thesis. This thesis concentrates on estimating moderate rainfall rates (3–10 mm hr^{-1}), which generate 36% of rain accumulation in southern UK, with dual-polarisation radar. At moderate rates, specific differential phase shifts (K_{DP}) are too small for accurate rainfall estimation, so Z_{DR} must be used. The noise in Z_{DR} means that using Z and Z_{DR} at each gate generates rainrates with error as much as a factor of 10. This thesis introduces a technique utilising the spread of Z and Z_{DR} data over an area, estimating drop concentration (N_{w}) over the area and hence 'a' in $Z = aR^{1.5}$. This generates an appropriate $Z - R$ relationship for the selected region, which can be utilised with each pixel's Z to give rainrates accurate to 25% while maintaining the high resolution of the data despite large noise in Z_{DR}. The thesis examines the use of the technique with operational radar, especially the Thurnham radar in the UK.

ACKNOWLEDGEMENTS

from the world of radar became necessary. I will also thank my father and stepmother *John* and *Elizabeth Thompson* whose support I always had despite the distance between us.

Finally my biggest thank you goes to my wife, *Claire Thompson [née Sharman].* Her unfailing love has been vital and despite putting up with me has always remained supportive, helping to provide a welcome shelter when the world got too much for me.

- Robert Thompson - August 2006

"Dual-Polarisation radar speaks with a forked tongue"

- Prof. Ian Cluckie - 2006

All science is either physics or stamp collecting.

- Ernest Rutherford (1871 - 1937), in J. B. Birks 'Rutherford at
Manchester' (1962)

Creativity is the sudden cessation of stupidity.

- Edwin Land

CONTENTS

CHAPTER 1:
INTRODUCTION

1.1 THE USE OF PRECIPITATION RADAR

Rainfall is probably the most important weather observable to the public: will it rain? If so, how much? Rain is possibly the most important part of any weather forecast. Rainfall information also affects many industries, notably agriculture, where rainfall predictions can influence sowing and harvesting times. Unfortunately, rainfall remains one of the most difficult features of the weather to forecast. Until very recently operational numerical weather prediction models operated with grid scales far too large to resolve rainfall so cloud and rain must be parameterised within the models. However, new high resolution models are being developed and introduced that reduce the resolution to 1-4 km, scales at which the rainfall is being much more accurately represented (for example, Golding *et al.*, 2005, demonstrate use of such a model in discussing the Boscastle flood of 2004). These parameterisations limit the accuracy of the rainfall forecasts. Possibly a larger problem however is that of the nature of rainfall. The spatial and temporal distribution of rainfall is variable and intermittent on small scales, and is probably the most chaotic of all atmospheric variables (Fritsch *et al.*, 1998). This will be discussed in more detail in chapter 4. This means that accurate predictions are difficult with lead times greater than just a few hours.

Rainfall is also a major hazard in the modern world, with flash flooding a regular feature of the news. Flooding is the result of a combination of problems. River floods are the result of prolonged, yet not necessarily intense, rainfall overloading the river drainage system. An example of river flooding is the the flooding of much of central Europe in 2002. The other type of flooding, flash flooding, is more dangerous, and happens when very intense rainfall occurs, which quickly overcomes the drainage systems. Flash

floods tend to be very strongly localised events, occuring frequently in urban (and hence inhabited) areas as the surface cannot absorb large amounts of water in a short time, flash flooding also often occurs in steep rural catchments. An example of flash-flooding is the event of 16th August 2004 in Boscastle. A flood swept through the Cornish village, destroying over 70 properties, damaging bridges and causing approximately 130 people to need airlifting to safety (Burt, 2005). Fortunately, no lives were lost due to the rapid response of the emergency services.

Although knowledge of the amount of rain falling will not allow for prevention of these floods, the warning that could be given from rainfall rate knowledge could save lives and damage to property.

One of the impacts of climate change according to the reports of the Intergovernmental Panel on Climate Change (IPCC) (Folland *et al.*, 2001) is an increase in extreme events, which would include flooding. It is a challenge to minimise the loss in both humanitarian and financial terms. Accurate rainfall measurement and surveillance will assist in prediction, warning and reaction to these high-impact events.

Rain gauges provide the traditional measure of the rainfall, although they are sparsely distributed and are just a point measurement. Rain gauges suffer from a number of sampling problems, including position, wind effects, small collecting areas and human error. But the chaotic behaviour of rainfall patterns mean that even the perfect rain gauge's ability to measure the rainfall distribution is very limited and depends on the rainfall in question. Convective cells can be very small (< 10 km), so gauges with spacing of as small as 10 km may record no rainfall despite very heavy rainfall between them. Stratiform rainfall shows similar variations but occurs over much larger scales. Precipitation radar can also be used to measure rainfall, and gives areal coverage over a large area (over $100,000$ km^2 for operational radars) with resolution to 1 km^2 at close ranges. Traditionally these radars measure just the reflectivity, Z (Section 2.2.1), of the target. The reflectivity is the empirically related to rainfall rate, R, by a simple $Z - R$ equation of the form

$$Z = aR^b. \tag{1.1}$$

However, these relations suffer from high errors (often quoted as a factor of 2 error in rainfall rate, but can be much larger in some cases) which mean that current radar is more of a qualitative tool than quantitative instrument. The radar suffers from a number of problems such as ground clutter (where the radar beam hits the ground, or similar static targets), the presence of hail and the bright band (caused by melting snow), these errors will be discussed later in this chapter. There also remains doubt in the values of both a and b with large numbers of these relations formulated over the years of radar meteorology, many of which appear in the book by Battan (1973). The likely cause of much of this variation is the variations in the drop size distributions, DSD, which naturally occur. It can be seen from many of the suggested forms of equation 1.1 that the $Z - R$ relations in stratiform (high b) and convective (low b) rainfall are considerably different. This could explain the different $Z - R$ relationships used by the UK and US operational networks. The UK, where stratiform rain is prevalent, uses $Z = 200R^{1.6}$, while in the US convective rainfall is more common, so a different relationship, $Z = 300R^{1.4}$, is used.

Modern technology allows the use of polarised radar beams, giving us more information on the scattering targets. Installation of these new dual polarisation radars has begun in the United Kingdom and France. With the extra information provided, more knowledge of the DSD can be obtained from the radar, improving rainfall estimation. Another benefit is that polarisation can be used to identify ground clutter, the bright band and hail. However the principal point of this thesis is for times when the radar beam is in rain (so short ranges - especially in the winter months). Dual polarisation techniques have been suggested as the way to better rainfall estimation, but this remains to be demonstrated in an operational environment.

It should be noted that weather radar cannot predict where rainfall will occur, but useful information can be obtained once the detection of the precipitation has occurred, and assists in nowcasting and weather forecasting such as the NIMROD system (Golding, 1998) operated by the Met Office, which forecasts up to a range of 6 hours.

1.2 RADAR METEOROLOGY

Radar[1] is a system that uses electromagnetic radiation for detection of targets and their positions. Although initially developed for aircraft, the potential of radar for meteorology was rapidly realised (Fletcher, 1990). This section will introduce the basics of dual-polarisation radar.

1.2.1 THE HISTORY OF WEATHER RADAR

Radar has its history in radio communications. Radar developed quickly after its invention by Watson-Watt in 1936 (although whether this was the true invention is debated). By the end of World War II radar had been well developed and was very successful, especially for the Allied forces. During the war, weather returns were generally considered a nuisance, but, before the end of the war, the Meteorological Office had a 10 cm radar. Since, radar has evolved, with improvements in all the technologies used in radar. Probably the greatest advances in radar were the invention of the transistor and the computer. The computer was especially important for radar meteorology, so that the large quantities of data generated can be utilised and archived.

The first work in the UK done on the accuracy of precipitation from radar was in the late 1940s. Meanwhile in Canada, Marshall *et al.* (1947) derived an early Z-R relation of the form of equation 1.1. However, it was not until 1967 that the use of radar to provide quantitative rainfall measurement in the UK was studied. This experiment used a 10 cm radar but suffered from a number of problems including a large beamwidth. Hence the radar was converted to 5.6 cm in 1973, reducing the beam to 1 °. In the early 70s the Dee Weather Radar Project based in north Wales pioneered research into the use of radar for rainfall rates, much of the work remains valid, though perhaps too confident, this project lead us to have the operational network we now have in the UK. This is now the operational radar band in the UK. This wavelength change means that the radar suffers more from attenuation of the radar beam in very heavy rain, but means that

---

[1]Radar is an acronym for RAdio Detection And Ranging

smaller radar antennas are required for the same beam width. In the UK and Europe, the very heavy, attenuating rains are less frequent than in the USA which is a major reason for the difference in radar wavelengths in these respective regions.

The advent of polarisation radar occurred in the early 1950s. Initially polarisation was exploited with circular polarisation, where promise was found for suppressing clutter. Drop shapes were found to depolarise the returns to the radar, leading to the development of the linear depolarisation ratio (see section 5.2). Seliga and Bringi (1976) used the shapes, sizes and orientation of rain drops to show differential reflectivity (see section 2.4.1) gave a measure of drop size, and when used in combination with Z has the potential to derive more accurate rainfall rate estimates. To measure differential reflectivity Seliga and Bringi (1976) suggested a radar design which utilised horizontally and vertically polarised pulses, measuring the returns at both polarisations. The CAMRa radar (see section 1.4) in Chilbolton was the first to implement this technique with alternate horizontally and vertically polarised beams, then as now this radar operated at S-band (note the operational radar network in Britain uses C-band). Sachidananda and Zrnić (1987) suggested the use of differential phase shift to improve rainfall estimation. The 1990s saw efforts into improved algorithms for rainfall estimation, both with traditional and dual-polarisation radars. Meanwhile, operational radar networks grew throughout the world at various frequencies, mostly operating at S-band in America, but at C-band in Europe and Japan. Recent years have seen the development and installation of the first polarisation radars in the operational environment.

1.2.2 THE MATHEMATICS OF RADAR: THE RADAR EQUATION

The power received from a distribution of meteorological targets is given by equation 3 of Probert-Jones (1962), often called the meteorological radar equation:

$$P_r = \frac{\pi^3 P_t \, g^2 \, \theta \, \phi \, h \sum |K|^2 \, D_i^6}{1024 \ln 2 \, \lambda^2 \, r^2}, \tag{1.2}$$

where

$$
\begin{array}{rcl}
P_r & = & \text{received power} \\
P_t & = & \text{transmitted power} \\
g & = & \text{antenna gain} \\
\theta & = & \text{beamwidth (horizontal)} \\
\phi & = & \text{beamwidth (vertical)} \\
h & = & \text{pulse length} \\
|K|^2 & = & \text{the dielectric factor (for rain } 0.93) \\
D_i & = & \text{scatterer diameters} \\
\lambda & = & \text{radar wavelength} \\
r & = & \text{distance between sample and radar antenna}
\end{array}
$$

with summation over a unit of volume. Equation 1.2 may be written as

$$
P_r = \frac{C \, |K|^2 \, Z}{r^2} \tag{1.3}
$$

where we have the radar constant, C, and the radar reflectivity factor, Z.

These equations make a number of assumptions:

- The targets are equally spread through the sample volume, are modelled as homogeneous dielectric spheres and have diameter smaller than the radar wavelength to ensure Rayleigh scattering.

- The reflectivity factor remains constant throughout the contributing region (gradients generate errors).

- The main beam power is described by a Gaussian function.

- Attenuation and multiple scattering are negligible.

- Polarisation of incident and backscattered waves are the same.

The radar reflectivity factor, Z, is usually referred to as simply "reflectivity" by radar meteorologists (which will be used in this thesis). Reflectivity is the summation of sixth power of diameter of all targets within a unit volume:

$$
Z\left[\text{mm}^6\text{m}^3\right] = \int_0^\infty \frac{|K|^2}{0.93} N(D) D^6 \, dD \tag{1.4}
$$

in linear units. The range of magnitudes of Z lead to its expression in logarithmic units, dBZ:

$$Z[\text{dBZ}] = 10 \log_{10} \left(Z \left[\text{mm}^6 \text{m}^3 \right] \right).$$ (1.5)

The radar observes P_r, which is then interpreted as the return from small spherical liquid water drops.

Radar system errors are given in Joss and Waldvogel (1990), and include beam blocking, attenuation (when atmospheric gases and particles reduce the power within the radar beam) and ground clutter. These errors can be minimised by:

- favourable radar site location to minimise beam blocking and ground clutter;

- appropriate choice of wavelength for the intended use;

- beam width and sensitivity for the intended purpose;

- good calibration;

- correction of attenuation and anomalous propagation.

1.2.3 DIFFICULTIES TRANSLATING Z TO R

Converting Z into R is not trivial. Although a relation of the form of equation 1.1 is accepted as representing the truth well, there remains a large number of problems.

When the radar beam hits the ground, or ground based objects (such as trees, buildings or masts) the reflectivity will be high, even without hydrometeors present. This will then mean that a Z-R translation will show a non-zero rainfall despite the lack of hydrometeors. When both clutter and hydrometeors are present within the radar beam the reflectivity is higher than for the hydrometeors alone, hence increasing the rainfall rate apparent from the Z-R translation.

When the radar beam encounters hail the reflectivity will be affected. Hail tends to have much larger diameters than rain drops. This means that when hail is present within the radar beam it dominates the reflectivity due to its dependence on the 6th power of

particle size (equation 1.2). This results in hail-infected returns having higher reflectivity than the rainfall would suggest once the hail melts (either in the fall or after impact with the surface).
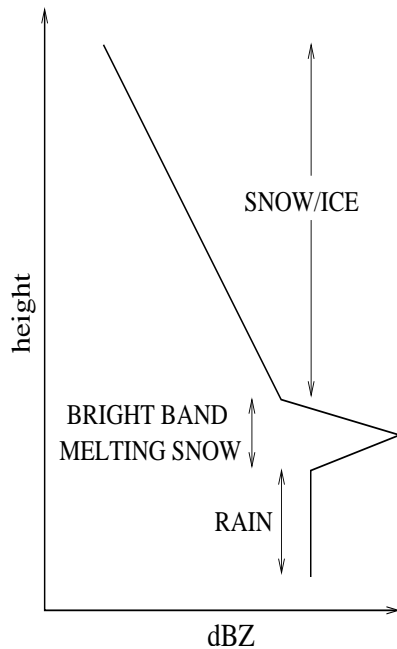
Figure 1.1 *Schematic plot of the vertical profile of reflectivity.*

Another problem occurs when the beam is sampling snow and ice. Reflectivity is reduced because the dielectric constant is different, but is increased by the larger size typical of the snow and ice particles. These snow and ice particles tend to also grow as they fall so the reflectivity can change as the same particles fall. An even more serious problem occurs once the snow flakes begin to melt. When this occurs the drop builds up water while maintaining an ice structure, so gains the dielectric constant of water, but with size of snow. This means that reflectivity is large, increasing by as much as 13 dB. A schematic of all of these effects can be seen in figure 1.1.

Even if all of these problems can be removed we still have difficulties calibrating the reflectivity recorded by the radar. This can be done using polarisation radar as will be seen in chapter 2. Finally the conversion from Z to R relies on a consistent raindrop size distribution, which is not present. This is why many different $Z - R$ relations have been suggested. These spectra will be discussed in the next section. Even if the rainfall rate is known perfectly from within the beam, low level growth or evaporation will change the rate by time the drop reach the surface, this cannot be corrected using dual polarisation radar.

1.3 THE RAINDROP SIZE SPECTRA

The drop size distribution is of vital importance to radar as it dictates the numbers and sizes of the drops in the sampled volume, affecting the returns via equation 1.4.

In the early years of meteorological radar research Marshall and Palmer (1948) suggested a simple exponential form of the raindrop size distribution:

$$N(D) = N_0 \exp -\Lambda D, \tag{1.6}$$

where $N_0 = 8000$ m^{-3} mm^{-1} and

$$\Lambda = 41 R^{-0.21}. \tag{1.7}$$

This drop spectrum only changes with rainfall rate, which would make converting reflectivity to rainfall a trivial task (which leads to $Z = 200 R^{1.6}$). Unfortunately the Marshall-Palmer drop spectrum does not represent the wide variation in drop spectra found in nature, which lead to the introduction variation of drop concentration. A gamma function for raindrops was suggested by Ulbrich (1983). However, variation in the shape parameter caused changes to the drop concentration required for the same rain properties, so a normalisation was added.

Natural raindrop size spectra are well-defined (Kozu and Nakamura, 1991) by a normalised gamma function:

$$N(D) = N_w f(\mu) \left(\frac{D}{D_o} \right)^{\mu} \exp \left(-\frac{(3.67 + \mu)D}{D_o} \right) \tag{1.8}$$

$$f(\mu) = \frac{6}{(3.67)^4} \frac{(3.67 + \mu)^{\mu+4}}{\Gamma(\mu + 4)}. \tag{1.9}$$

In this equation there are three variables:

Shape parameter μ. High values of μ imply a more truncated spectrum. See figure 1.2.

Drop Concentration N_{w}, normalised so that, despite changes in μ, liquid water content remains constant. See figure 1.3.
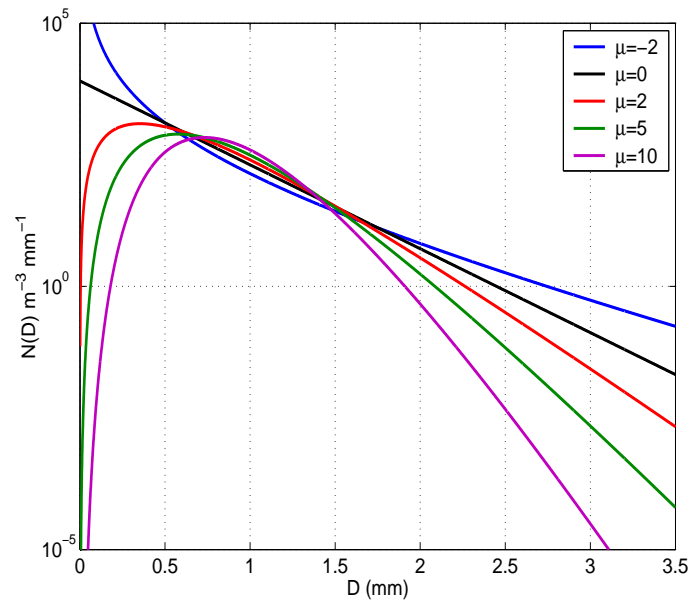
Figure 1.2   *Normalised gamma distribution, with μ variations. For this plot D_o is 1 mm and N_w is 8000 $m^{-3}mm^{-1}$.*
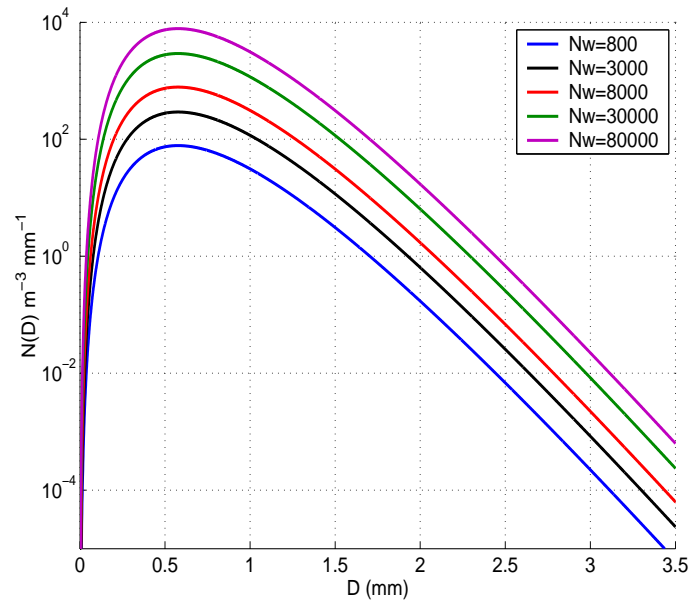
Figure 1.3   *Normalised gamma distribution, with N_w variations. For this plot D_o is 1 mm and μ is 5.*

Median drop diameter D_o, the diameter of the drop of which there is an equal volume of water in drops of greater and lesser sizes. See figure 1.4.
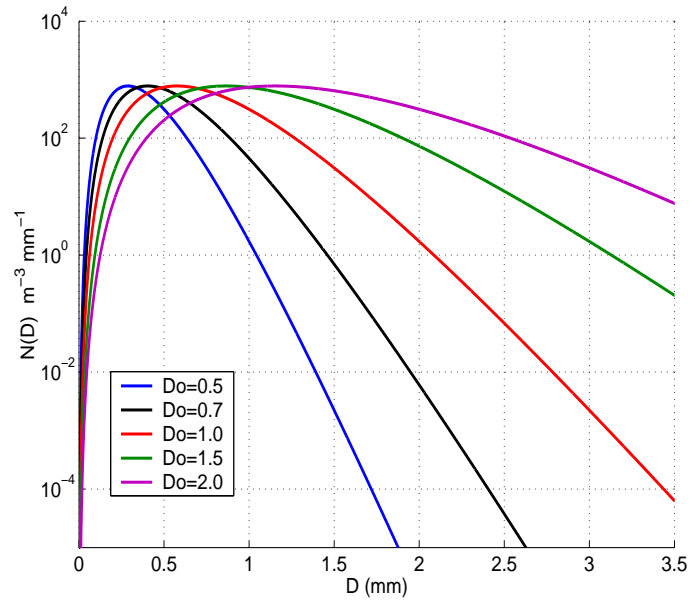
Figure 1.4 *Normalised gamma distribution, with D_o variations. For this plot N_w is 8000 $m^{-3}mm^{-1}$ and μ is 5.*

This normalised spectrum is preferable (Illingworth and Blackman, 2002) to the non-normalised gamma function of Ulbrich (1983) as it gives N_w a more reliable meaning. With $\mu = 0$ the normalised gamma function reduces to a simple exponential form.

Ulbrich (1983) used the many $Z - R$ relations of Battan (1973) to find a range of variables in the gamma function (not-normalised) known as the "Ulbrich" range. He deduced a μ range from -1 to 5. Illingworth and Blackman (2002) questioned the validity of the mathematics of the derivation of the "Ulbrich" range (and showed evidence of data outside realistic bounds, as an example a rainfall rate of 40000 mm/hr results from a spectrum within the "Ulbrich" range), but it is now common practice to derive polarimetric rainfall techniques using the "Ulbrich" range. Comparison with observations of disdrometer (Kozu and Nakamura, 1991) found an average value of μ would be about $4 - 6$. Using disdrometer observations in Chilbolton, UK, Illingworth and Johnson (1999) found a mean value of $N_w = 8511$ m^{-3} mm^{-1}, with a standard deviation of a factor of 3.6, with 96% within a factor of 13. Bringi and Chandrasekar (2001) found a similar value of $N_w = 10,000$ m^{-3} mm^{-1} from a disdrometer in Darwin, Australia and

$D_\text{o} = 1.25$mm.

These techniques have a problem with sampling the less common large drops due to the sampling area. A larger volume with a better sample of the larger drops is found using radar. Wilson *et al.* (1997) used differential Doppler velocity, DDV (difference in Doppler velocities at horizontal and vertical polarisations). They show that DDV as a function of Z_DR is dependent on the value of μ. They find a range of $\mu = 2 - 10$ with a mean of 5.

1.4 THE CHILBOLTON ADVANCED METEOROLOGICAL RADAR

The Chilbolton Advanced Meteorological Radar (CAMRa), (Goddard *et al.*, 1994a), is an S-band radar ($\lambda \approx 10$ cm, 3 GHz) with a very large (25 m diameter) fully steerable dish to give very high resolution radar data and sensitivity (the world's largest steerable pointable meteorological radar). The radar (pictured in figure 1.5) is located at Chilbolton Observatory, in Hampshire (near Winchester), UK and run by the Rutherford Appleton Laboratory (RAL). The radar operates with an alternate pulse system (described in section 2.4.3) for polarimetric measurements and also has Doppler capability. For information on the hardware of the radar see the paper of Goddard *et al.* (1994a). A key feature of the CAMRa radar is the very large antenna, which gives a very narrow $0.28°$ beam ($1°$ is more normal). This means that the radar data has much higher spatial resolution than other radars. The use of data from this radar will be extensive throughout this thesis.

The maximum range resolution is limited by the pulse length, and the range is limited to the product of the speed of light and pulse length divided by 2 for the return trip. The radar data acquisition system averages 64 pulse pairs at each gate. Additionally, for most operations 4 gates in range are averaged to make a range resolution of 300 m. The effects of this averaging will be discussed in more detail in chapter 3.

The wavelength of 10 cm is larger than operational radars in the UK, which tend to
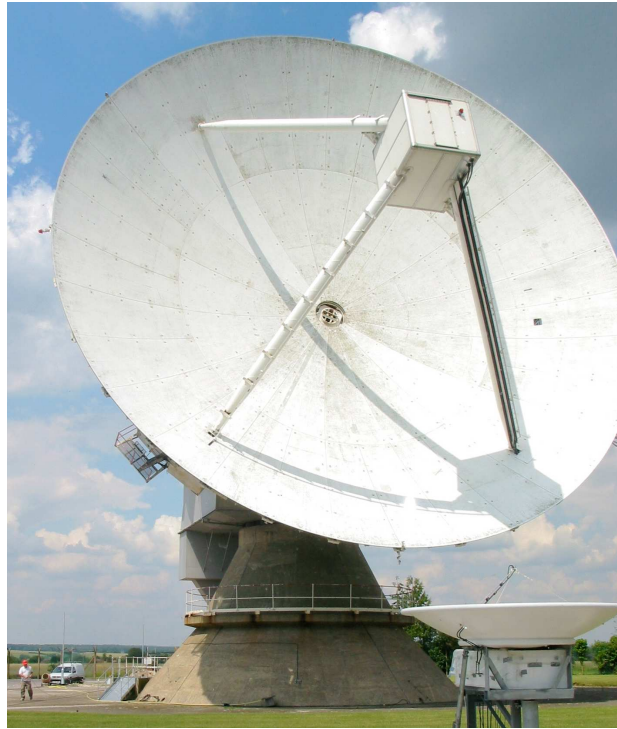
Figure 1.5 Photograph of the CAMRa radar in Chilbolton.

operate in C-band ($\lambda \approx 5.6$ cm), but the same as used in the USA. This means that attenuation of the radar signal, by both hydrometeors and atmospheric gases, will be less significant. Attenuation is a result of absorption and scattering of the radar beam as a result of passing through the extinction cross section of the target particles. In the Rayleigh regime, where drops are much smaller than the radar wavelength, the extinction cross section is proportional to the drop volume. The attenuation of the radar beam will be larger as wavelength decreases. For example rainfall of 40 mm/hr attenuates the beam by approximately 0.5 dB km^{-1} at C-band, whereas at S-band this is less than 0.1 dB km^{-1}.

1.5 THESIS OUTLINE

This thesis focuses on the use of an area-integrated method to accurately estimate moderate rainfall rates. This chapter has shown the need for more accurate rainfall rates, described the basics of radar meteorology, introduced the normalised gamma distribution

Frequency	3.0765 GHz
Wavelength	10 cm
Antenna diameter	25 m
Beam width	0.28 °
Pulse width	0.5 μm
PRF	610 Hz
Max. range resolution	75 m
Max. digitised range	160 km
Peak power	560 kW
System noise figure	1.3 dB
Elevation slew rate	1 ° s^{-1}
Azimuth slew rate	2 ° s^{-1}
Cross-polar isolation	-34 dB
Noise at 1 km	-36.7 dBZ
Unambiguous velocity	15 m s^{-1}

Table 1.1 *Properties of the CAMRa system.*

of raindrop size and gave details of CAMRa, the radar used for much of the work in this thesis.

Chapter 2 examines the current state of rainfall estimation from radar, initially with conventional radar, moving into dual-polarisation radar. The new radar variables available from the dual-polarisation will be described as they are encountered in this chapter. This chapter will demonstrate the need for integrated techniques when using polarisation parameters, especially in the operational environment.

The natural variability of rainfall is considered in chapter 3. Using polarisation radar parameters we look into the changes in parameters we record and show the variabilities are the effect of true changes in the rainfall, not simply the effect of the sampling.

The statistics of rainfall are considered in chapter 4, examining the occurrence of rainfall events, the decorrelation of the rain and the related effects of non-continuous

sampling of rain when estimating accumulations as performed by a radar network.

In chapter 5 the integrated Z/Z_{DR} technique is described along with precautions necessary to avoid problems with output. This chapter is followed by a number of examples showing the results of the technique and explanations of the physical processes giving rise to the results, in chapter 6.

Chapter 6 also demonstrates the evaluation of the integrated Z/Z_{DR} technique and comparisons to other methods of rainfall estimation.

The use of the integrated Z/Z_{DR} technique in the operational environment is considered in chapter 7. Here we detail the differences that occur in the operational environment compared with use on research radars. This poses significant problems to most polarisation methods due to the increased noise of the operational systems. This chapter introduces the Thurnham operational dual-polarisation radar.

Chapter 8 gives a conclusion and comments on possible future work into the described method. Finally the potential for this technique to become part of the UK's operational system is discussed.

CHAPTER 2:
RAINFALL ESTIMATION WITH RADAR

2.1 INTRODUCTION

This chapter will investigate the various methods of estimating rainfall rate using radar, from the simple reflectivity relationship used on the UK operational network to the modern combined and integrated polarisation radar techniques.

2.2 Z-R, WITHOUT POLARISATION

2.2.1 'TRADITIONAL' REFLECTIVITY RAINFALL RATE METHODS

A traditional non-polarised radar will measure only the reflectivity at each gate (often these radars actually use a polarised beam, but lack the capability to receive or transmit in the orthogonal polarisation. Currently these radars are dominant in the operational networks of the world.

Empirical relations of the form

$$Z = aR^b, \tag{2.1}$$

using only the reflectivity to estimate rainfall, may suffer from errors of a factor of two in rainfall rate. This is caused by variability of rain drop spectra, as

$$Z = \sum ND^6, \tag{2.2}$$

but

$$R = \sum ND^{3.67}, \tag{2.3}$$

where N is the number of drops and D is the drop diameter, in mm. Oft-quoted is the

Marshall and Palmer (1948) relation $Z = 200R^{1.6}$ derived from the Marshall and Palmer (1948) drop size spectra of equation 1.6.

The variation in drop spectra explains the wide variety of $Z - R$ relations reported, and this will be analysed in more detail in chapter 3. Many have been proposed, such as those in Battan (1973). Battan went on to suggest that it may be more appropriate to assign a $Z - R$ based on the type of rain event considered, suggesting equations of the form of table 2.1.

Rainfall Type	$Z - R$	Author
Stratiform	$200R^{1.6}$	Marshall and Palmer (1948)
Orographic	$31R^{1.71}$	Blanchard (1953)
Thunderstorm	$486R^{1.37}$	Jones (1956)

Table 2.1 $Z - R$ *relation for different rain types suggested by Battan (1973).*

Use of an adjustable $Z - R$ would, however, require a reliable method of defining the event "type" operationally, though radar-gauge adjustment has be implemented in some work (e.g. Wilson and Brandes, 1979), this does not truly differentiate rain type, and may partly correct miscalibration. Although these simple techniques have been used for over 50 years, modern technology can improve our precipitation estimation.

2.3   RAINDROP SHAPES

Why is polarisation important for weather radars? The answer is that raindrops (and other hydrometeors) are not perfect spheres. If all targets were perfectly spherical, the returns from all polarisations would be the same, even if sizes varied. Raindrop shapes are related to their size. Drops smaller than 1 mm are spherical, but become increasingly oblate as the size increases, as shown in figure 2.1. These shapes are a result of the high surface tension forces of water in the drop, and the aerodynamic effects caused by the drop falling under gravity. Also, turbulence in the air causes raindrops to have a distribution of angles, where the major axis deviates from the horizontal, known as "canting angles" (Beard and

Jameson, 1983). The radar will see drops with a variety of canting angles, but an average value of close to $0°$. Raindrops larger than 1 mm in diameter oscillate about a mean shape (Beard and Tokay, 1991). The effects of these oscillations will average to zero for a large number of drops. The combination of canting and oscillation means that a radar does not view the maximal horizontal and minimal vertical extent of the drops. To interpret polarisation returns the raindrop shapes must be known well.
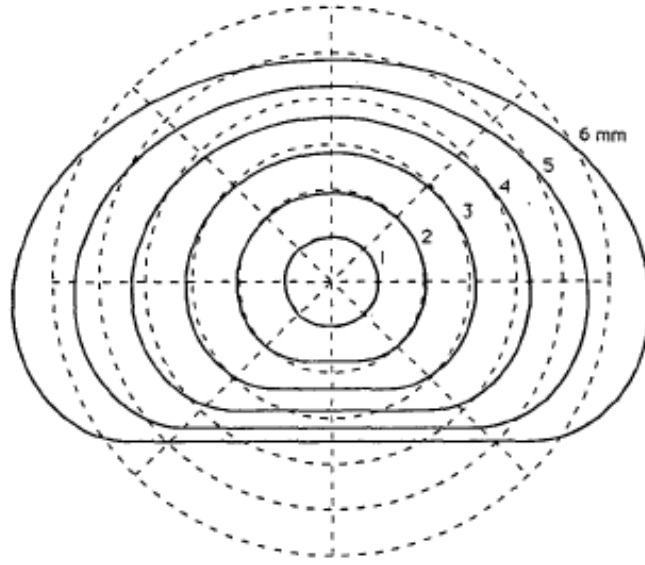
Figure 2.1   *Horizontal view of equilibrium shape of raindrops of 1-6 mm diameter, with shape for spherical drops of the equivalent volume. The dashed lines show the size of the equivalent volume sphere. From Beard and Chuang (1987).*

Pruppacher and Pitter (1971) suggested a simple linear relationship between drop axial ratio, r, and drop diameter, D (mm):

$$D < 0.5 \, \text{mm} \quad \Rightarrow \quad r = 1$$
$$D > 0.5 \, \text{mm} \quad \Rightarrow \quad r = 1.03 - 0.062D, \tag{2.4}$$

which was commonly used until recently. Goddard *et al.* (1982) formulated a new model:

$$D < 1.1 \, \text{mm} \quad \Rightarrow \quad r = 1$$
$$D > 1.1 \, \text{mm} \quad \Rightarrow \quad r = 1.075 - 0.065D - 0.0036D^2 + 0.0004D^3, \tag{2.5}$$

which was calculated from comparison of radar and disdrometer. This answered a problem that observations (of Z_{DR} and comparison with disdrometer 150 m below the radar beam) suggested the linear shapes were too oblate for drops smaller than 2.5 mm. This implied the drops should be more spherical than the linear model predicts.

More recently, use of strobe photography in long wind tunnels has led to the proposal, by Andsager *et al.* (1999), of the polynomial:

$$D = 1.1 - 4.4 \, \text{mm} \quad \Rightarrow \quad r = 1.102 - 0.01445D - 0.001028D^2. \tag{2.6}$$

These models predict distributions as shown in figure 2.2.
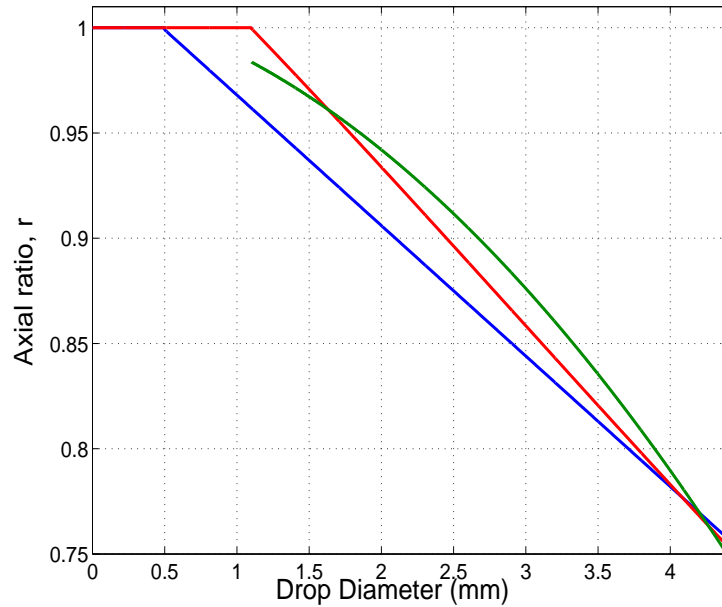
Figure 2.2 *Plots of different raindrop shape models: linear Pruppacher and Pitter (1971) model (blue), Goddard* et al. *(1995) model (red) and Andsager* et al. *(1999) model (green).*

2.4   THE ADDITION OF DIFFERENTIAL REFLECTIVITY

2.4.1   WHAT IS DIFFERENTIAL REFLECTIVITY?

Seliga and Bringi (1976) suggested that rainfall rate estimations could be improved using differential reflectivity (Z_{DR}). This is defined as the ratio of reflectivity at horizontal and

vertical polarisations:

$$Z_{\mathrm{DR}} = 10 \log \left(\frac{Z_{\mathrm{HH}}}{Z_{\mathrm{VV}}} \right). \tag{2.7}$$

This parameter is independent of drop concentration and hence gives information on the mean shape (reflectivity weighted) and hence size of the drops. Using this parameter provides information on the variation in the drop size distribution, hence allowing more accurate rainfall rate estimation.

2.4.2 WHY USE DIFFERENTIAL REFLECTIVITY FOR ESTIMATING RAINFALL RATES?

The use of Z_{DR} gives the ability to reduce the effect of variability in the drop size spectra by adding extra information about drop size. In what follows it is assumed that the natural variability of DSDs is captured by the normalised gamma function (section 1.3) and assumes that $\mu = 5$.

By knowing the relationship between drop shape and size, Z_{DR} gives the D_{o} of the target drops (assuming constant μ). For a given D_{o}, Z and R both scale with N_{w}, so Z/R can be calculated as a function of Z_{DR}. This results (at S-band) in the formula of Illingworth and Blackman (2002):

$$\mathrm{dB}Z - \mathrm{dB}R = \frac{Z}{R} = f(Z_{\mathrm{DR}}) = 21.48 + 8.14\,Z_{\mathrm{DR}} - 1.385\,(Z_{\mathrm{DR}})^2 + 0.1039\,(Z_{\mathrm{DR}})^3. \tag{2.8}$$

A plot of this equation can be seen in figure 2.3. In the thesis of Lee (2003), however, it is suggested that it is better to use:

$$\frac{Z}{R} = f(\log Z_{\mathrm{DR}}), \tag{2.9}$$

where f is an empirical polynomial, which will give better Z/R at low values of Z_{DR}. Using this formula, the rainfall rate at each point can be calculated, using the Z and Z_{DR} values. It is known that at constant Z_{DR}, Z and R both scale with N_{w}. So given Z_{DR}, a value of reflectivity can be found using 2.9 for the case where rainfall rate is 1 mm hr^{-1}. Rainfall rate R, in dBR, is given by

$$\mathrm{dB}R = \mathrm{dB}Z_{obs} - \mathrm{dB}Z_{1\mathrm{mm/hr}}, \tag{2.10}$$
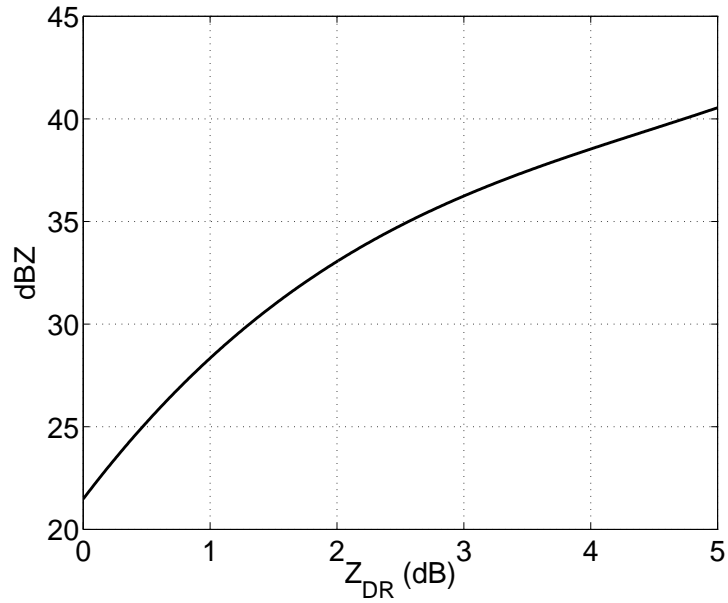
Figure 2.3 *Plot of the reflectivity required at a given Z_{DR} for a rainfall rate of 1 mm/hr as formulated in Illingworth and Blackman (2002).*

where dBZ_{obs} is the observed reflectivity and $Z_{1\mathrm{mm/hr}}$ is reflectivity in the case described above. Recall that

$$R \,=\, 10^{\left(\frac{\mathrm{dB}R}{10}\right)}. \tag{2.11}$$

When considering this in linear terms, this becomes

$$R \,=\, c\,Z\,g(Z_{\mathrm{DR}}). \tag{2.12}$$

This is similar in form to the equation of Bringi and Chandrasekar (2001):

$$R \,=\, c\,Z^{\alpha}\,Z_{\mathrm{DR}}^{\beta}. \tag{2.13}$$

Figure 2.3 shows that if the drops present are generally smaller than an average spectrum, then Z_{DR} is smaller, and would suggest the rainfall is higher than a simple $Z - R$ would predict (Z for 1 mm/hr drops as $Z_{\mathrm{DR}} \to 0$). When only very large drops are present (in the early stages of a convective shower for instance) the dependence of Z on the sixth power of drop size means that the reflectivity is high, but rainfall not especially heavy. This can be seen at high Z_{DR} (large drops) where a much higher Z is required to achieve 1 mm/hr of rainfall.

While in theory equation 2.13 yields a good estimate of R, large errors result especially when Z_{DR} is small. Bringi and Chandrasekar (2001) suggest a more robust estimate is found if considering Z_{DR} in linear terms:

$$R = c_1 \, Z^{\alpha_1} \, 10^{\, 0.1 \beta_1 \, Z_{DR}}. \tag{2.14}$$

The coefficients are chosen by regression using the "Ulbrich" range of parameters in the normalised gamma distribution of drop sizes (Ulbrich, 1983). Bringi and Chandrasekar (2001) propose $c_1 = 0.0067$, $\alpha_1 = 0.93$ and $\beta_1 = -3.43$ at S-band. Estimators of the form of (2.14) are now becoming more widely used (Brandes *et al.*, 2002; Ryzhkov *et al.*, 2005b). However, it is difficult to explain physically any value of α_1 not equal to 1. Equations 2.10 and 2.11 show that Z and R scale together so α_1 must be 1 or this would not be the case. The only possible cause of a non-unity α_1 is a result of systematic changes in μ with rainfall rate. Use of linear drop shapes and the Ulbrich range (Gorgucci *et al.*, 1994; Chandrasekar and Bringi, 1988; Chandrasekar *et al.*, 1990) lead to an overestimate of rainfall rate by as much as a factor of two.

It should be noted that for 25% accuracy at rainfall rates of $3 - 10$ mm hr^{-1}, Z_{DR} must be measured to within 0.1 dB. The reason for requiring this level of accuracy in Z_{DR} can be seen in figure 2.3. The slope of the curve at reflectivities around 30 dBZ mean that a 0.1 dB error in Z_{DR} will result in a 1 dB error in Z for 1 mm/hr, equivalent to 25%. This accuracy of rainfall rate will also require Z to be calibrated to 1 dB. This constraint will be discussed in section 2.6.1.

2.4.3 SAMPLING NOISE IN DIFFERENTIAL REFLECTIVITY

The radar measurement of Z_{DR} is subject to a number of errors. Errors caused by antenna imperfections are believed to be small for the Chilbolton 3 GHz radar and as it has no radome, radome errors are not introduced. However, fundamental errors caused by the sampling statistics cannot be avoided. This statistical noise will be unavoidable as it imposes a fundamental limit on the accuracy of the measurement of Z_{DR}.

The statistical noise for the Chilbolton radar is a result of the combination of non-

simultaneous sampling of Z_{HH} and Z_{VV} (the Chilbolton radar uses alternate pulse mode where a horizontally polarised wave is transmitted and response in both polarisations received, then the next is transmitted with vertical polarisation, and both channels receive; this sequence is a pulse pair) and the number of independent samples. Assuming a perfect alternate pulse radar (no errors introduced by the antenna), the recorded values of Z_{DR} will have mean equal to the true value, with a standard deviation given by:

$$SD(\hat{Z}_{DR}) = 10 \log_{10} \left\{ 1 + \left[\frac{2}{N} \sum_{l=-(N-1)}^{N-1} \left(1 - \frac{|l|}{N} \right) \left(|\rho[2l]|^2 - |\rho[2l+1]\rho_{hh,vv}[0]|^2 \right) \right]^{1/2} \right\},$$

(2.15)

according to Bringi and Chandrasekar (2001). $\rho_{hh,vv}[0]$ is the correlation between power of horizontal polarisation reflectivity and vertical polarisation reflectivity when not time lagged (i.e. interpolation is needed if an alternate pulse system is used). In equation 2.15

$$|\rho[n]| = exp \left(-\frac{8\pi^2 \sigma_v^2 n^2 T_s^2}{\lambda^2} \right) = exp \left(-8\pi^2 n^2 \sigma_{vn}^2 \right)$$

(2.16)

where σ_{vn} is the normalised spectrum width (normalised to the maximum unambiguous velocity measured by the radar), given by:

$$\sigma_{vn} = \frac{2\sigma_v}{\lambda(PRF)}.$$

(2.17)

In these equations, $\rho[n]$ the signal correlation with a time lag n, N is the number of samples of H and V pairs (64 for the Chilbolton 3 GHz radar), T_s is the time spacing between samples, σ_v is the spectral width of the targets and λ is the radar wavelength (10 cm).

These equations are best explained physically. Figure 2.4 shows a schematic of a time series taken from observations of high spectral width (a measure of the rate of reshuffling of the target scatterers) and high correlation between the horizontally and vertically polarised beams. Each red cross indicates the time a measurement is made (note they are alternate). The plot shows that the targets reshuffle quickly and that the H and V beams correlate with each other very well. However, this case will only have a good estimate of Z_{DR} if the spectral width is not too high. If spectral width is too high, the estimate will be
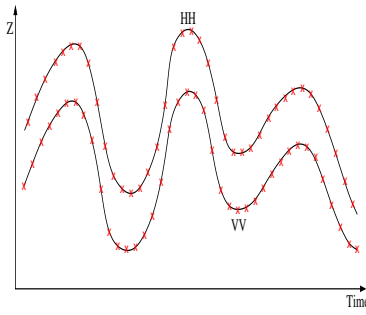
Figure 2.4 *Schematic showing the time series of Z_H and Z_V for data of high correlation and high spectral width*
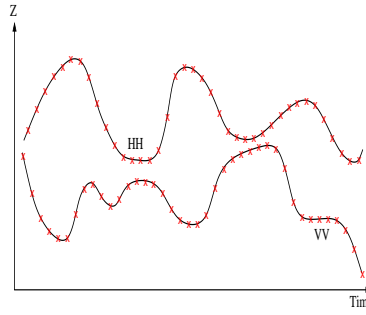
Figure 2.5 *Schematic showing the time series of Z_H and Z_V for data of low correlation and high spectral width*
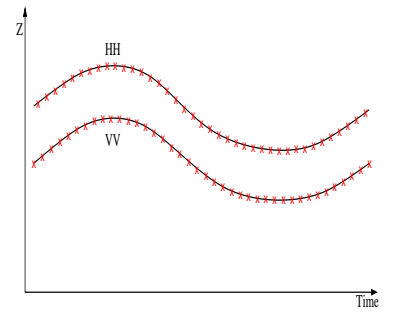
Figure 2.6 *Schematic showing the time series of Z_H and Z_V for data of high correlation and low spectral width*

poorer as the reshuffling will be so rapid that alternate pulses will sample reshuffled (and hence unrelated) targets within the beam. Figure 2.5 shows a schematic of a time series with high spectral width but low correlation. It can be seen that the measured reflectivity is fluctuating rapidly but that the horizontal and vertical time series do not correlate well, meaning that the Z_{DR} estimate will be poor. Figure 2.6 shows a schematic of a time series with low spectral width but high correlation. In this case, the high correlation would improve the Z_{DR} estimate, although the low spectral width means that the alternate samples are in fact not independent. This means the number of samples is in effect lower, making the estimate worse.

These effects are quantified in figure 2.7. It shows that, as the co-polar correlation approaches unity, the error in Z_{DR} is reduced. It can be seen that an ideal situation would have normalised spectral width of about 0.08. For Chilbolton, this corresponds to $\sigma_v = 2.4 \ m \ s^{-1}$, with values either side of this leading to an increased standard deviation in measured Z_{DR}. Higher spectral width will lead to increased error as the drops reshuffle more rapidly, making H and V less related; lower spectral width increases the error because the number of independent samples is effectively reduced. It has been found by Illingworth and Caylor (1991) that for rain with Z_{DR} of around 1 dB, $\rho_{hh,vv} \approx 0.99$, using CAMRa. In heavy rain in the UK, the spectral width is often found to be of order $\approx 1 \ m \ s^{-1}$ ($\sigma_{vn} = 0.03$), too small for optimal Z_{DR} measurement. This leads to a
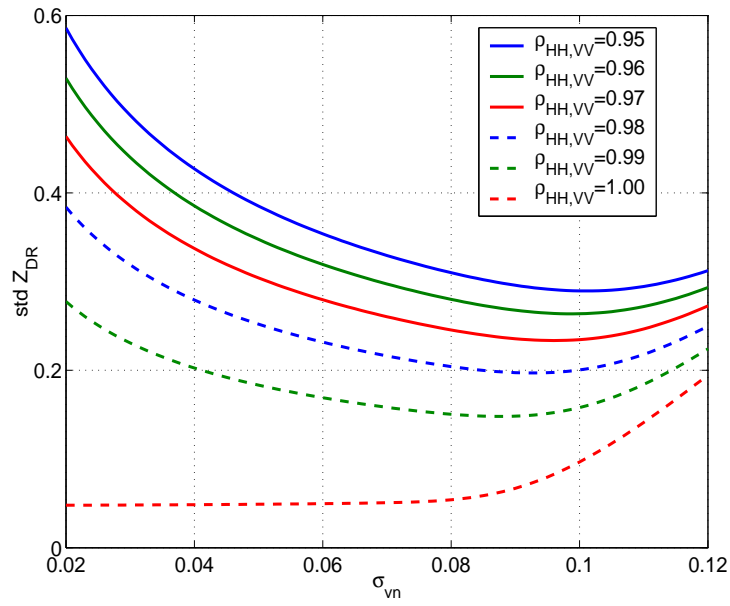
Figure 2.7 *A graph showing the effect of spectral width on the error in Z_{DR} for various values of co–polar correlation, for $N = 64$. Note that this is for a single gate.*

seemingly counter-intuitive problem: the spectral width is too low for good estimation of Z_{DR}.

Spectral width is caused by a number of effects (Nastrom, 1997):

- atmospheric turbulence at scales smaller than the radar beam volume;

- wind shear across the sample volume;

- finite beam-width;

- radar configuration and geometry.

These mean that a larger beam volume will lead to higher spectral widths. As the spectral width of Chilbolton is too low for optimal Z_{DR} measurement, this implies that the resolution of Chilbolton is too high for good Z_{DR} estimates. A larger volume would lead to more turbulence in the beam and higher wind shear, showing that an operational $1°$ beam may, from statistics alone, give a better Z_{DR} measurement, the wider beam nearing the optimal $\sigma_{vn} = 0.08$. However, current operational radars utilise "hybrid mode" where

each beam is transmitted with $45°$ polarisation, hence interpolation of the horizontal and vertical signals is not required, so the spectral width only affects the accuracy of Z_{DR} in terms of the number of pulses that are independent. Use of hybrid mode will be discussed in more detail in chapter 7.

2.4.4 PROBLEMS WITH DIFFERENTIAL REFLECTIVITY FOR RAINFALL RATES

So a statistical noise limit in Z_{DR} has been shown, that is a result of sampling that cannot be overcome. For CAMRa this limits us to a Z_{DR} accuracy ≈ 0.15 dB on a 300 m gate, larger than the limit for 25% rainfall rate accuracy. Using the noisy Z_{DR} at each gate to calculate rainfall rates will give noisy, and biased results. Also at low Z_{DR} values, the curvature of the Z/R line is high. This means that the rainfall rate increase caused by reducing Z_{DR} by a small amount is larger than the reduction caused by an equal increase in Z_{DR}.

To demonstrate this, examples from figure 2.8 will be used. Example 1 is for an observation of 32 dBZ and $Z_{\mathrm{DR}} = 0.65$ dB. This Z_{DR} leads to $Z/R = 26.5$ dBZ mm^{-1} hr, and hence a rainfall rate of 5.5 dBR (3.5 mm hr^{-1}). Now add an error to the Z_{DR} measurement of ± 0.2 dB. For the lower Z_{DR} limit of 0.45 dB; $Z/R = 25$ dBZ mm^{-1} hr and hence rainfall rate is 7 dBR (5 mm hr^{-1}); for the upper Z_{DR} limit of 0.8 dB, $Z/R = 27.5$ dBZ mm^{-1} hr and rainfall rate is 4.5 dBR (2.8 mm hr^{-1}). This is showing that lowering Z_{DR} increased rainfall rate by 1.5 mm hr^{-1}, while raising Z_{DR} decreased R by only 1.2 mm hr^{-1}, demonstrating an 8.6% bias.

Example 2 is for 43 dBZ and 1.5 dB Z_{DR}. Following the blue line to the blue cross, $Z/R = 31.6$ dBZ mm^{-1} hr, hence dBR= 11.4 (13.8 mm hr^{-1}). The same ± 0.2 dB error is applied (green), in this case leading to dBR, of 12.3 dB and 10.6 dB (17 to 11.5 mm hr^{-1}), showing a 6.5% bias.

But there remains perhaps a bigger problem, that of negative Z_{DR}. The statistical noise means that areas of naturally low Z_{DR} will occasionally be observed with negative
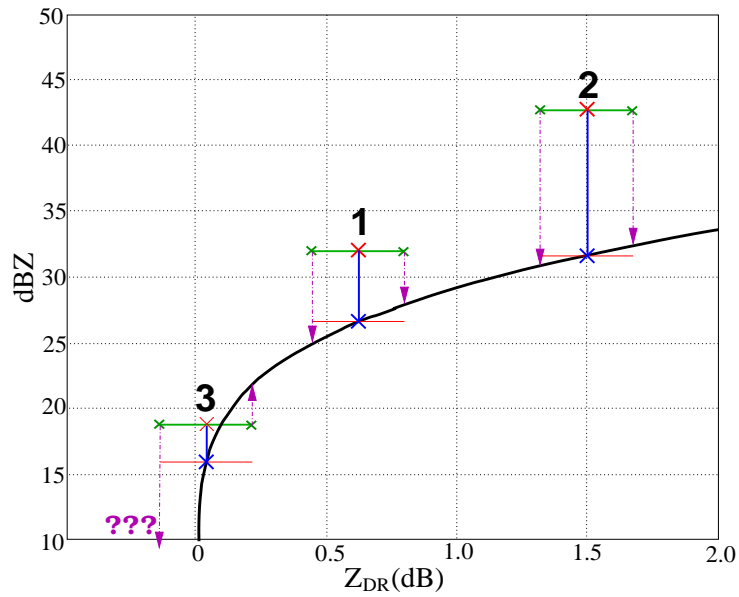
Figure 2.8 *Diagram showing the cause of the bias from gate-by-gate $R = f(Z, Z_{DR})$. Also shown is the problem caused by negative Z_{DR}.*

Z_{DR} (for a true $Z_{DR} = 0.3$ dB with a 0.2 dB standard deviation measurement error, 7% of points will record $Z_{DR} < 0$). For rainfall, negative Z_{DR} is unphysical, as it would be a result of drops having their major axis vertically. This explains the asymptote at $Z_{DR} = 0$ dB of the Z/R line. As can be seen in figure 2.8, example 3 has low Z_{DR}. If the estimate gives a lower value it may suggest a negative Z_{DR}. Here we have a conundrum: should these data points be simply thrown away or estimated using a standard Z-R? The combination of this problem, and the bias, are shown in figure 2.9.

2.5 DIFFERENTIAL PHASE SHIFT

2.5.1 WHAT IS DIFFERENTIAL PHASE SHIFT?

The velocity of a polarised radar wave is slowed when travelling through raindrops as a result of the index of refraction difference between air and water. This means that if the beam passes through a volume containing oblate raindrops, the horizontally polarised
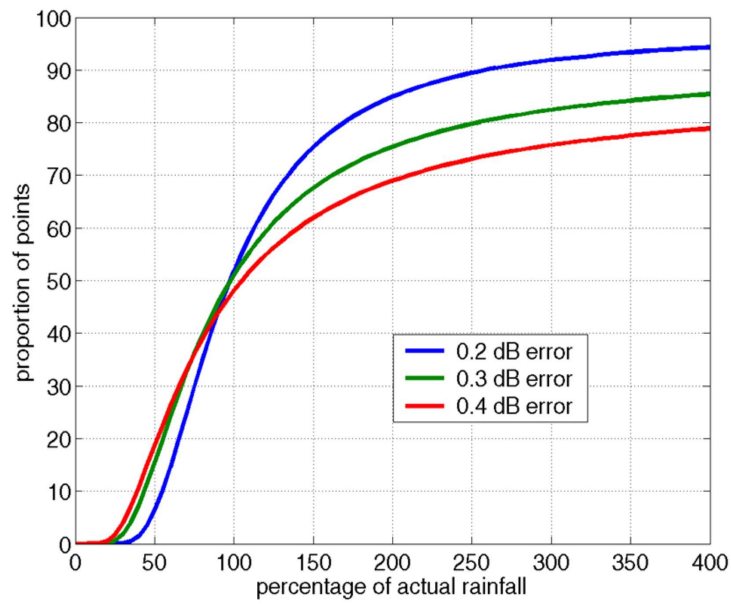
Figure 2.9 *A plot demonstrating the bias in rainfall rates caused by Z_{DR} noise. This plot uses 30 dBZ with mean Z_{DR} of 0.4 dB. The colours show the cumulative distribution for three different values of Z_{DR} estimator noise. The lines show that as the Z_{DR} noise increases, more points have extremely high rainfall rates (due to near-zero Z_{DR}). More points also do not appear on this graph, where Z_{DR} has become negative, hence no rainfall rate can be calculated.*

wave takes slightly longer to travel than vertically polarised equivalent. The phase of the
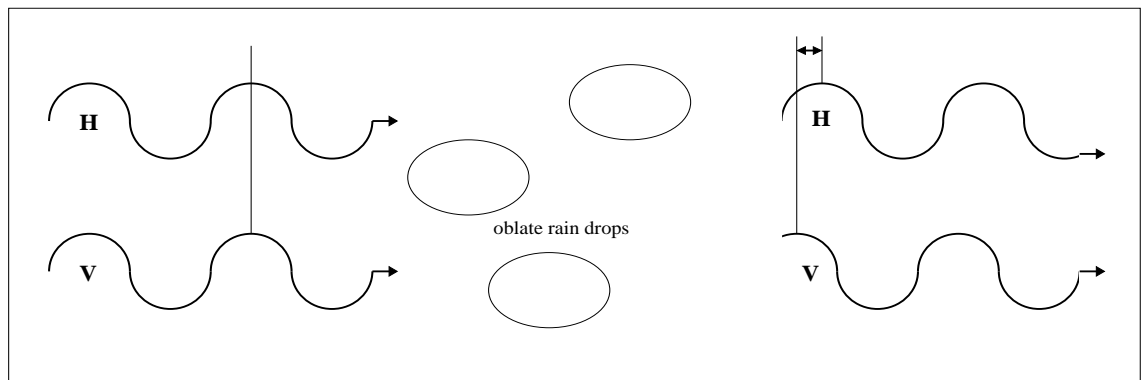
Figure 2.10 *Diagram showing the cause of differential phase shift, ϕ_{DP}; a result of the slower propagation of the H wave than the V wave in a volume containing oblate (large) raindrops. Figure from Illingworth (2004).*

horizontal returned signal lags behind the vertical, hence the differential phase,

$$\phi_{DP} = \phi_V - \phi_H, \tag{2.18}$$

usually will increase with distance from the radar.

The "specific differential phase", K_{DP}, is defined as the rate of change in ϕ_{DP} along the beam (units of $^{\circ}$ km^{-1}). As ϕ_{DP} increases with range, K_{DP} should be positive, and increase with rainfall rate.

2.5.2 WHY USE SPECIFIC DIFFERENTIAL PHASE FOR RAINFALL RATES?

Sachidananda and Zrnić (1986) and Sachidananda and Zrnić (1987) suggested that rainfall rates could be derived from K_{DP} using an equation

$$R = \mathcal{A}K_{\mathrm{DP}}{}^{\mathcal{B}} \tag{2.19}$$

with $\mathcal{B} = 0.866$.

Use of differential phase shifts gives a number of advantages over using reflectivity, because the value of $\mathcal{B}$ is near unity, so the conversion from K_{DP} to R is more linear than the conversion of Z to R (equation 2.1). This near-linearity is important as since R and K_{DP} scale with N_{w}, if the relationship is linear they do not depend on N_{w}. One of the set backs for Z-R relations is that it is difficult to calibrate Z (as it is difficult to dwell the radar at a target with known reflectivity), and this leads to errors in calibration of Z and hence R. Since K_{DP} uses phase change it does not require the calibration so it is not a significant problem for K_{DP} to R translation. $Z - R$ translation methods suffer from reduction of beam power due to attenuation in high rainfall. For K_{DP} this becomes the strength, the attenuation goes hand in hand with phase shift. Phase shifts do not become large until attenuation is significant, so K_{DP} is favourable, over Z, for rainfall estimation in very heavy rain, when the K_{DP} becomes large. This also leads to why differential phase shifts cannot be used for moderate rainfalls that are to be determined in this thesis. For moderate rainfall rates the phase shifts will be very small, masked by the noise in

measuring them. The estimations used in the thesis assume no attenuation, although once the attenuation is present the phase shift signal becomes large enough to be useful in heavy rains.

The K_{DP} to R translation also shows improvement in the presence of hail. The large hydrometeor sizes in hail lead to large reflectivities being measured, while in K_{DP} the tumbling of the hail removes the effect of the large hydrometeors. Finally, where the radar beam is partially obscured, the radar beam has a much reduced power, so estimates of Z in regions with blocked radar beams are reduced and likely unusable. However, the phase shifts are unaffected by the obscuration so estimation of rainfall using K_{DP} will be possible.

The difficulty with $R(K_{\mathrm{DP}})$ relations is that the phase shifts in all but the heaviest rainfall are small at S-band. Even at C-band, phase shift only becomes significant at heavy rainfall rates. However, to achieve good accuracy of the method, ϕ_{DP} is required to $1°$ accuracy, although the measurement is more noisy than this, in a similar way to that of Z_{DR}, especially in the operational environment. This problem is compounded by the need for K_{DP}, the differential of the noisy ϕ_{DP} signal, resulting in very large noise levels in K_{DP}. This restricts use of K_{DP} for rainfall estimation operationally to only the heaviest of rains in the UK.

2.5.3 SAMPLING NOISE IN DIFFERENTIAL PHASE

Similarly to the noise in Z_{DR} (section 2.4.3), the measurement accuracy of phase shift will be affected by the continual rearrangement of hydrometeors, leaving a fundamental limit on the accuracy of ϕ_{DP}. With the alternate sampling of the CAMRa radar, interpolation between pulses is needed for estimating ϕ_{DP}, as with Z_{DR}, the accuracy of the interpolation being limited by the Doppler width of the target. This follows a similar pattern to section 2.4.3, meaning that for the CAMRa radar, a standard deviation of ϕ_{DP} of $\approx 2°$ is expected.

In practice, this theoretical limit in accuracy of ϕ_{DP} is not achieved because of various

problems. If one side of the radar beam experiences more phase shift than the rest, this can cause negative K_{DP}. If the gradients occur along the beam, K_{DP} becomes biased. Gradients in the rainfall nature within the beam are obviously more common and more extreme when the beam width is large, hence gradients will be a larger problem for operational radars than for a radar with resolution as high as with the Chilbolton radar. The effect of the radar sidelobes on K_{DP} are very large, so even slight mis-matching of the horizontally and vertically polarised waves will add random noise to K_{DP}. A sidelobe with reflectivity of 1% of the main-lobe return introduces a $5°$ noise in ϕ_{DP}, which will become a major problem operationally where mis-matched sidelobes may be a more significant problem and will add to the already higher noise expected. Ground clutter returns randomly in phase, so leads to a similar problem to sidelobe mis-matching, with small amounts of clutter causing large levels of noise in ϕ_{DP}. When the target hydrometeors are very large they leave the Rayleigh scattering regime and enter into the Mie scattering regime, adjusting the backscattering, leading to a local maximum in the ϕ_{DP} profile, which in turn can lead to negative K_{DP}, because the scattering regime is a result of the particle size relative to wavelength. The Mie-scattering will be a bigger problem at C-band than S-band where Testud *et al.*, 2000 suggest the problem is small enough to be negligible.

These various problems combine to give a typical noise in ϕ_{DP} of about $3°$ (Ryzhkov and Zrnić, 1995) at S-band; easily enough to cause negative K_{DP}. Ryzhkov and Zrnić (1996) suggest that use of the modulus of K_{DP} in equation 2.19 would avoid the negative value problems, but there is no physical justification for this. Overall, this means that K_{DP} can not be used for accurate rainfall rates on a gate-by-gate basis.

2.5.4   PROBLEMS WITH SPECIFIC DIFFERENTIAL PHASE FOR RAIN-FALL RATES

The $R = f(K_{\mathrm{DP}})$ estimator is very sensitive to the chosen drop shape model. The use of linear drop shapes may account for the underestimation of rainfall rate (e.g. May *et al.*,

1999, Petersen *et al.*, 1999 and Brandes *et al.*, 2001) found from equation 2.19. Bringi and Chandrasekar (2001) calculated $R(K_{\mathrm{DP}}) = 40.5(K_{\mathrm{DP}})^{0.85}$ with linear drop shapes, but suggest use of more realistic drop shapes, yielding $R(K_{\mathrm{DP}}) = 50.7(K_{\mathrm{DP}})^{0.85}$.

The near-linearity of equation 2.19 is considered a major advantage of the $R(K_{\mathrm{DP}})$ method. Assuming a more typical $\mu = 5$ (the shape parameter in the normalised drop spectrum, see section 1.3) at S-band, the relationship is $R = 50.1(K_{\mathrm{DP}})^{0.7}$ ($K_{\mathrm{DP}} = 0.00417R^{1.4}$). This index is almost as large as the 1.5 for $Z(R)$, mitigating many of the advantages of the $R(K_{\mathrm{DP}})$ technique. Changes on the drop concentration will also have a major effect on the accuracy of the technique, an underestimate of a factor of two in R being caused by a factor of ten increase in N_{w} (not unreasonable; see section 1.3).

The final problem to be considered is the error in rain rate estimates as a result of the error in measuring K_{DP}. The error means that, at low to moderate rainfall rates, the errors are several hundred percent, while at 50 mm hr^{-1}, the error is 40%. This could be improved by increasing dwell time. However, this will lead to scan rates too slow for an operational radar. This means that an operational radar could not reliably use K_{DP} alone for rain rate estimation.

2.5.5 USING SPECIFIC DIFFERENTIAL PHASE AND OTHER PARAMETERS

Next this chapter will examine the potential use of differential phase shift with other radar parameters to estimate rainfall rates.

2.5.5.1 RAIN FROM DIFFERENTIAL REFLECTIVITY AND SPECIFIC DIFFERENTIAL PHASE

This method uses a similar argument to that of $R(Z, Z_{\mathrm{DR}})$ (section 2.4.2). With Z_{DR} providing information on drop size, it leads to an equation of the form:

$$R = c_2 \, K_{\mathrm{DP}}{}^{\alpha_2} \, Z_{\mathrm{DR}}{}^{\beta_2}. \tag{2.20}$$

Gorgucci and Scarchilli (1997) suggest $c_2 = 51.0$, $\alpha_2 = 0.968$ and $\beta_2 = -0.462$, although this is unstable as Z_{DR} approaches 0 dB, with a return to the problem of negative Z_{DR} from section 2.4.4. A more desirable form uses linear Z_{DR} where the unphysical Z_{DR} values remain numerically stable:

$$R = c_3 \left(K_{\text{DP}} \right)^{\alpha_3} 10^{\,0.1\beta_3 \, Z_{\text{DR}}} \tag{2.21}$$

(Gorgucci and Scarchilli, 1997). They use $c_3 = 67.1$, $\alpha_3 = 0.954$ and $\beta_3 = -1.230$. Bringi and Chandrasekar (2001) suggest using $c_3 = 90.8$, $\alpha_3 = 0.93$ and $\beta_3 = -1.69$.

This method suffers hugely from the large amount of error. As both K_{DP} and Z_{DR} have significant errors as discussed in sections 2.4.3 and 2.5.3, the produced rain rates will have very large error, above that of the standard $Z - R$. Also, use of Z_{DR} means that the hail independence of K_{DP} is lost as hail reduces Z_{DR}. The increased error particularly means that gate-by-gate combination of Z_{DR} and K_{DP} parameter methods are unsuitable for operational radar algorithms.

2.5.5.2 RAIN FROM REFLECTIVITY, DIFFERENTIAL REFLECTIVITY AND SPECIFIC DIFFERENTIAL PHASE

Given that the normalised gamma distribution contains three variables (N_{w}, D_{o} and μ), it would appear that using the three radar parameters, Z, Z_{DR} and K_{DP}, a more accurate estimate of the rainfall rate could be obtained. However, the three radar parameters are not independent: with Z and Z_{DR} known, K_{DP} can be calculated.

2.6 POLARISATION METHODS: INTEGRAL TECHNIQUES

This chapter has shown that the three useful parameters (in terms of rainfall estimation as this thesis concerns) available from dual polarisation, Z, Z_{DR} and K_{DP}, are too inaccurate to improve operational rainfall rate resolution while maintaining good spatial resolution. However, integrated parameters may provide a valuable constraint for improvement on

the traditional $Z - R$ relations. These integrated techniques will be especially important in the operational polarisation radar environment, where the gate-by-gate noise will be high but the underlying signal will still be useful.

2.6.1 CALIBRATION OF REFLECTIVITY

Calibration of Z is of crucial importance if rainfall rate is to be derived from it. Traditionally the calibration is performed by comparison to rain gauges (or use of a signal generator and gauge adjustment), but this suffers from representivity problems comparing the large radar beam volume to the small area of the rain gauge as well as changes in the fall from beam to gauge. This means that calibration of Z is only as good as a factor of two. Many operational systems have a built in rain gauge comparison which is used to ensure good calibration. Goddard *et al.* (1994b) showed that K_{DP}/Z_H is nearly independent of μ and can be calculated from Z_{DR}. The technique uses individual Z and Z_{DR} along the ray to estimate K_{DP}. This allows prediction of the phase shift, ϕ_{DP}, along the ray. This is compared with the observed phase shift. The calibration of Z is then performed by adjusting Z until the predicted and observed phase shifts agree.

The technique does not have the high noise of K_{DP}, and if the technique is used on a ray, the phase shift before and after the heavy rain can be used for accurate estimation of the phase shift as data can be averaged (see figure 2.11). The technique can obtain 0.5 dB accuracy if a $10°$ phase shift can be recorded to $1°$. Rays with particularly noisy polarisation parameters can be removed and not considered. As we are considering high phase shifts of heavy rain, Z_{DR} is at 1 to 2 dB and the accuracy in Z_{DR} required is 0.4 dB, for a calibration of Z good to 0.5 dB, which can be achieved. This calibration method would be ideal for operational radar. The accurate calibration of Z will be essential for all methods likely to be implementable with the noise of an operational radar.

Concern has been expressed (Le Bouar *et al.*, 2001) that attenuation of Z and Z_{DR} will pose a problem. At X-band this would be a major problem, but at C-band, if the phase shift is not too high ($10°$), the attenuation of Z is under 0.5 dB, which is not large
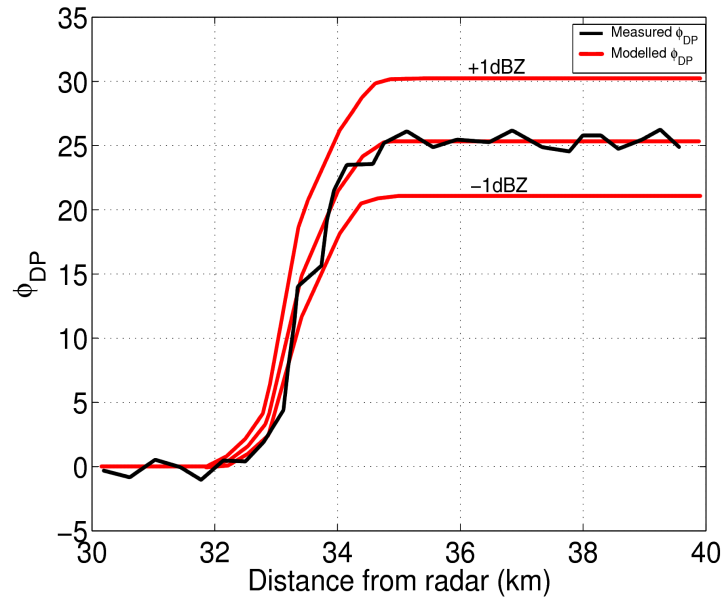
Figure 2.11   *Example of the calibration of Goddard* et al. *(1994b). The red lines show the predicted phase shift from Z and Z_{DR}. Different Z gives different phase trace predictions and comparison with observation fixes Z.*

enough to pose problems (Illingworth, 2004). Phase shifts above that level would suffer attenuation, so care must be taken at C-band to avoid these attenuated regions.

2.6.2   THE 'ZPHI' TECHNIQUE

The 'ZPHI' technique was described by Testud *et al.* (2000) and has shown good results (for example, Le Bouar *et al.*, 2001) at C-band in the heavy tropical rainfall of Darwin, Australia. The method uses the total phase shift, ϕ_{DP}, along a ray of observed Z as a constraint to fix the drop concentration, hence a, (2.1). The full technique uses phase shift to correct for attenuation, which can be significant at C-band where current operational dual polarisation radars in Europe operate, and shorter wavelengths (such as X-band).

This thesis will describe the ZPHI method only at non-attenuating wavelengths. It can be shown that, given naturally occuring raindrop size spectra are represented well by a normalised gamma function, the value of b should be 1.5 assuming that N_w is not a function of D_o. A log-log plot of K_{DP}/N_w against Z/N_w (with changing D_o) is close

to a straight line with little dependence on the shape parameter of the drop spectrum, μ. Hence suitably weighted integration of the drop spectra gives the expression

$$K_{\mathrm{DP}} = f N_{\mathrm{w}}^{1-g} Z^g, \tag{2.22}$$

where f and g are constants. Integration along the beam gives:

$$\phi_{DP} = f N_{\mathrm{w}}^{1-g} \int Z^g dr. \tag{2.23}$$

As the constants, f and g, are known, the phase shift ϕ_{DP} and the reflectivity along the ray can be used to calculate N_{w}, which fixes a in equation 2.1. The combination of this appropriate N_{w} and attenuation correction leads to the rainfall rate improvements reported by Le Bouar *et al.* (2001).

The method has the advantage of not using the noisy K_{DP} profile, therefore reducing the noise by integration, making it especially appropriate for the operational environment. The line of $K_{\mathrm{DP}}/N_{\mathrm{w}}$ against Z/N_{w} is not linear where Z/N_{w} is less than 1 (for a Marshall-Palmer $N_{\mathrm{w}} = 8000$ m^{-3} mm^{-1} this would be $Z = 39$ dBZ), although this is not a problem as it does not correspond to the heavy rain with large enough phase shifts for the technique.

The technique is particularly sensitive to the calibration of Z as an error in Z will translate to an error in N_{w} and hence a. Le Bouar *et al.* (2001) suggested that the climatological N_{w} could be used to calibrate Z.

Although the method shows great promise, it is only appropriate at very high rain rates. To estimate rainfall rates to 21% at C-Band, a phase shift above $32°$ is required. This is achieved by 10 km of 50 mm hr^{-1} or 75 km of 10 mm hr^{-1} rainfall, both unlikely to occur in the UK often. For 32% accuracy these can be divided by five as the phase shift required reduces to $6°$, so requiring 2 km of 50 mm hr^{-1} or 15 km of 10 mm hr^{-1} rainfall; more common, but rain above 10 mm/hr constitutes just 0.01% of the time and 19% of the accumulation. This means that the improvements from 'ZPHI' are only realised in areas of very heavy rainfall or very widespread moderate rainfall, neither of which are frequently observed in the UK environment. The constant N_{w} along the ray is also quite

restrictive and is likely to be unrealistic due to the large scale compared to the scale of variations in rainfall. The beam can be divided into 'sections', but each segment must have a phase change of at least $6°$, so the sections can only be small enough to alleviate this problem if the rain is widespread. The technique is also sensitive to hail, so hail recognition is needed or else it will lead to errors in the inferred N_w and hence a.

The 'ZPHI' technique is especially applicable to tropical regions, where heavy rainfall unaffected by hail is most common. Matrosov *et al.* (1999) shows scope to extend the technique to moderate rainfall rates at short wavelength X-band radar. The technique is excellent for use operationally for estimating heavy rainfall. This thesis will concentrate on the estimation of the moderate rainfall rates of 3 to 10 mm/hr which occur for just 0.67% of the time, but accounts for 36% of the accumulated rainfall at Chilbolton. The techniques are aimed to be appropriate for liquid rain where phase shifts are low (hence the attenuation of the radar beam is negligible).

CHAPTER 3:
THE NATURAL VARIABILITY IN REFLECTIVITY AND DIFFERENTIAL REFLECTIVITY

3.1 INTRODUCTION

This chapter will examine the variability that is seen in the observations of reflectivity, Z, and differential reflectivity, Z_{DR}. In section 2.4.3 Z_{DR} was shown to have an inherent noise from its sampling, which is quite large, especially for operational radars. This sampling noise is reduced by increasing the number of independent samples, dictated by the spectral width (normalised by the folding velocity). The optimal normalised spectral width for accurate Z_{DR} measurement is ≈ 0.09. This chapter initially examines the effects on radar measurements of the three drop size distribution parameters.

One of the advantages of dual polarisation radar, which led to its introduction to the operational environment, is the potential improved rainfall estimation offered. However, if this advantage is to be obtained, one must allow for the noise in the observed data. If the radar parameters are to be utilised for moderate rainfall rates, the Z_{DR} data available must be accurate to within 0.1 dB. This would require careful calibration, which may not be a trivial task. This will be considered within this chapter. The "true" nature of the rainfall is found within the sampling noise. This chapter will show how it may be possible for moderate rainfall rates to find the signal from within the noise and to estimate the drop size distribution and therefore reduce the inaccuracies in rainfall rate estimation. This chapter examines the patterns of Z and Z_{DR} expected, and discusses how one may reduce the noise in the data and examines the information that is available despite the

noisy measurement.

3.2 DROP SIZE SPECTRUM EFFECTS ON Z AND Z_{DR}

In this section the effect of adjusting the three parameters of the normalised gamma distribution of rain drops described in section 1.3 will be described. Recall that the three variables are the drop concentration, N_{w}, the median drop diameter, D_{o} and the shape parameter μ. Each of these parameters will affect the position of a point in Z/Z_{DR} space.

3.2.1 EFFECT OF DROP CONCENTRATION

The drop concentration term is the most straightforward to describe and explain the effect on Z and Z_{DR}. Increasing N_{w} merely means that there are more drops present, but their relative sizes remain the same. This means that reflectivity measured at both horizontal and vertical polarisations is increased with the drop concentration. Since Z_H and Z_V are both scaled with N_{w} the ratio of them remains constant, hence the Z_{DR} remains constant. Section 1.3 stated that N_{w} varies over a large range, 96% of recorded values lying within a factor of 13, and this variation will transfer to reflectivity resulting in a variation of 11.1 dBZ.

In summary, an increase in N_{w} raises Z, but has no effect on Z_{DR}.

3.2.2 EFFECT OF MEDIAN DROP DIAMETER

As the target drops increase in size, the reflectivity increases by D^6. The same factor applies to the reflectivity at both polarisations, although rain drop shapes mean that as the drop grows, it becomes more oblate, increasing the difference between the horizontal and vertical drop sizes that are used in D^6. This difference means that Z_{DR} increases with the median drop diameter, approximately weighted by the seventh moment.

In summary, an increase in D_{o} increases both Z and Z_{DR}.

3.2.3 EFFECT OF THE SHAPE PARAMETER

The effect of μ is more difficult to examine. Higher values of μ mean a less diverse spectrum of drop sizes. The effect is plotted in figure 3.1. It can be seen that the change appears to be solely vertical. However this is because of the slope of the plot; in fact the move is diagonal. Given the N_{w} of 8000 mm^{-1} m^{-3} and D_{o} remaining the same, the μ
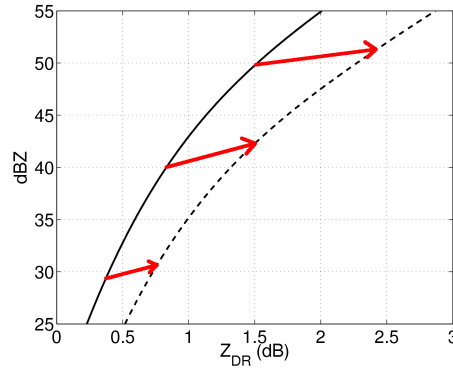
Figure 3.1 *dBZ and Z_{DR} expected for rain of constant N_{w} of 8000 mm^{-1} m^{-3}, and constant μ. The solid line shows the plot if $\mu = 0$, the dashed line is for $\mu = 5$. The red arrows show the true movement that is occuring if there is no change other than μ.*

effect is as follows: the reflectivity if '$\mu = 0$' is slightly higher than if '$\mu = 5$' because of the effect of the higher weighted tail of large drops (the large drops have a large effect from the D^6 relation for reflectivity). The Z_{DR} is also larger from lower μ as the large drop tail is more influential on differential reflectivity as it has an approximate seventh moment dependence on drop size. Consider the example where N_{w} is 8000 mm^{-1} m^{-3}: with $\mu = 0$, when Z is 40 dBZ, Z_{DR} is 0.8 dB. When $\mu = 5$ with the same other spectrum parameters, these values become 42 dBZ and 1.5 dB.

This will be relevant when estimating drop size distribution parameters using Z and Z_{DR}. When estimating N_{w} from Z and Z_{DR}, a value of μ must be assumed, but changes in the assumed μ will have an effect very similar to changing N_{w}. This problem is demonstrated in figure 3.2. However, to estimate rainfall, this consideration of μ is less serious than it would appear. The effect of μ upon rainfall rate is reversed, almost cancelling out the error induced. From the example above, the rainfall rates from the DSDs differ by
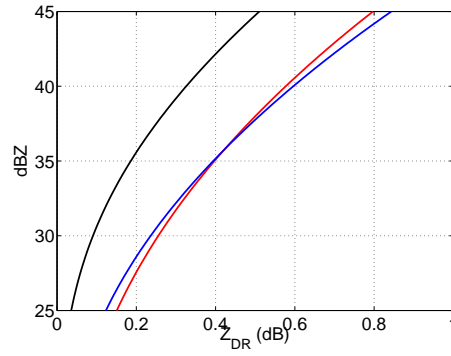
Figure 3.2 *Plot demonstrating the problem in distinguishing between a change in μ and a change in N_{w}. The black line shows the case when N_{w} is 8000 mm^{-1} m^{-3} with $\mu = 5$. If one now alters this so that $\mu = 0$, the red line is obtained (higher Z_{DR} is found as a result of the greater presence of large drops). However, this line is very similar to the blue line, which is the line where N_{w} is 1600 mm^{-1} m^{-3} with $\mu = 5$. Given the noise levels in even the very accurate CAMRa data, the red and blue lines will be indistinguishable.*

just 6%. This means that although one will suffer from μ variation if estimating N_{w}, but not if one simply wishes to derive rainfall, using N_{w} as a route to that end. This will be seen again later in the thesis.

3.3 Z_{DR} OFFSET AND CALIBRATION

Any methods to derive rainfall properties from differential reflectivity measurements will require Z_{DR} to be accurately calibrated. Erroneous calibration of Z_{DR} will be evident as an offset in values of recorded Z_{DR}. For the purposes of this thesis, where moderate rainfall rates are being examined, Z_{DR} is required to an accuracy of 0.1 dB (see section 2.4.2).

To calculate the offset in the Z_{DR} data (to enable correction) comparison must be made between the observed Z_{DR} in a portion of data where the expected value is known and well defined; generally this means where the value of Z_{DR} is expected to be 0 dB. This will mean viewing particles that will have a invariant (to a good approximation) circular shape when viewed from the radar. Three options will be considered.

Viewing the sun This option happens with operational radars "accidentally", after sunrise and before sunset. The radar will view the sun at low elevations and should see the sun's radiation as unpolarised returns; being unpolarised, the Z_{DR} should be 0 dB. The problem is that viewing the sun considers only the received channel of the radar, but does not consider transmission, where calibration may also be a problem if the transmitted power at each polarisation is not equal. Viewing the sun is sometimes used for calibrating the positioning of radars, Collier (2001).

Vertical Dwells When viewing vertically the radar sees only the undersides of the hydrometeors, which will show no preferential alignment unless in the presence of a strong electrostatic field. An example of data from a vertical dwell is shown in figure 3.3. This means that, on the average of a large number of targets, they will have an apparent circular shape. When viewing vertically, sidelobes become a problem, as the ground clutter returns from the sidelobes may be quite high and need careful removal. The ideal conditions for a vertical dwell are a layer of thick high level cirrus cloud. Here the signal in Z will be strong enough to allow use of L_{DR} (L_{DR} is the linear depolarisation ratio, it is defined as the ratio of vertically polarised return and horizontally polarised return from a horizontally polarised transmitted beam, this is useful as when the ground is the target the returned echo is depolarised so L_{DR} is high) for distinguishing clutter. The background noise is a returned factor in both horizontal and vertical channels, so if Z is small, the background noise in the opposite channel will be a significant percentage, hence L_{DR} will be high. The return will be a reasonable distance from the radar (~ 10 km), limiting potential near field problems. (When in the near field radar the illumination of the radar dish is not complete. In the near field, the Z recorded is lower than "true" values. Near field correction can be applied, as discussed at W-band and Ka-band by Sekelsky, 2001. Although differential reflectivity should be unaffected, any illumination pattern differences between the horizontally and vertically polarised beams may introduce an error in Z_{DR}.)

Light rain In light rain or drizzle the hydrometeors are small. Small drops are spherical
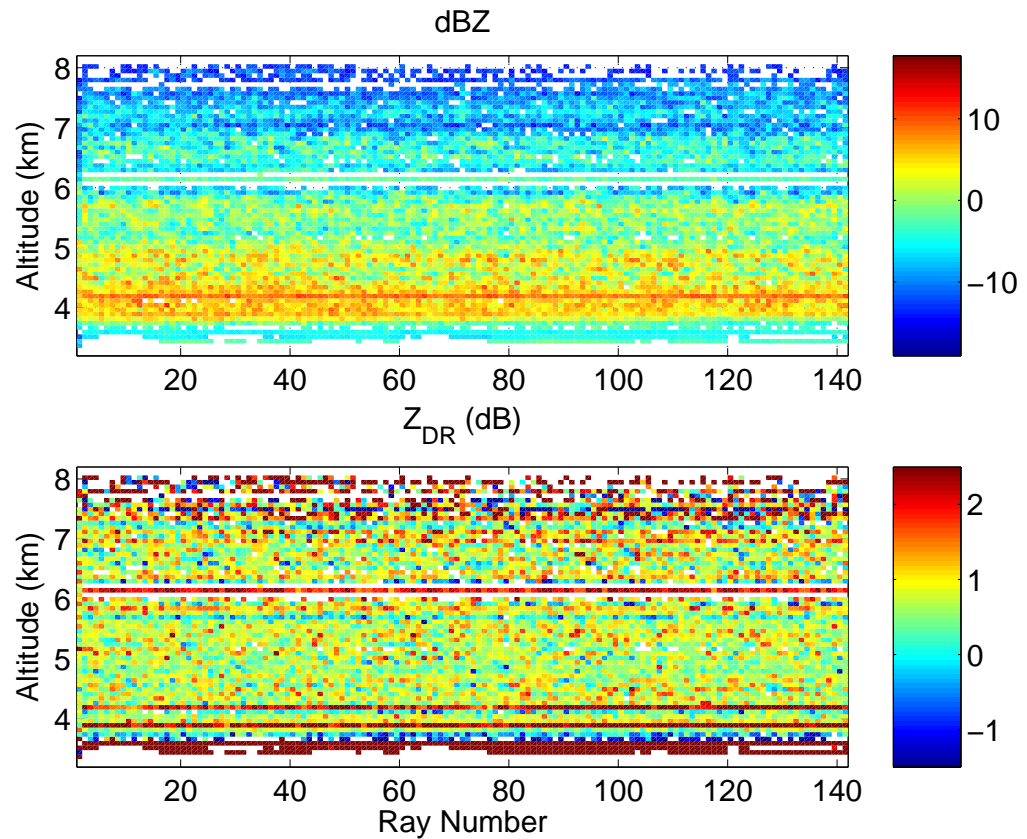
Figure 3.3 *dBZ and Z_{DR} data from a (30s) dwell with the CAMRa radar pointing vertically. This data was taken on 04 March 2004, in the presence of a cirrus cloud.*

(section 2.3) so appear circular at all angles when viewed by the radar. However, for calibration, the rain to be examined must be clearly defined as being all small drops. Low reflectivities but high differential reflectivities are possible when a very low concentration of large drops are present. This occurs in the early stages convective rain.

Each of these options have both advantages and disadvantages.

Viewing the sun does not require special time in the scan routine as it will occur twice a day operationally. This would seem an excellent possibility but confirming only the receive (not transmit power) will not be a thorough calibration, so will not have the prerequisite accuracy. Calibrating the receive channel may have other uses, although

viewing the sun is not suitable for Z_{DR} calibration.

Vertical dwells will give a good calibration. The conditions where the hydrometeors align are quite unusual and easily recognised so the calibration using the vertical dwells will be good in terms of reliability. However, performing a vertical dwell requires time in a scan strategy and in an operational system, time within the strategy is at a premium. A vertical dwell requires not just the time to perform the dwell, but also the time to move the dish to point vertically and then return to its near horizontal position. A further possible problem occurs where the radar antenna may warp under the stress caused by the weight, as the metal of the antenna is very heavy (the Chilbolton 25 m dish weighs 400 tonnes). The warping may change the shape of the antenna slightly so it does not have the correct curvature in all pointing directions. The stresses will be rather different in vertically and horizontally pointing positions so these are where the largest effect of warping would be expected. The effect of the dish warping is likely to be small, but the largest change would likely be vertical to horizontal so calibrating at vertical for horizontal use may have small error, but with a well designed antenna this error should be negligible.

Using **light rain** for Z_{DR} calibration will be considered next. Light rain will be seen by the radar regularly, and will be easy to detect. Using light rain for Z_{DR} calibration will not require additional scans in a scan strategy, a plus point in an operational system. However, to use light rain for calibration one must be sure the rain is formed by small drizzle drops, not just low concentrations of larger drops. Differentiating between few large drops and a large number of small drops before calibration of Z_{DR} may be non-trivial. Even at low reflectivities of 0-10 dBZ the Z_{DR} will be non-zero, predicted for Marshall-Palmer rain ($Z_{DR} = 0.005$ dB). With a gamma distribution with shape parameter $\mu = 5$ this value is 0.001 dB (note that these are well below the accuracy we require).

Once one has found data known to have average Z_{DR} of 0 dB, examination of the data will show a spread in Z_{DR} as expected from the sampling, as described in section 2.4.3. However, the average of the data will be zero. To calculate the offset one simply must find the average Z_{DR}. However, saying "simply" find the average Z_{DR} is ignoring
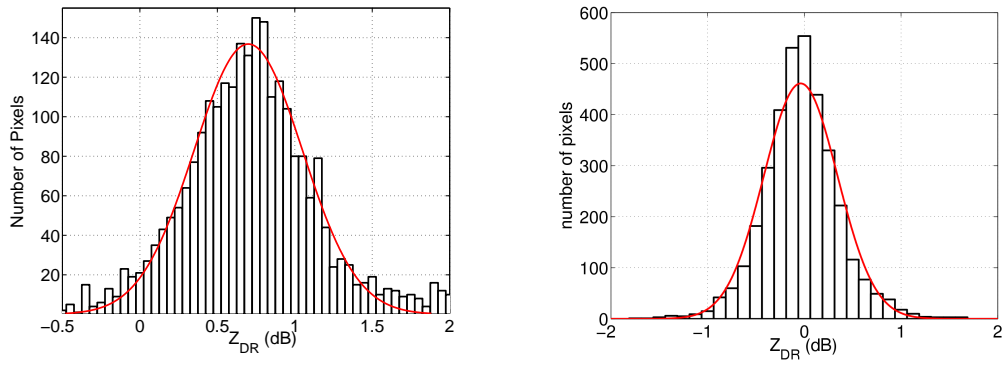
Figure 3.4 *Histograms of Z_{DR} data. [Left] Data from figure 3.3. Overlayed is a Gaussian distribution with same total, mean (0.70 dB) and standard deviation (0.35 dB). [Right] Data taken from a similar case (with larger bin widths). Overlaid is a Gaussian distribution with same total, mean (-0.04 dB) and standard deviation (0.38 dB).*

a possible problem. Figure 3.4 shows histograms of Z_{DR} data from vertical dwells. To be entered into these histograms the point must have at least 0 dB reflectivity, L_{DR} less than -10 dB and appropriate altitude (for the left panel this is between 4 km and 7 km). These criteria remove clutter and data where signal to noise ratio will make the data unreliable. The histogram shows that there is more data in the tails of the distribution, which shows the data is not quite normally distributed. This non-normality is shown by the difference between mean ([left] 0.70 dB, [right] -0.04 dB) and median ([left] 0.66 dB, [right] -0.00 dB). The difference between these is small however (0.04 dB in both examples), so not a problem for calibration when using vertically pointing dwells is (recall that 0.1 dB accuracy is required). So despite the slight non-normality of the distribution, calibration is well within the 0.1 dB tolerance and is the best option for calibrating Z_{DR}.

When considering the option of examining the Z_{DR} values of light rainfall, the histogram is more likely to be skewed than for the vertical dwell. Because of drop size spectrum changes, larger oblate drops may become abundant, a result of extreme spectra, but there is no spectrum option to give a reverse of this as prolate drops are unphysical. Figure 3.5 shows an example of Z_{DR} from light rain (defined as having $0 < dBZ < 10$). In this case the distribution is near normal, with very little skew. However, this example
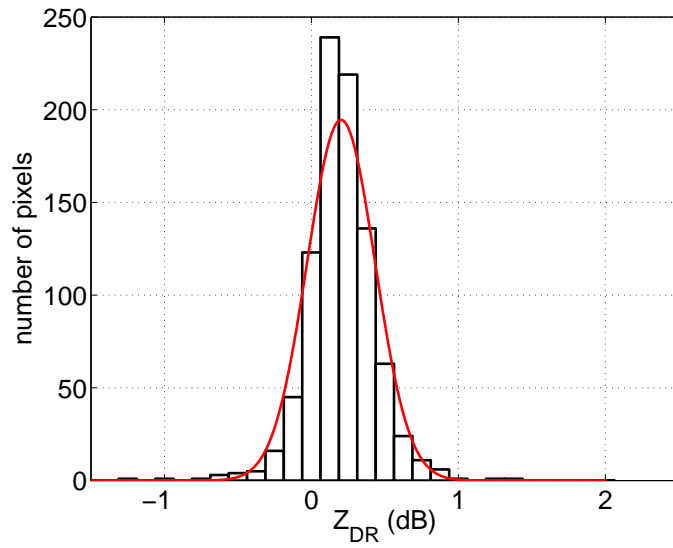
Figure 3.5 *Histogram of Z_{DR} data from light rain ($0 < dBZ < 10$). Overlaid is a Gaussian distribution with same total, mean (0.2021 dB) and standard deviation (0.2307 dB).*

has a small number of points that are a long way from the peak (± 5 dB), which have a large effect on the mean and standard deviation despite the small numbers because of the large variations they represent. To remove the effect of these points all data not within 3 standard deviations of the mean are removed before calculating the mean for calibration. The cause of the extreme points is likely to be small amounts of ground clutter, which can have a large effect on Z_{DR} yet little effect on L_{DR}. This example shows that the data is offset by 0.20 dB, which should be corrected before use in rainfall estimation algorithms.

In conclusion, the Z_{DR} calibration is vitally important when using Z_{DR} for estimating rainfall rates. Its calibration is performed by checking its value where it is known it should be zero. The recommended method for this is to use vertical dwells with the radar, with checks for consistency in light rain when scanning horizontally. Although vertical dwells are a problem in terms of time involved in a scan strategy the calibration will not drift rapidly so the scans will not be required to repeat frequently and given the importance of calibration time should be allowed.

3.4 Z VARIATION

The accuracy of reflectivity is dependent on the number of independent pulses available. Each pulse measures the reflectivity, but the random positioning of individual drops means that the scattered waves interfere (both constructively and destructively). However the random movements of rain drops and other scatterers rearrange the interference pattern, so if a number of pulses are averaged, the reflectivity estimate is improved. So the more individual pulses are used for measurement, the better the measurement, although this comes at the expense of scanning speed. The time spent pulsing per ray is known as the dwell time. From dwell time and pulse repetition frequency (PRF) the number of pulse pairs can be easily found. The Chilbolton CAMRa radar uses 64 pulse pairs (a pulse pair is a single horizontally polarised transmitted pulse, followed by a vertically polarised pulse), but as the standard, four range gates are further averaged to improve the estimate. An operational radar will be able to measure reflectivity to an accuracy of 1 dB, with random normally distributed sampling noise around the "true" value, using the calibration technique of Goddard *et al.* (1994b) described in section 2.6.1. This level of accuracy is acceptable for attempting to estimate rainfall rates to within 25%.

3.5 Z_{DR} VARIATION AND THE EFFECTS IT CREATES

Measured Z_{DR} data shows a spread of values. This spread is a result of the combination of two spreading effects: random errors from the sampling (described in section 2.4.3) and the natural variability of the rainfall adjusting drop spectra. An increase in mean drop size, generally, will increase Z_{DR} (generally is used here because if it happens that D_{o} increases a little while μ also increases, the lack of larger drops from the μ effect actually decrease Z_{DR}). These two effects will be constantly present. However it is possible to limit the effect of the spread caused by natural variability by examining data from very small areas (where natural rain changes will be small) or considering low reflectivity where drops are all small so the natural variations have little effect on Z_{DR} despite large drop spectrum changes. Using low reflectivity areas to ensure natural variations are small

may not be perfect: in convective rain it is possible to have a very small number of large drops, which individually have high reflectivity, but with so few, the integrated result over the radar is a rather small average.
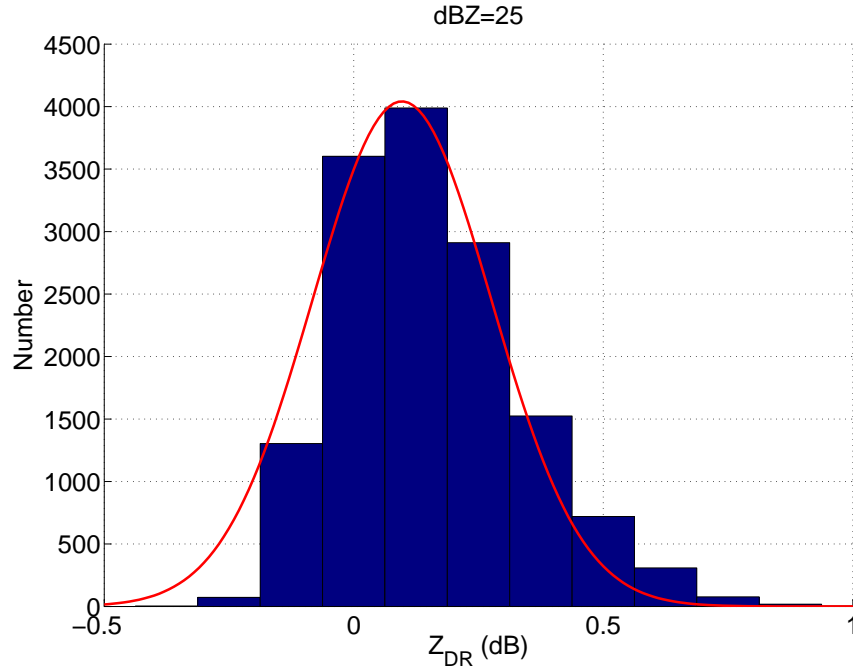
Figure 3.6 *Histogram showing the distribution of Z_{DR} data from 18/08/2000. This data is for all data points passing and L_{DR} threshold of -20 dB with ranges between 15 and 60 km and $24 - 26$ dBZ. Also shown is a normal distribution with the same mean, standard deviation and total as the data for comparison.*

Figure 3.6 shows a histogram of Z_{DR} data from a large area of data (so DSD variations will be large), but only where a 2 dB band of reflectivity is considered. The small band so that Z_{DR} variations as expected from rain of constant N_w are small. The data is also chosen to be within light rain so that nearly all drops are spherical, hence natural drop spectrum changes have little effect on the drop shapes. The plot has a normal distribution of the same mean (0.10 dB), standard deviation (0.19 dB) and integral total points overlaid for comparison. The distribution can be seen to follow a normal distribution well within two standard deviations, but with a higher weighted positive tail compensated by less well represented negative tail. Since this data is showing predominantly the distribution caused by a sampling problem, with little natural variation, averaging over four data points would be assumed to halve this spread ($\frac{1}{\sqrt{4}} = \frac{1}{2}$). However, averaging does not

have the expected effect on standard deviation of the distribution. By averaging points from alternate gates and rays and then repeating the histogram of figure 3.6, this leads to a distribution with mean of 0.11 dB and standard deviation of 0.16 dB (reduced by just 16%). The reason for this is that the averaging mixes in data from other reflectivity bands (where Z_{DR} would be expected to be different) rebroadening the distribution of Z_{DR}, disguising the effect of the averaging.

Now this will be considered for a very small area of 16 points of data. The sixteen points are considered as 4 boxes, each containing four data points of Z and Z_{DR} data (see figure 3.7). For each box the mean Z_{DR} ($\overline{Z_{\mathrm{DR}}}$) and standard deviation of Z_{DR} ($\sigma_{Z_{\mathrm{DR}}}$) are calculated. With only four points, the variations in these values will be quite large, although from these one can calculate the standard deviation of Z_{DR} at grid scale level by

$$\sigma_{grid} = \frac{\left(\sigma_{Z_{\mathrm{DR}}}^{ABEF} + \sigma_{Z_{\mathrm{DR}}}^{CDGH} + \sigma_{Z_{\mathrm{DR}}}^{IJMN} + \sigma_{Z_{\mathrm{DR}}}^{KLOP}\right)}{4}. \tag{3.1}$$

The noise of the data when 4 points are averaged is given by

$$\sigma_{4pts} = \mathrm{std}\left(\overline{Z_{\mathrm{DR}}^{ABEF}} + \overline{Z_{\mathrm{DR}}^{CDGH}} + \overline{Z_{\mathrm{DR}}^{IJMN}} + \overline{Z_{\mathrm{DR}}^{KLOP}}\right). \tag{3.2}$$

In these equations superscripts are used to define the grid boxes (from the left of figure 3.7) used to calculate that average or standard deviation, not powers. This procedure is
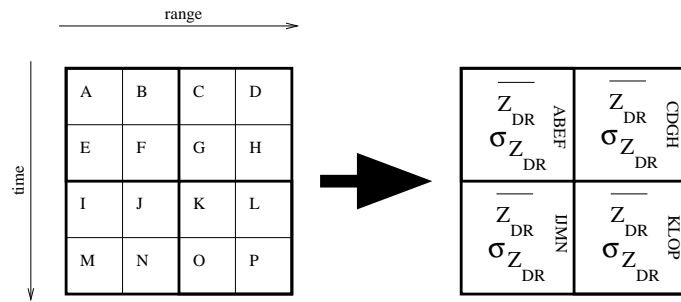
Figure 3.7 *Schematic to demonstrate how the effect of averaging Z_{DR} points can be examined.*

repeated over a large number of positions for a dwell. When the radar is pointed and measurement is performed with the radar static in this position, this results in a time

series of data. This gives the result of Z_{DR} dropping by 48%, near the 50% the statistics would expect (the value of 48% is derived from 207 sets of sixteen points).

For averaging 4 points there are three sensible possibilities: averaging two points in range and two in time as in figure 3.7, averaging four points in range to have 4 boxes (ABCD, EFGH, IJKL and MNOP) or four boxes in time (AEIM, BFJN, CGKO and DHLP). These yield a 53% drop and a 40% drop in Z_{DR} spread respectively.

The reason for the halving occurring with this method of comparison is that Z_{DR} is averaged and spread considered only from the local points (the values of Z are never seen). Mixing of Z changes are part of the 16 point method, but sorting by Z does not occur, and the Z has no impact on the spread calculation.

The natural variability of rainfall means that the variations in recorded Z_{DR} increase as the reflectivity increases because the large (and hence larger and therefore oblate) drops become increasingly important. This can be seen in figure 3.8. This plot shows that the Z_{DR} generally increases (with Z) as expected for rain of constant N_{w}, shown by the red lines. The spread shows variation in N_{w} is larger at lower reflectivities. However this is a result of smaller changes in Z_{DR}, at a fixed reflectivity, from variations in N_{w}. Generally the number of points in each histogram decreases with increasing reflectivity for this rain event.

3.5.1   EFFECT OF Z_{DR} SPREAD ON DERIVED RAINFALL RATES

The spread in Z_{DR} will obviously have an impact on the rainfall rates derived using point measurements of Z_{DR}. This effect can be easily seen in figure 3.9: changes horizontally on this plot adjust the rainfall rate.

The previous chapter demonstrated that Chilbolton data had a Z_{DR} spread with standard deviation of ~ 0.2 dB. This shows again the problem of negative Z_{DR} (discussed in section 2.4.4) when Z (and hence Z_{DR}) are low. Negative Z_{DR} is less common at increased reflectivities as can be seen in figure 3.8, so incalculable rainfall rates become less common in heavier rain. Along with negative Z_{DR} are very low values of Z_{DR} where
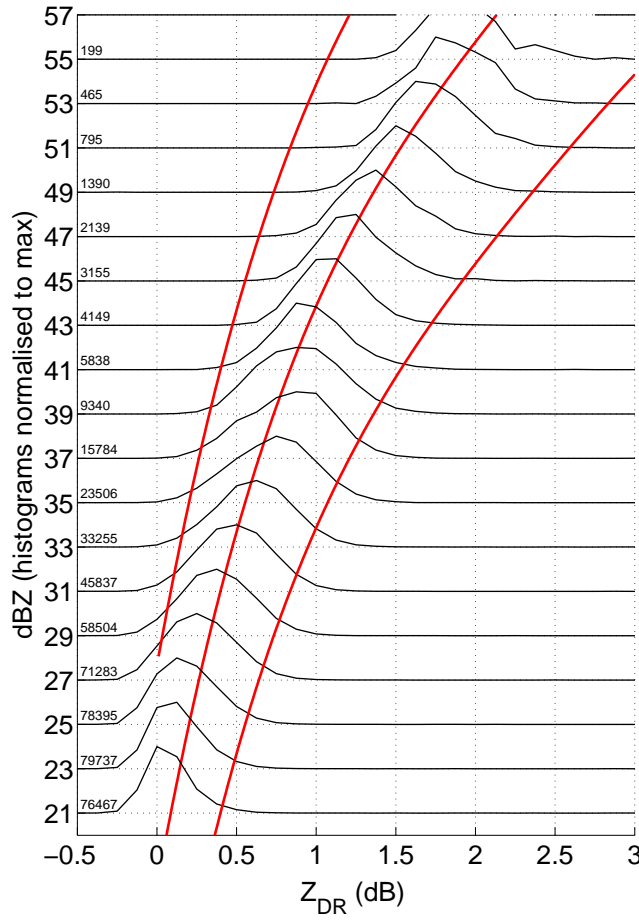
Figure 3.8 *Plot showing the distribution of Z_{DR} data from six PPI scans over 2.5 hours on 18/08/2000. This data is for all data points passing an L_{DR} threshold of -20 dB with ranges between 15 and 60 km. The data is selected by reflectivity; a histogram is made for each division. The histograms are then normalised to have the same peak values. These normalised histograms are then plotted together in order, so each black curve is the normalised Z_{DR} histogram at the Z-band shown on the Y-axis. The number to the left, above each line is the number of pixels which were used to make that histogram. Overlaid are three red curves which show the curves predicted by rain of constant N_w of 80 000, 8 000 and 800.*

very small changes in Z_{DR} imply large changes in rainfall rates, which can be seen by the colour gradient horizontally in the lower-left corner of figure 3.9.

Now consider the data that one would expect to be recorded. Figure 3.10 shows typical data expected for an area where $N_w = 1700$ m^{-3} mm^{-1}. The blue crosses show simulated data with a Z_{DR} error of 0.2 dB, with red crosses where that noise is 0.5 dB. This plot really shows the problem that the error causes when calculating rainfall rates. First consider the smaller error. The 0.2 dB error is similar to the data from the Chilbolton radar, which is a very accurate research radar. Also plotted on the figure are the lines where the drop concentration is different by a factor of four ($N_w = 6770$ m^{-3} mm^{-1} and $N_w = 425$ m^{-3} mm^{-1}). These lines are similarly spread to the blue crosses of the simulated observations, so the Z_{DR} variations adjust the rainfall rates calculated gate-by-gate by a factor of 2.5. This is a very large error, showing that even with an extremely
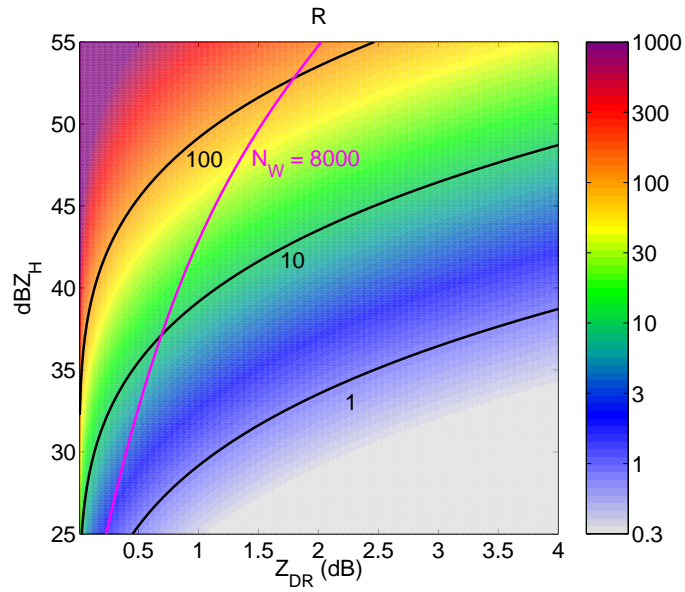
Figure 3.9   *Theoretical plot of Z_{DR} against Z. Colours show rainfall rate (on a logarithmic scale) calculated by the method of Illingworth and Blackman (2002). Note that the colour scale has been set to saturate at 0.3 mm/hr and 1000 mm/hr; these are not limits. Also plotted are black lines of constant rainfall rate, labelled in mm/hr and a magenta line of $N_w = 8000$. This plot does not cover negative unphysical values of Z_{DR}.*

accurate research radar gate-to-gate Z and Z_{DR} will actually worsen the errors in rainfall rates at these reflectivities/rain rates. However, it is clear from the figure that the crosses do show a common line: they average to the solid black line as shown, so if this line can be estimated, much more accurate rates can be achieved. The 0.5 dB noise points (in red) show data that would be typical for the same region, but for a good operational radar. Here, data shows large variations, and negative Z_{DR} occurs even above 35 dBZ. This spread would result in as much as a factor of 10 error in rainfall rate, although even to the eye the average of the data is clearly near to the solid black line. If this could be estimated, much improved rain rates would be available.

Previously it was shown that by averaging the data the errors in Z_{DR} can be markedly reduced. However, averaging reduces the resolution, so loses much of the power of using radar. Another minor point to consider is that averaging of Z and Z_{DR} does not average the N_w (due to the curvature of lines when remaining constant). The large errors
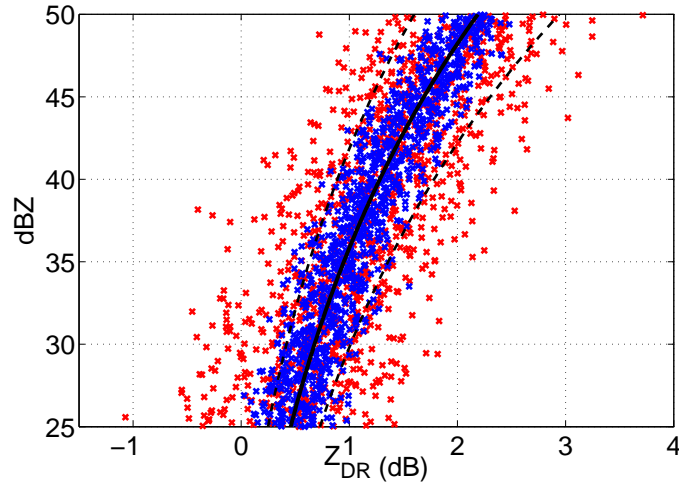
Figure 3.10 *A plot showing the expected Z_{DR} spread. The solid line shows the position of Z and Z_{DR} given $N_{\mathrm{w}} = 1700~m^{-3}~mm^{-1}$. The blue crosses show typical data give this distribution, with a standard deviation of 0.2 dB in Z_{DR} from the $N_{\mathrm{w}} = 1700~m^{-3}~mm^{-1}$ line. Red crosses show the same except with higher 0.5 dB noise. The two dashed lines show the position of $N_{\mathrm{w}} = 6770~m^{-3}~mm^{-1}$ and $N_{\mathrm{w}} = 425~m^{-3}~mm^{-1}$.*

in rainfall rates acutely show the need for integrated techniques for rainfall calculation if simple $Z-R$ relation techniques are to be improved upon, especially for operational radar systems, so as to maintain the high resolution available, but with the extra information made available by the new polarisation parameters.

3.6   SUMMARY

This chapter has examined the variability of radar data in reflectivity and differential reflectivity. The data of both shows variations from two separate sources, sampling noise and natural variability of rainfall (in the drop size distribution).

The response of Z and Z_{DR} to changing each of the three parameters of the normalised gamma distribution of rain drops was examined. N_{w} was shown to scale with Z, but because Z_{DR} is a ratio of reflectivities, it has no alteration from N_{w}. Changes in the median drop diameter increase both Z and Z_{DR}, from the sixth and seventh moments of

size. The effect of μ is based on the amount of large drops present within the distribution. Lowering μ slightly increases reflectivity, but has a larger effect on Z_{DR}, in which the large drops have a greater effect. The μ change has a similar effect when viewing lines in Z/Z_{DR} space to that of changing N_w, so any detected change in N_w may in fact be the result of μ. Fortunately, the rainfall rate is similarly affected so the erroneously estimated N_w would still yield a good rain rate estimate.

If one is to use Z_{DR} data for rainfall estimation it needs to be precisely calibrated. Three options for calibration of Z_{DR} have been discussed, and conclude that vertical dwells are the best method, checked with light rain in near horizontal scans to ensure warping of the antenna is small.

When removing the noise in data one must be cautious. Selecting data by reflectivity and performing statistics on the Z_{DR} does not yield the expected results of averaging. The changes in Z_{DR} that occur hand in hand with changes in Z increase the spread in values, apparently reducing the effect of averaging. It was shown with use of boxes of sixteen pixels that the averaging of data does improve the accuracy of Z_{DR} as expected (critically this is at the expense of resolution which may not be desirable). Averaging four points reduces the standard deviation in Z_{DR} by 48%; close to the expected 50%.

The effect of the noise in Z_{DR} when measuring rainfall rates is examined, showing that an operational radar would be so prone to the noise in Z_{DR} that point by point methods utilising it will suffer greater noise (possibly as much as a factor of ten) than a simple $Z - R$ relation.

CHAPTER 4:
RAIN STATISTICS

4.1   INTRODUCTION

To demonstrate the effectiveness of any rainfall measuring technique, it must have its outputs compared with a ground truth. Traditionally one uses rain-gauge measurement to compare against our radar derived rainfall accumulations (e.g. Brandes *et al.*, 2001), especially using hourly accumulations (e.g. Collier, 1986 and Ryzhkov *et al.*, 2005b). In this chapter, the effect of the frequency of measurements will be examined using a drop counting rain-gauge. A harsher test would be to compare the rainfall rates measured by both gauge and radar, as accumulations have the effect of averaging out variations in rate. The longer the accumulation considered, the greater the averaging (an example of assessment from averaging is Harrold *et al.*, 1974).

Variations in rainfall rates at a location (which goes hand-in-hand with spatial rainfall distribution) have far wider use than simply for radar comparison. Rainfall statistics are important for a wide range of engineering applications, for hydrological applications, predictions of river flow, erosion and design of urban drainage. Statistics of rain are also important to the telecommunications industry, who have concerns about the fade statistics of microwave communication links.

Rainfall has a chaotic nature, with large fluctuations on small spatial and temporal scales. This means that if one only measures the rainfall rate at sparse intervals the accumulation may not match the "truth". See figure 4.1, which shows the rainfall accumulations at a 30 s time resolution, and the accumulations measured when one measures for 30 s only once every 15, 5 and 2.5 minutes. The total accumulations which result from these four time series are also seen to be different.

The effect of frequency of measurement is especially important for radar meteorology.
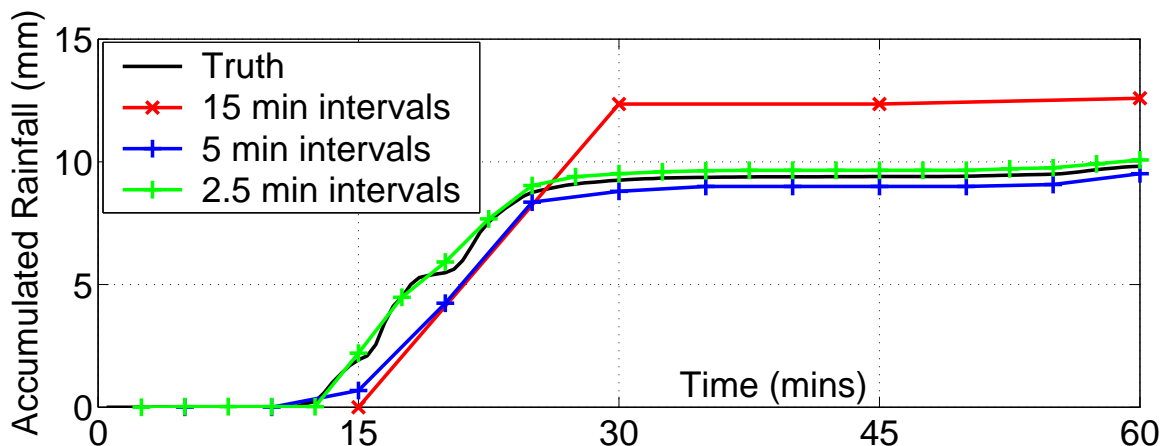
Figure 4.1   *A plot showing the rainfall accumulations over an hour. The black line shows the "Truth" from the drop counting gauge (30 s time resolution); the coloured lines indicate the accumulation from taking a 30 s snapshot only every 15, 5 or 2.5 minutes. The snapshots are taken from the middle time between crosses.*

It is common to compare radar rainfall estimates with rain-gauge measurements using accumulations, but the return period for the radar measurements will significantly affect the accumulation calculated. The very nature of rainfall means that rain-rates are rarely consistent for more than a few minutes, often with large peaks and troughs. This means that if one measures the instantaneous rainfall rate during the peak, the accumulated rainfall will be much larger than the truth. However, if the measurement occurs during a trough in the rainfall rate the accumulation will appear smaller than the truth. Figure 4.1 shows examples of both cases. For the 15 minute repeats an above average rate is measured and therefore the accumulation is overestimated. The 5 minute repeats initially underestimate, but "catch up" much of the difference by overestimating the end of the main shower. To demonstrate the effect numerically see table 4.1. Here the effect of sampling at only half the times are seen, and then just a quarter. Both cases result in an underestimation.

Rates																				Accumulation
0	1	1	2	2	3	5	9	6	4	4	3	3	2	2	2	4	7	3	1	**64**
0		2		4		10		12		8		6		4		8		2		**56**
		4				20				16				8				4		**52**

Table 4.1 *A numerical demonstration of the effect of different sampling frequencies. In this case the less sampled sets show smaller accumulations.*

4.2   INSTRUMENT: DROP COUNTING RAIN-GAUGE

For this work a rapid response drop counting rain-gauge (Norbury and White, 1971) will be used, located at Chilbolton. This instrument collects rainfall and counts water droplets of known volume falling from the reservoir. The gauge has a 150 cm^2 collecting area and a time resolution of 30 s, giving a quantisation of 0.48 mm/hr as each drop corresponds to 0.004 ± 0.0004 mm of rainfall. The quantisation of the data will affect the results when considering very low rainfall rates. The data used was from 1st May 1999 to 31st March 2005, with a total of 61 months of data available ($39,936$ hours), covering all seasons. This data set includes $7,990$ rain events (defining separate events to have five minutes of zero accumulation between them) with a mean duration of 24 minutes and accumulation per storm averaging 0.47 mm.

4.3   PDFs OF RAINFALL RATES

Of the $4,792,320$ rain rates in the data set, 95% have no rain. The data is plotted in figure 4.2 to show the rainfall occurrence. This figure shows to the lower right the noise resulting from the low number of events of very high rainfall rates causing Poisson noise. Rainfall rates of above ≈ 5 mm/hr show an exponential distribution, although there is a more curved pattern below this rate.

Alternatively this can be shown as the probability of a rainfall rate above a value, shown in figure 4.3. This demonstrates that moderate or heavy rainfall (> 3 mm/hr) is measured 1% of the time. Also shown on this plot are curves supplied by Goddard (per-
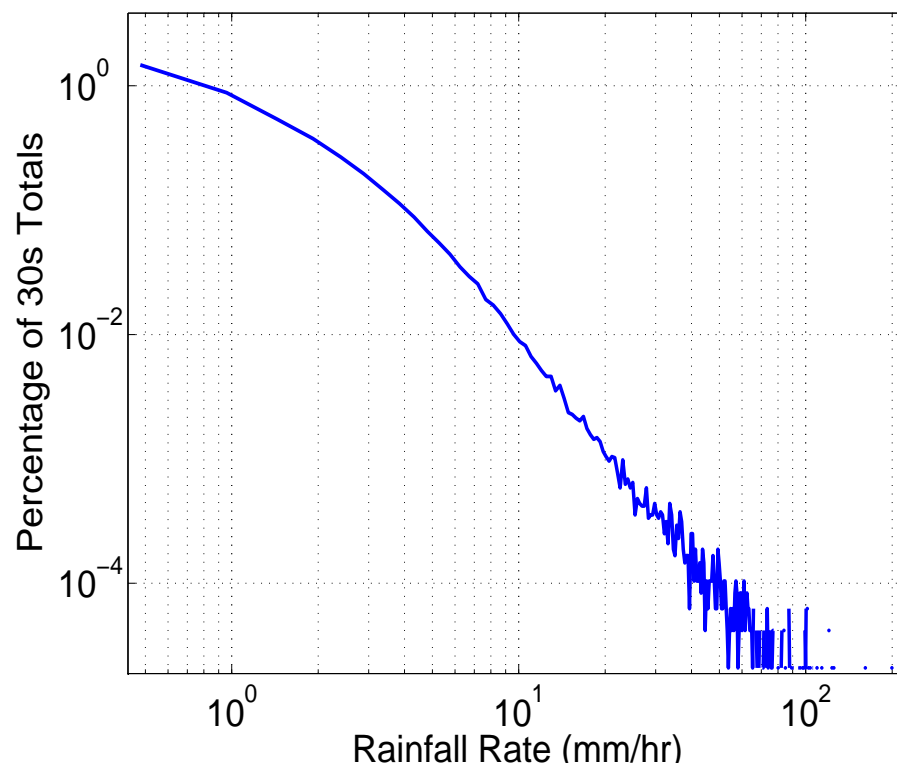
Figure 4.2 *Plot showing the frequency of rainfall rates. The noise occurs to the lower right as a result of the very few events with the highest rainfall rates. The curvature (suggesting less low rates than a linear model would suggest) initially may be a result of a gauge sampling effect, although it will shortly be seen that this is is not instrumental.*

sonal contact, 2006). These show similar statistics for a rain gauge located in Sparsholt (located 7.5 km South-East of Chilbolton), rates derived from Chilbolton radar and suggested from the ITU-R (International Telecommunication Union - Radiocommunication Sector) model. It happens that Chilbolton lies on the border of two zones (climate E and climate F, which describe climate types) of the ITU-model so both are shown on this plot. These plots also show the curvature for low rates (implying that low rates are less likely than they would be if a linear model were used). This indicates that the curvature is a physical effect and not the result of gauge error. This physical effect of curvature is also shown by Jones and Sims (1978) for all of the defined climatic regions. They also show that in the climatic region of Chilbolton (maritime temperate) this curvature is especially pronounced.
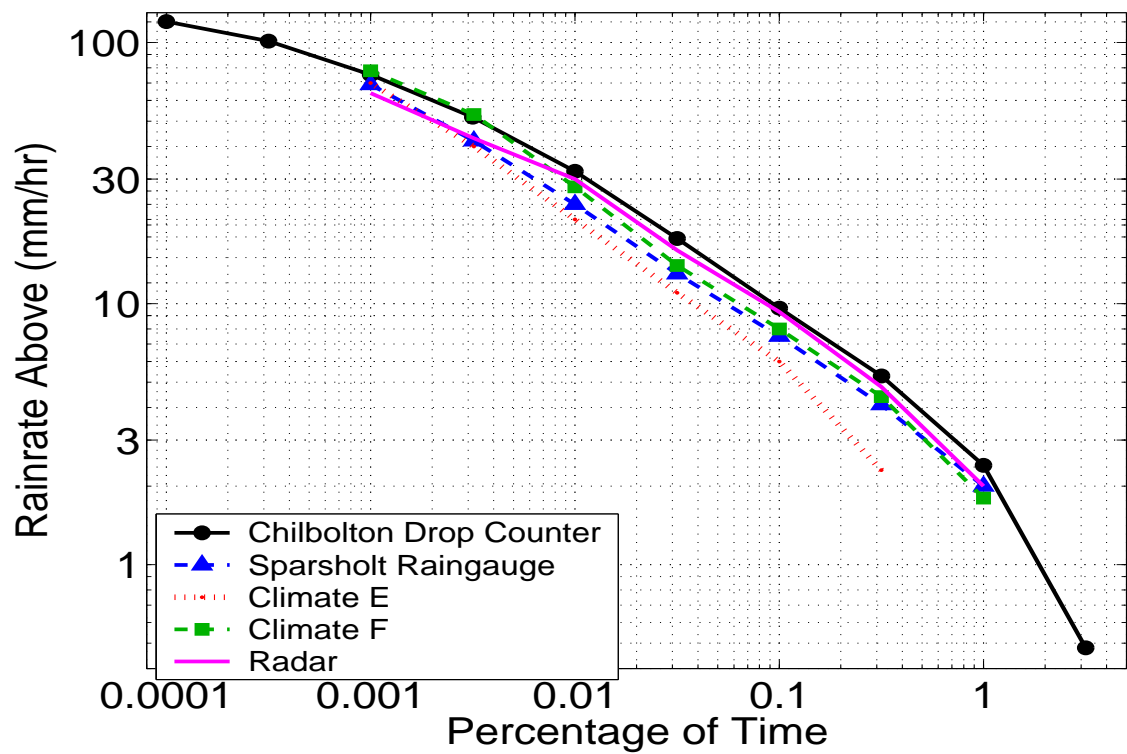
Figure 4.3 *Plot showing the regularity of occurrence of rain rates. Here the plot shows the probability of rainfall above a chosen rate. Also shown are curves from Goddard (2006), personal communication, for a rain gauge at Sparsholt (∼ 7.5 km from Chilbolton), rain derived from the Chilbolton radar and ITU-R recommended model statistics for the two zones (climate E and climate F) of which Chilbolton is on the boundary.*

The hourly rainfall accumulations have been calculated from this data. From these, 82% of hours have no rainfall. Next the rainfall rates occurring in each accumulation will be examined. Even in the hours with the largest accumulations, many 30 s samples contain no rain.

From the data set, the possibility of a universal relationship between rain rates falling within hours of any accumulation will be examined. The first step is to calculate the proportion of 30 s samples for each rain rate. At this point it should be noted that the instrument dropper imposes a measurement quantisation of

$$120(\text{number of samples in hour}) \times 0.004(\text{size of one drop}) = 0.48\text{mm/hr}. \qquad (4.1)$$

The results of plotting the proportions is shown in figure 4.4, where a similar pattern for all accumulations is seen, suggesting a universal relationship may be applicable. The events within the accumulation categories decrease dramatically as the accumulation increases, with 1187 cases of 1 mm within an hour, but just 8 cases of 10 mm within an hour. The reason for this discrepancy is clear from figure 4.3. However, this plot has too
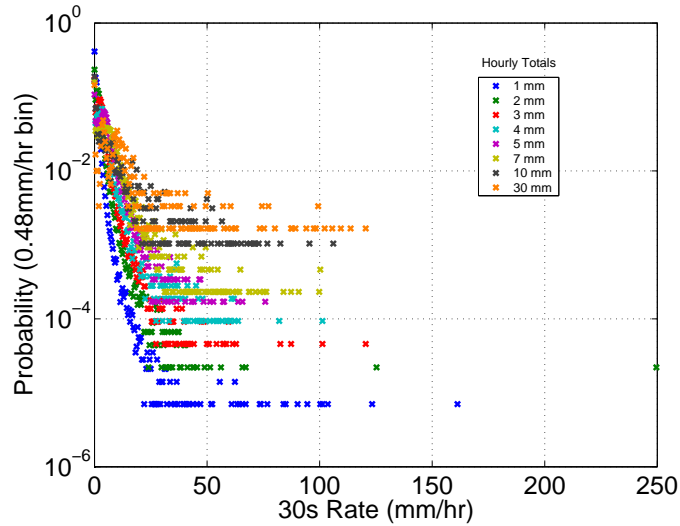
Figure 4.4 *Plots showing the proportions of 30 s rain rates recorded during different hourly accumulations. Horizontal axis: linear.*

little emphasis on the lower rainfall rates, so to improve on this the horizontal will also be given a logarithmic scale, resulting in figure 4.5.

In this plot it is easier to see the differences between the accumulation levels. In general the probability of any given large rainfall rate (>10 mm/hr) increases as the hourly accumulation increases as would be expected. Also, lower rates are more common in hours of small accumulation. Most importantly these lines all show similar pattern, but are offset in both dimensions. Next the rainfall rates will be rescaled. A similar plot to figure 4.5 will be created, replacing the horizontal axis with rainfall rate as a proportion of hourly average:

$$P_{HA} = \frac{R_{30s}}{R_{HA}}, \qquad (4.2)$$

where HA stands for "hourly average". This yields figure 4.6. In this plot the turn-
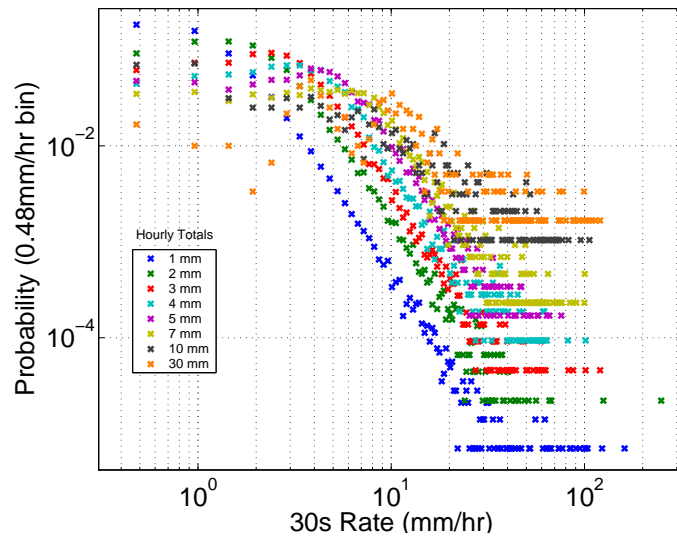
Figure 4.5   *Plots showing the proportions of 30 s rain rates recorded during different hourly accumulations. Horizontal axis: logarithmic.*
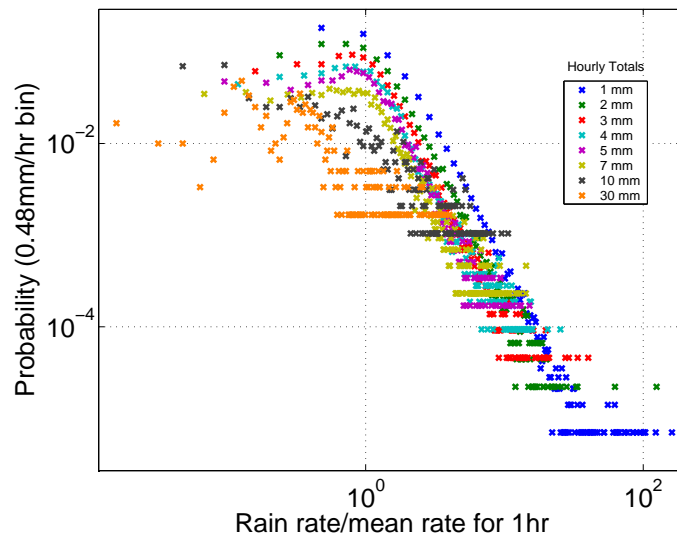
Figure 4.6   *Plots showing the proportions of 30 s rain rates (vertical), as proportion of hourly average recorded (horizontal) during different hourly accumulations (shown by colour).*

ing point of all colours (accumulations) occurs at the same point. However the lines maintain the vertical displacement, showing that a proportional rate of 0.48 (0.48 mm/hr for a 1 mm accumulating hour, 2.4 mm/hr for a 5 mm accumulating hour) is more likely for lower rainfall rates. This effect is however caused by the quantisation of

rates from the counter. For the 1 mm hourly accumulation, the quantisation occurs at 0.48 mm hr^{-1}/mm hr^{-1}, although, for a 30 mm accumulation the minimum recordable P_{HA} is 0.016 mm hr^{-1}/mm hr^{-1}. To examine the probability of any rainfall rate a correction for this effect must be applied. To do this the vertical axis is changed to be the proportion of 30 s rates per 1 mm hr^{-1}/mm hr^{-1}.

$$\text{probability of 30s rate per bin width}$$
$$= \text{proportion of hourly average} \times \text{quantisation proportion} \tag{4.3}$$

The result is shown in figure 4.7a.

Figure 4.7 shows that different hourly accumulations have the same distribution; for rain-rates much above the hourly average, a power law fall off is seen. This power law has slope of -3. A constant probability is observed for occurrences less than the hourly average. If the function is defined to be continuous, have a power law relationship with slope -3 and be constant for lighter rainfall than average rainfall, the constant value can be found via integration. This model must satisfy the two important integrals. First consider the probabilities: the total probability must be one, and the problem must be considered in linear space:

$$\int_0^1 C dr + \int_1^\infty C r^{-3} dr = 1, \tag{4.4}$$

where r is the normalised rainfall rate. Integration yields that $C + \frac{1}{2}C = 1$, so $C = \frac{2}{3}$. Next check the average; mean r must again be one.

$$\int_0^\infty Pr dr = 1 = \int_0^1 \frac{1}{3} r dr + \int_1^\infty \frac{1}{3} r^{-3} r dr. \tag{4.5}$$

Integration reveals that this is satisfied. So the constant value for rainfall rates below the average is $\frac{2}{3}$, which, in the log space of figures 4.7, is -0.18.

This procedure was then repeated, changing the accumulation period to 15 minutes (figure 4.7b) and 3 hours (figure 4.7c). Similar distributions of rainfall rates are found, all showing the turning point occurring at the hourly average rainfall rate.

(a) 1 hour accumulation

(b) 15 minute accumulation

(c) 3 hour accumulation
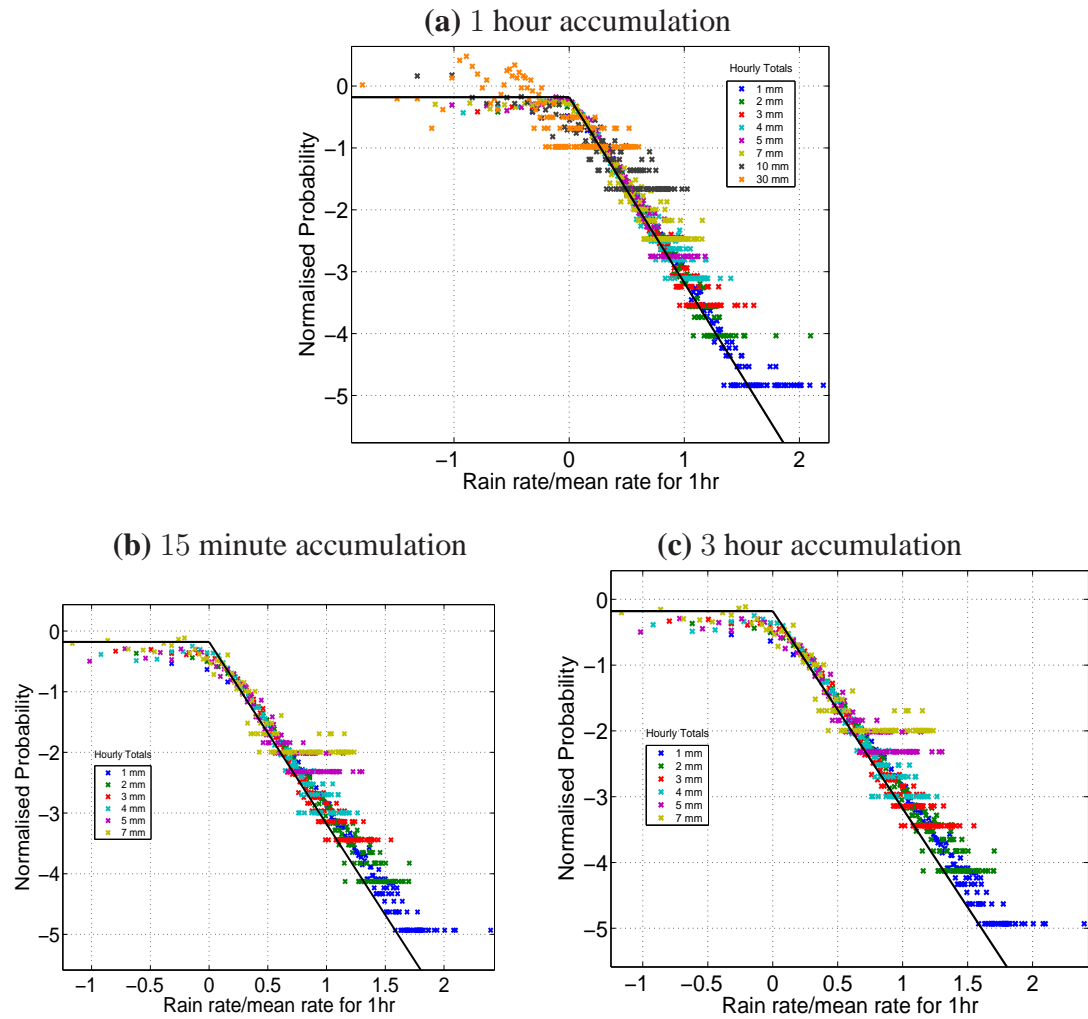
Figure 4.7 *Rainfall rates occurring as a proportion of the accumulation over a period shown. The data has been normalised to allow for the probability of occurrence and quantisation of rainfall rates. Also plotted is the fitted model in black.*

This tells us significant information on the nature of rainfall. In absolute terms, an hour of 3 mm of rain shows little variation in rainfall rate, whereas a very heavy event of 20 mm shows large variations. However, in relative terms, these variations in rate are the same. One would expect this behaviour to occur for any high resolution rainfall data set, including high resolution numerical model grid boxes.

4.3.1 DATA REQUIRED TO DEMONSTRATE THIS BEHAVIOUR

The amount of data needed to see the behaviour described above will be important for confirmation of models. Figure 4.8 shows examples of data from three of the wettest days of the dataset ([a] 42 mm, [b] 24 mm and [c] 34 mm falling during the days). The plots show similar behaviour to that expected by the model presented above, but there is some variation. Figure (a) shows a curve over the turning point, (b) shows a large peak at the mean rate for the 4 mm/hr category and (c) shows less lower rainfall rates than average for all categories.
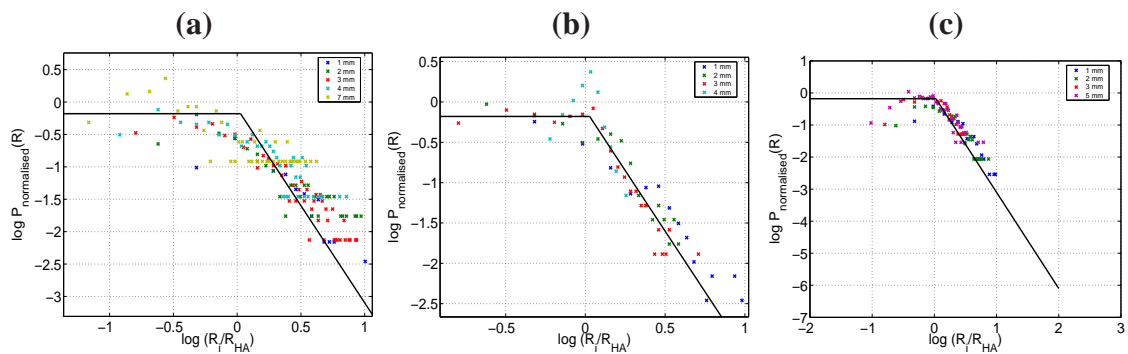
Figure 4.8 *Rainfall rates occurring as a proportion of the accumulation over an hour. These examples each show data from one very wet day [each a separate day] (accumulation of > 20 mm).*

Although the expected behaviour can be seen from a single day of heavy rain the best test would involve a longer record for statistics.

4.3.2 RAIN RATE BEHAVIOUR FROM RADAR DATA

The distribution of rainfall can be examined using radar data as well as rain gauge data. We will calculate rainfall rate at each radar pixel using a simple $Z - R$ relationship, then instead of considering the rainfall rates as a proportion of a time average rate, they will be considered as the proportion of the average rate over an area. Figure 4.9 shows that the radar data shows similar characteristics to the gauge, but the lower rainfall rates appear to be rather reduced, with the increase in rates near the mean. This may be an effect of the radar having poor measurement at low rainfall rates.
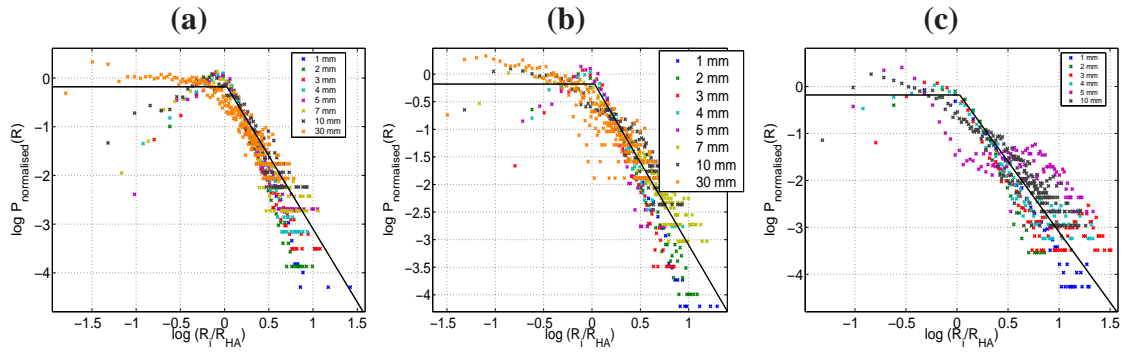
Figure 4.9   *Rainfall rates occurring as a proportion of the average over an area. The area for averaging is (a) $5.6°$ azimuth by 4.5 km range, (b) $11.2°$ azimuth by 9 km range and (c) $22.4°$ azimuth by 18 km range. The radar data was chosen to be free of non-rain targets ($L_{\mathrm{DR}} < -20$ dB) with ranges between 15 km and 60 km. The data was taken during the passing of a front over Chilbolton on 18/08/2000.*

Similar analysis has been performed for another radar scan (figure 4.10). In (a) and (b) the low rates are less frequent than expected, but in (c) this effect is not seen. This indicates that this behaviour is only seen if the averaging area (or time) are large enough.
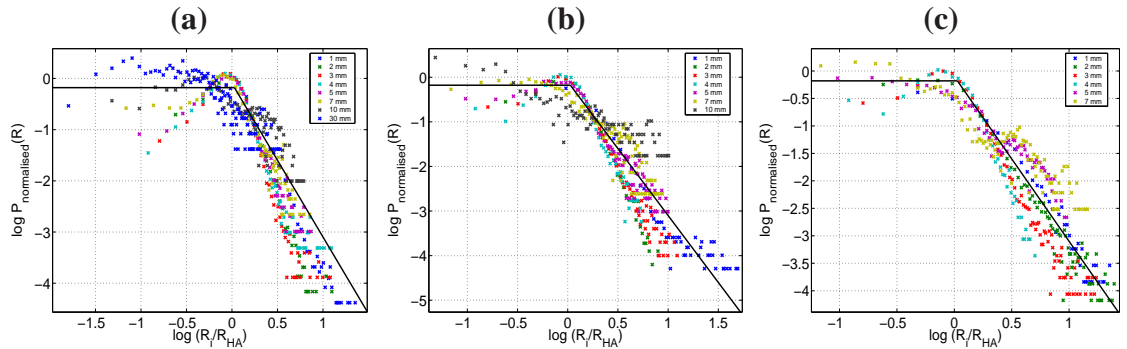
Figure 4.10   *Rainfall rates occurring as a proportion of the average over an area. The area for averaging is (a) $5.6°$ azimuth by 4.5 km range, (b) $11.2°$ azimuth by 9 km range and (c) $22.4°$ azimuth by 18 km range. The radar data was chosen to be free of non-rain targets ($L_{\mathrm{DR}} < -20$ dB) with ranges between 15 km and 60 km. The data was taken during the passing of a front over Chilbolton on 09/10/2000.*

The behaviour of rainfall rates from the radar have shown how the model of rainfall rate distributions can be applied to uses beyond simple rain gauges. It is important for numerical models to also obey these statistics, to ensure rainfall is correctly simulated.

4.4 ERRORS DUE TO FINITE NUMBER OF RADAR SCANS

To examine the effect of the regularity of "snapshots", the effect of measuring the rainfall every 2.5, 5 and 15 minutes will be studied, this is briefly discussed by Harrold *et al.* (1974). This involves selecting one measurement in the required time period and calculating the apparent hourly accumulation with the "truth". For this, the errors in the measurement must be calculated. The errors are controlled by Poisson statistics so that the error is given by

$$\frac{\Delta R}{R} = \frac{\sqrt{N}}{N},$$ (4.6)

where N is the number of tips during in the time period concerned. To reduce the errors, "snapshots" are taken from one minute accumulations (from successive samples). To compare the different accumulations from the timing possibilities the two will be compared using these errors. To compare a 15-minute repeating cycle of "snapshots" first see figure 4.11. This plot shows some extreme outliers, with the largest errors occurring from overestimated rainfall accumulations. The size of the errors are also seen: the errors for the 15 minute repeats are larger as the total sampling time is just 2 minutes of the hour (hence low N), where the whole hour is used for the "truth" (so high N).

A similar plot for examination at 5 minute intervals is shown in figure 4.12. This is quite a significant improvement, with much fewer points with large discrepancies.

The errors caused by the sampling effect will now be examined. The data will be divided up into a number of rain-rate categories. For each category the bias, the mean modulus of the error, the root mean square error and standard deviation of error are calculated. The sampling of the counter means that a small error will occur as a result of measurement and this error cannot be improved upon. This error as a result of the "counter" sampling increases with rainfall rate in an absolute sense, but decreases in a fractional sense, which can be seen visually as the black lines in figures 4.13 (absolute) and 4.14 (percentage).
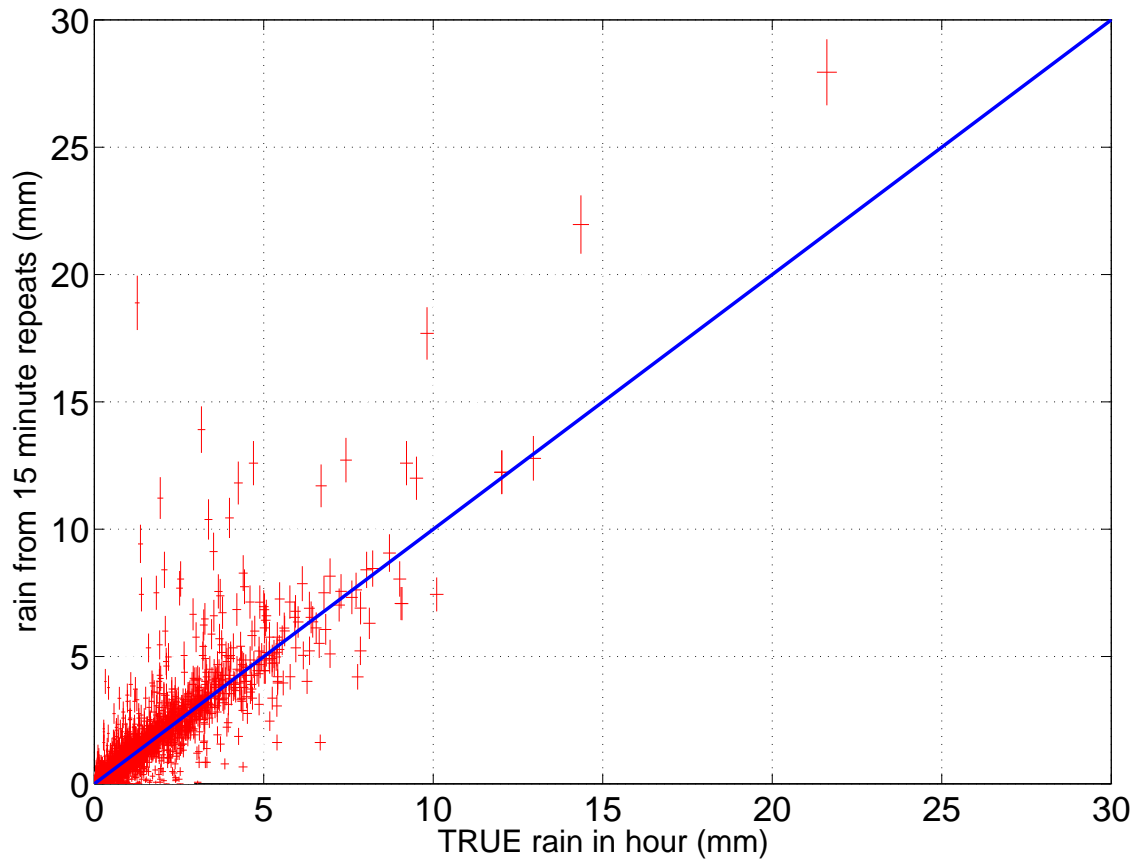
Figure 4.11 *A comparison of hourly accumulations between the "truth" (horizontally) and apparent accumulation from sampling once every 15 minutes (vertical). The blue line plots where the two are the same, red crosses show the positions of all hours of the 61 months which contain rain and the size of the cross indicates the errors on this value.*

4.4.1 BIAS

$$bias = \overline{recorded\,vaulue - true\,value} \qquad (4.7)$$

The bias will show any systematic errors occurring as a result of the reduced snapshot distribution. The bias is calculated and plotted in figure 4.13 for rainfall categorised by true hourly rainfall. The black curves show the error expected as a result of sampling the entire hour of rainfall. There will be significant bias if the calculated bias for a sampling return period lies outside of this. The figure shows that all show no significant bias allowing for errors except for the case of 15 minute sampling of rainfall between 8.5 and
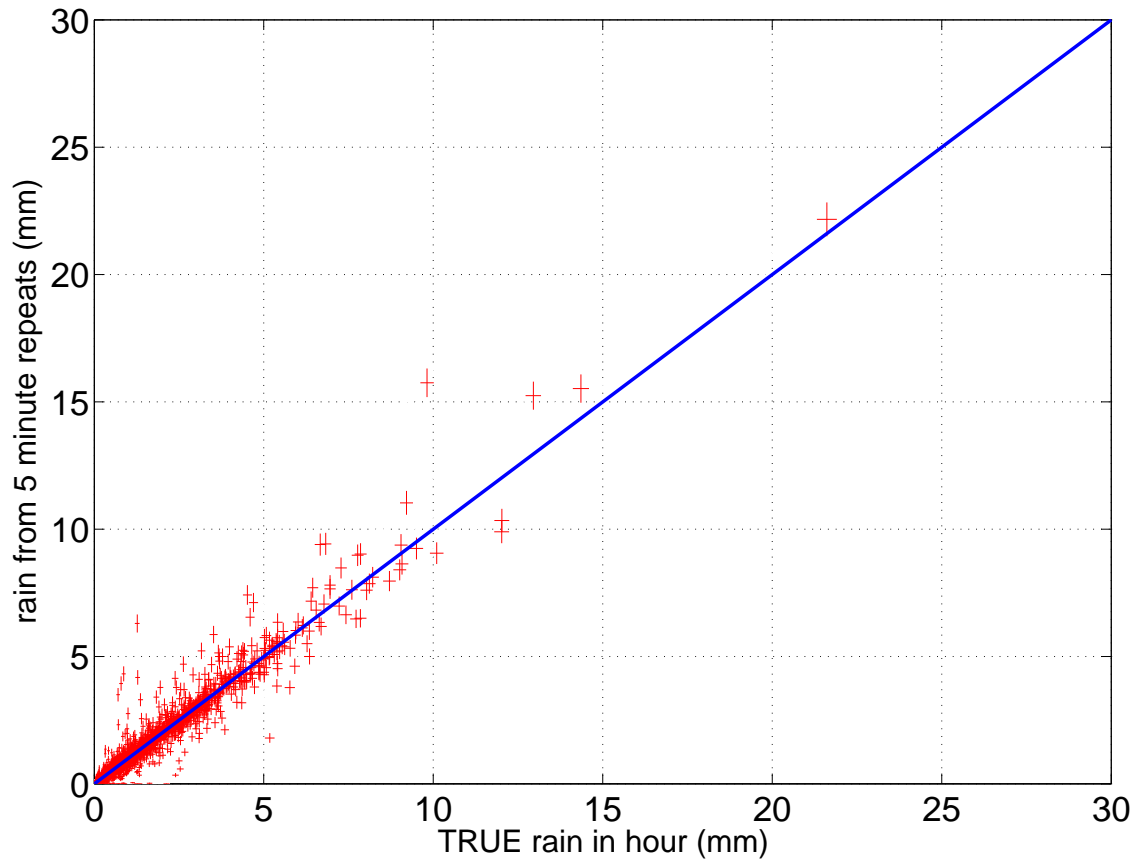
Figure 4.12 *A comparison of hourly accumulations between the "truth" (horizontally) and apparent accumulation from sampling once every 5 minutes (vertical). The blue line plots where the two are the same, red crosses show the positions of all hours of the 61 months which contain rain and the size of the cross indicates the errors on this value.*

11.5 mm within the hour. However, this comprises just 8 cases in the record. So the sampling period does not bias the total derived rainfall within an hour.

4.4.2 ROOT MEAN SQUARE ERROR

$$RMS = \sqrt{\left[(recorded - truth)^2\right]} \qquad (4.8)$$

The root mean square is a measure of the average error in the data. We examine the mean square error to determine the error in rainfall rate caused by longer sampling return period. Figure 4.14 shows the root mean square error in terms of percentage error. Again
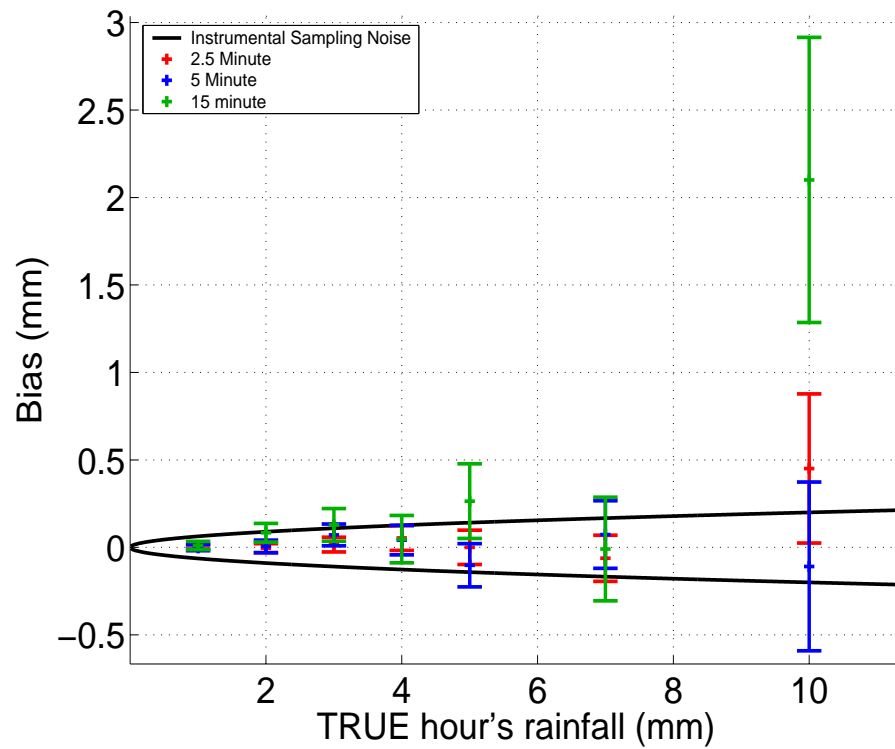
Figure 4.13   *Plot showing the bias caused by sampling return period.*

the expected error caused by the sampling of the dropper is plotted in black; if the RMS errors lie above this line, the error is significant. It can be seen that as the sampling return period is decreased the error in calculated hourly totals is reduced, and that the largest percentage errors occur at low rainfall rates. It should be noticed that the errors occurring are all significant.

These errors found however comprised the combination of two error distributions: the sampling error of calculating the "truth" from the counter and the error which is the result of the increased sampling return period. Assuming both errors are normally distributed this can be expressed as:

$$\left(\sigma_{total}\right)^2 = \left(\sigma_{counter}\right)^2 + \left(\sigma_{return\ period}\right)^2. \tag{4.9}$$

This means that to calculate the error that is caused by the sampling return period the
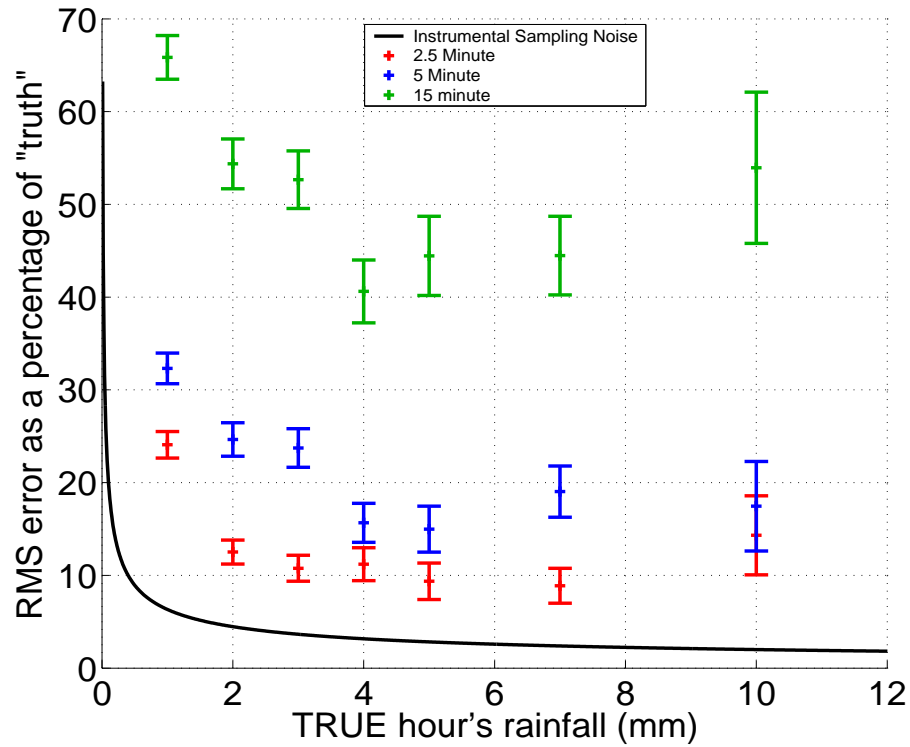
Figure 4.14 *Plot showing the effect of sampling return period in percentage error of "true" rainfall rate.*

formula

$$\sigma_{return\ period} = \sqrt{\left(\sigma_{total}\right)^2 - \left(\sigma_{counter}\right)^2} \qquad (4.10)$$

is used.

This will give an indication of the error that would be expected from a radar measuring hourly rainfall accumulations (figure 4.15), showing limitations from the variability of the rain and requirements for a scan strategy to measure rainfall accumulations accurately.

Figure 4.15 shows that for rainfall rates of order 5 mm/hr an accumulation of 15% accuracy can be achieved by a return period of 5 minutes, although if the return period is 15 minutes, this error has increased to 45%. This means that a radar measuring the accumulation from four scans per hour will show a 45% error given a PERFECT radar-rainfall algorithm. In actuality the radar-rainfall algorithm will generally be significantly in error in measuring rainfall rates, which will add to the error caused by scan strategy.

However, the effect of how regularly one samples rainfall on measured accumulations
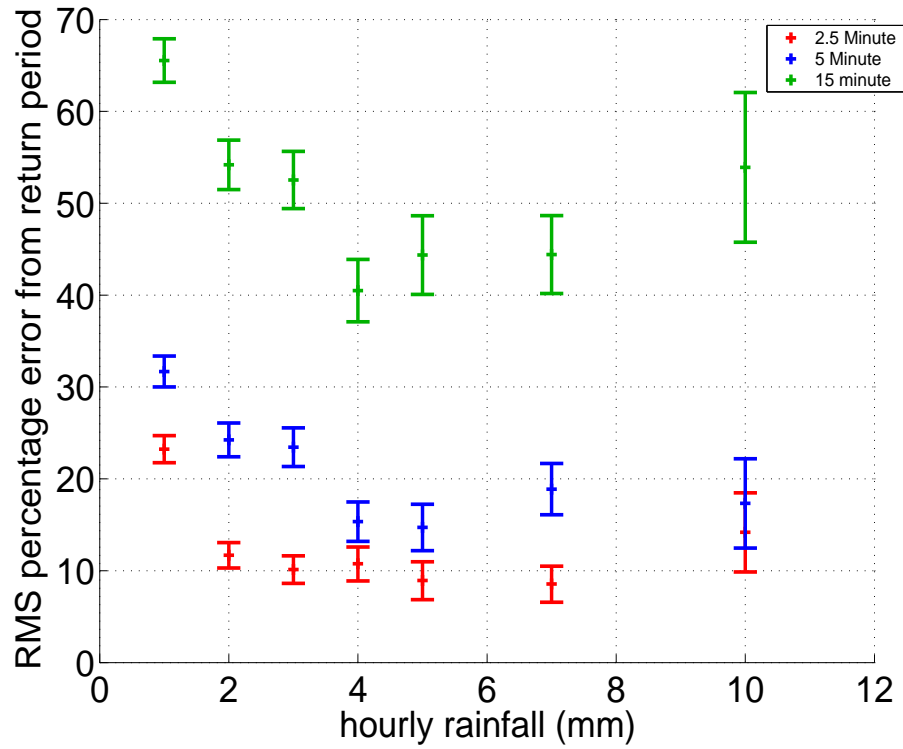
Figure 4.15 *Plot showing the effect of sampling distribution of "snapshots" in percentage error of hourly rainfall rate, having removed the effect of sampling using the drop counting gauge.*

can be examined in another way: autocorrelations.

4.5   DECORRELATION TIME OF RAINFALL RATES

The "memory" in the system will be examined by calculating the correlation of the rainfall rate with the rainfall rate a time before (the autocorrelation function). For this the Pearson's correlation is calculated for the rainfall rate at time t and the rain-rate τ seconds later, $t + \tau$:

$$\rho_\tau = \frac{\sum \left(R_t - \overline{R}\right)\left(R_{t+\tau} - \overline{R}\right)}{\sum \left(R_t - \overline{R}\right)^2}. \tag{4.11}$$

Calculation of the autocorrelation demonstrates that the correlation decreases with time lag as shown in figure 4.16. The decorrelation is exponential as expected from pre-

vious work (Zawadzki, 1973, 1987; Drufuca and Zawadzki, 1975) showing decorrelation time to $\rho_\tau = 0.5$ of 4.5 minutes or decorrelation to $\rho_\tau = e^{-1}$ of 9.3 minutes. Burgueño, A. and Vilar, E. and Puigcerver, M. (1990) derived decorrelation times of 3.5 and 5.4 minutes for a rain gauge in Barcelona. The data from Chilbolton has a longer decorrelation time, related to the relative prevalence of convective rainfall in Barcelona (this will be examined shortly). The decorrelation time is much lower than that reported by Zawadzki (1987) (~ 20 minutes) for Montreal. This is likely to be a result of the time resolution of the available data: he used data smoothed over 5 minutes of tipping bucket rain gauge data.

These decorrelations can be converted into a spatial decorrelation scale from the speed of rain storm progression using a "synthetic storm" (Drufuca and Zawadzki, 1975), assuming that the time series from a fixed point rain gauge is the result of advection of spatial variations. Using an assumed mean storm progression speed of 10 m s^{-1} (36 km/hr) the decorrelation distance to e^{-1} is 5.5 km.

It is seen that after just 5 minutes the correlation has dropped to 0.5, and by 15 minutes it has fallen to just 0.3. This shows the amount the rainfall is related to the rate before, so only 30% of the rain-rate now is related to the rain-rate 15 minutes ago. This clearly shows the need for regular repeats when calculating accumulations from rainfall rate "snapshots".

4.5.1   SEASONAL AUTOCORRELATION

By dividing the data into seasons (winter: DJF, spring: MAM, summer: JJA, autumn: SON) the effect of the time of year on rainfall correlations can be shown. The autocorrelations for all four seasons are shown in the left panel of figure 4.17. The summer season is seen to have higher correlation than the winter for short lag periods, although after 4 minutes the correlation is lower, continuing to decrease as the lag increases. This pattern can be easily explained by the predominant precipitation during these seasons. Convective rainfall is more common during the summer, while stratiform rain dominates
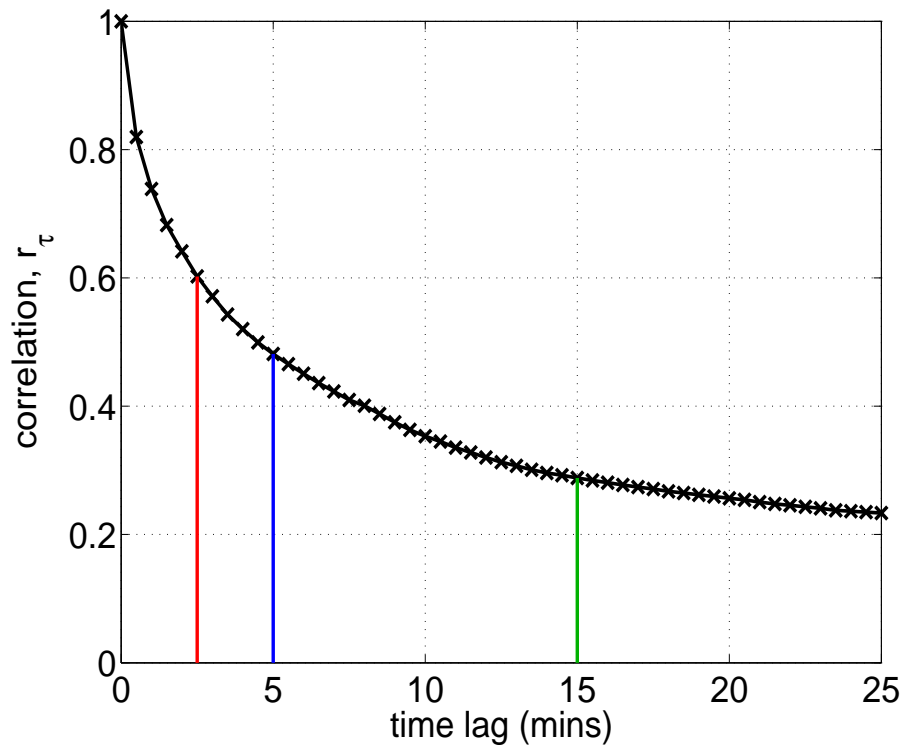
Figure 4.16 *Plot showing the autocorrelation function of rainfall rates. Marked on are the correlations at* 2.5, 5 *and* 15 *minute lags to correspond to the tested return periods for hourly accumulations.*

during the winter months (see figure 4.17 right panel). Stratiform rain's large scale nature mean that the variations over even long periods are rather small, indicated by the high correlations (> 0.5) at time lags as far as 25 minutes (decorrelation to 0.5 occurs in 26.8 minutes, to decorrelate to e^{-1} is 51.9 minutes), whereas convective rain occurs in short sharp "bursts", so is poorly correlated for long lag periods (decorrelation time to 0.5 of 5.1 minutes and falling rapidly so as the decorrelation to e^{-1} takes 8.9 minutes). These times are longer than the times for the full data set as only the heavy rain is considered (so comparison should only be made between convective and stratiform, not with the overall data set). As expected spring and autumn lie between summer and winter.

With operational radar scan strategies having low level scans at 5 minute intervals the seasonal effect on accumulation accuracy is small as it is near the crossing point.
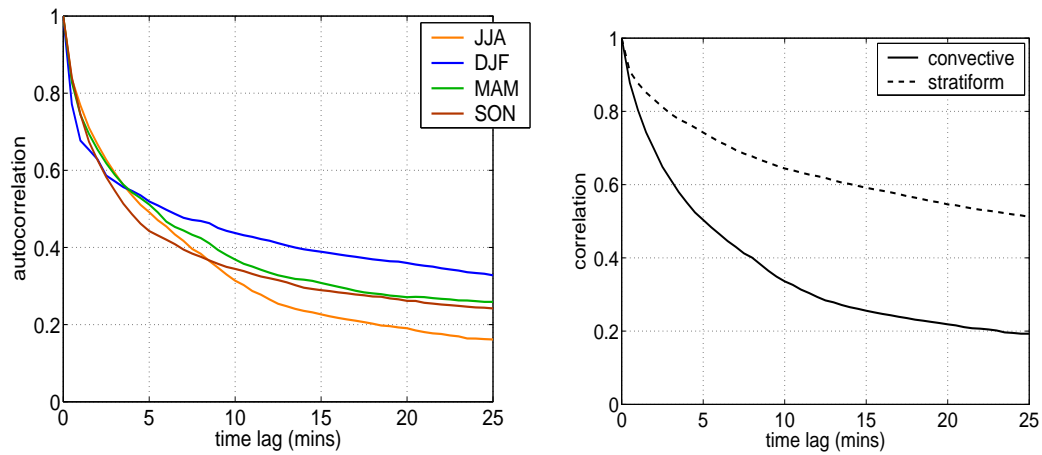
Figure 4.17   *[LEFT] Plot showing the autocorrelation of rainfall rates for 4 seasons.   [RIGHT] Plot showing the autocorrelation of rainfall rates for convective and stratiform rainfalls. These have been defined as rain from days where more than 10 mm of rain fell. Stratiform rain has a daily maximum rain rate less than 22 mm/hr, if the daily maximum was greater than 22 mm/hr the rain was considered convective. This gives 58 days of data of each type.*

4.6   RAINFALL POWER SPECTRUM

This section will examine the power spectrum of the rainfall data from the rain gauge. Together with the auto-correlation function the power spectrum density provides a Fourier transform pair. Physically, we know that rain varies on a number of scales. The rain varies from mesoscale (10^3 km) processes, such as weather systems, to microscale variations (1 cm), such as drop interactions. This means a model of the temporal spectrum of the rainfall (in actuality this will be of log of rainfall as will be seen shortly) can be formulated. Veneziano *et al.* (1996) combine the segmented spectra of previous authors to gain a spectrum as shown in figure 4.18. They suggest that ω_1 occurs at the scale of convective cell clusters (7-15 km, Crane, 1990 [~ 20 minutes]), with lower frequencies showing a $-5/3$ slope, converting to -3 at this point, this is the energy input scale. The next conversion, to the -1 slope segment, ω_2 occurs as the microscale is represented at the rain input scale of 3-7 km (Crane, 1990) [10 minutes]. Finally ω_3 occurs at the very small scales, where the slope returns to $-5/3$ (Veneziano *et al.*, 1996 suggest this occurs at 30-90 s). Horizontal turbulence invalidates the theory used to derive these plots at high frequency when considering time rather than space variations; the effect is an increased
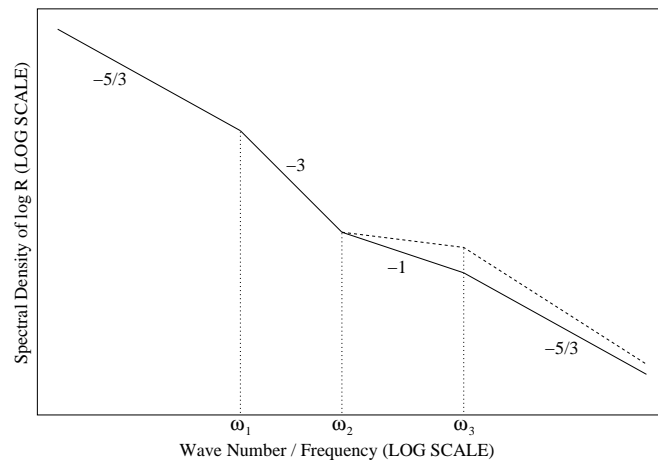
Figure 4.18   *Idealised spectrum of log rainfall rate, based on figure 1 of Veneziano et al. (1996). The solid line shows the spectrum by wave number, with dashed line showing the frequency scale plot. The difference is qualitative, being a result of horizontal turbulence.*

power at the high frequencies.

Figure 4.19 shows the rainfall rates of one event lasting just over 2 hours. The upper
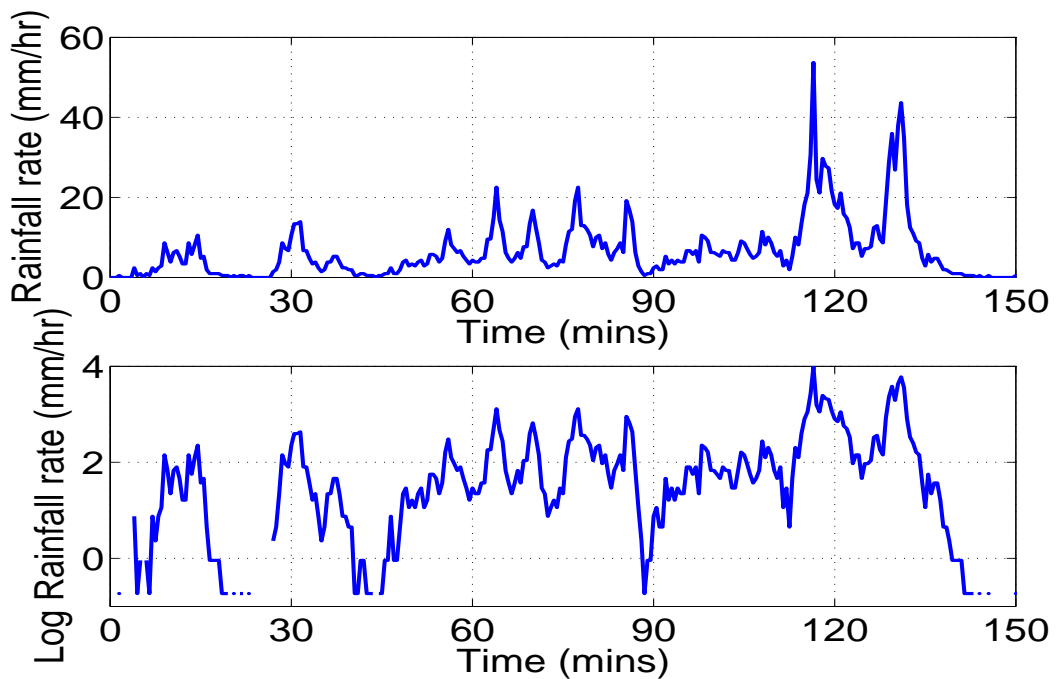
Figure 4.19   *An example of a rain event demonstrating why the log of rainfall rate is considered instead of the linear rainfall rate.*

plot shows the rainfall rates, the lower showing the natural logarithm of the rain rate. The amplitudes of the high frequency changes in rainfall rate are dependent on the average rainfall rate at the time. This is shown similarly in the log plot, where the high frequency variation has the same size at all levels, implying that the variations are multiplicative, so the log scale should be used for creating a power spectrum. The use of the logarithm of rainfall rate was also made by Crane (1990) and Veneziano *et al.* (1996).

To estimate the power spectrum density (PSD), first a discrete Fourier transform is computed from the log rainfall rates. Taking the logarithm of the rainfall means that zero values must be removed before computation of the Fourier transform. PSD is calculated by squaring the result of the Fourier transform and scaled by frequency. The PSD that is derived has very large noise, so this is smoothed to see the true signal. This smoothing is performed with a moving average, shown in figure 4.20. Generally this average is from
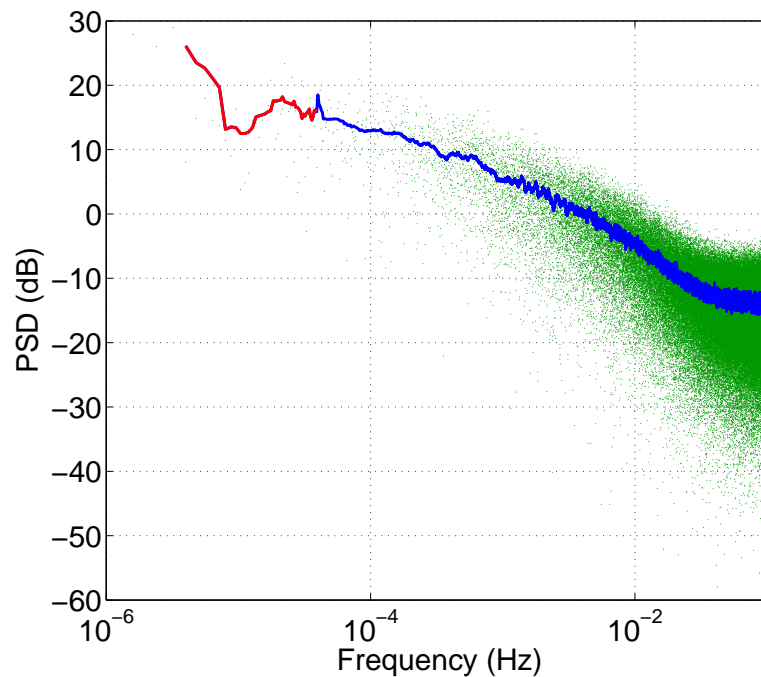
Figure 4.20   *Periodogram of the natural log of rainfall rate (after removing zero rainfall rates). Green dots show all data points; blue and red lines show moving averages as described in the body text.*

the 101 nearest points (from a total of 131073), shown by the blue line. However, the very low frequency has few data points but retains some information, so for the lowest

frequencies, the moving average is calculated from just 11 points of the derived PSD. This is the red section of the line (this is why the noise level on this segment of the line is larger). Note that these are running means from the calculated PSD, not of the rainfall data used for calculation.
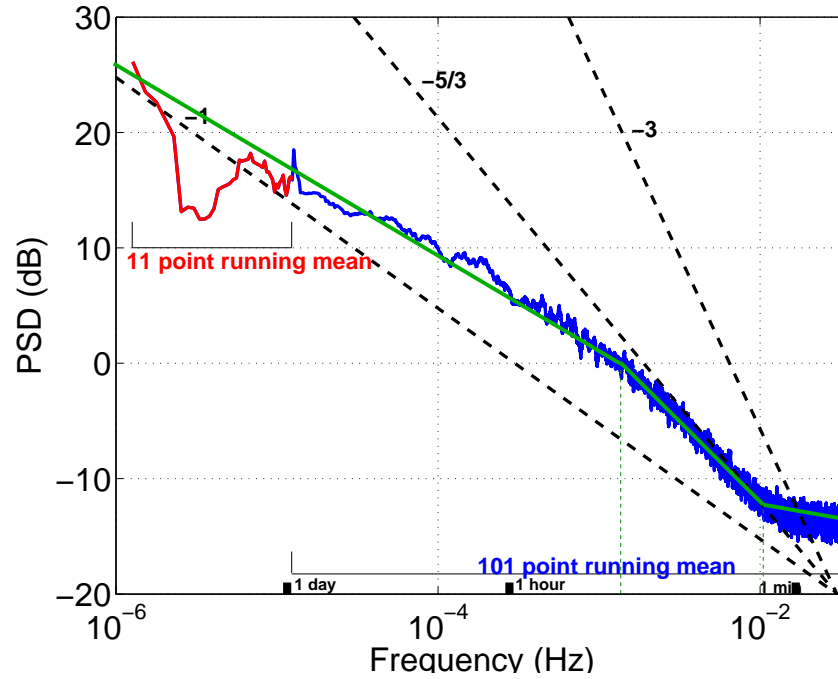
Figure 4.21 *Periodogram of the natural log of rainfall rate (after removing zero rainfall rates). The dashed lines show slopes of -1, $\frac{5}{3}$ and -3 for comparison. Overlaid in green, is a segmented spectrum to fit the data.*

Figure 4.21 shows that moving average again, but this time the plot also shows the slopes expected from Veneziano *et al.* (1996) (dashed black lines), and a segmented model fitted to the data (in green). This green model shows three of the segments from the model of Veneziano *et al.* (1996), the missing segment being after ω_3. This is missing as the frequency this is expected to occur at is too small, so not detectable with the 30 s resolution of the rain gauge data used in this study (ω_3 is also missing in Crane (1990) presumably for the same reason). The first spectral turning point, ω_1 occurs at 12.4 minutes, ω_2 occurring at 1.6 minutes. Both turning points are found to occur at higher frequencies with the Chilbolton data set than suggested from the storms used in

the Veneziano *et al.* (1996) study (16.1 min and 4.8 min respectively). However, the ω_1 value found lies within one standard deviation (factor of 1.5) of the mean, the second corner (ω_2) is within two standard deviations (factor of 1.8). Veneziano *et al.* (1996) found the final corner point, ω_3, to have an average value of 35 s, with standard deviation of a factor of 1.2. Assuming the trend of finding the turning points for Chilbolton data occurring at higher frequencies than Veneziano *et al.* (1996) found, ω_3 is likely too small to be measured by the drop counter with 30 s resolution.

The other comparison with the model is of the slopes of each segment. Each segment has slope shallower than the model predicts, where the model suggests it should be $-5/3$ (-1.67) the Chilbolton data shows -0.85. The middle segment where the model suggests the slope should be -3, the data in this study has slope of -1.53. The final section shown by the drop counter record has slope of -0.2, which is again shallower than the model predicts, although this was expected as this study is working with temporal spectrum rather than spatial. The effect of the difference between considering spatial and temporal spectrum was shown by a dashed line in figure 4.18, caused by the Taylor hypothesis not holding at higher frequencies due to horizontal turbulence.

4.7 SUMMARY

Statistics of rainfall were calculated showing a general form of rainfall rates within a longer term mean. These statistics should be obeyed at any point, so has implications for high resolution numerical modelling. Any equivalent high resolution numerical model grid box (especially cloud resolving or large eddy models) should obey the same rainfall statistics as shown by the rain gauge. It has been shown that the decorrelation time to a correlation of e^{-1} is 9.3 minutes, indicating rain has a spatial decorrelation scale of ~ 5 km. The power spectral density forms the Fourier transform pair of the auto-covariance function. The power spectral density is shown to have a similar segmented pattern to the model of Veneziano *et al.* (1996), but with shallower slopes and higher turning point frequencies.

This section on the timing of sampling when examining accumulations has an important significance when considering comparisons between radar and rain gauges. A rain gauge measures the rainfall integrated over the considered period whereas the radar measures instantaneous rate at a single time, imposing a limit on the comparisons. It has been shown that the decorrelation of rainfall is the cause of the errors, and that this decorrelation is dependent on the type of rainfall being measured (and therefore season it is measured during).

CHAPTER 5:

THE INTEGRATED

REFLECTIVITY/DIFFERENTIAL

REFLECTIVITY TECHNIQUE:

METHOD

5.1   INTRODUCTION

As was shown in chapter 2, Z_{DR} and Z can be used for rainfall rates on a gate-by-gate basis (2.4.2), although this requires Z_{DR} be accurate to 0.1 dB for rainfall rates, R, of $3-10$ mm/hr. Unfortunately large errors in Z_{DR} are observed, caused by the statistics of the returned echoes (Bringi and Chandrasekar, 2001) resulting in about 0.2 dB noise for the CAMRa. Radar antenna problems are small for CAMRa, although in the operational environment are likely to be significant (because in the operational environment financial and reliability constraints lead to smaller, less perfect antennas and radar setups, with radomes, which can affect results, especially when wet). The NEXRAD-KOUN radar (Ryzhkov *et al.*, 2005a) has 0.4 dB noise in Z_{DR}, while at C-band, for a UK operational radar the noise may be still larger. This means that gate-by-gate rainfall estimation using Z and Z_{DR} is noisy and may be biased. This noise averages out over time and space, but this remains a great drawback for instantaneous point rainfall rates. This gate-by-gate method does not allow for the possibility of unphysical, but statistically feasible, negative Z_{DR} observations (see section 2.4.4). This chapter will show a method of using Z and Z_{DR} over a domain to estimate the rainfall rate at each pixel. This will benefit from the increased information on the drop size distribution given by Z_{DR}, but will not suffer

as a result of the random noise of Z_{DR}, by averaging this noise to zero. A number of problems with the method will be examined, also considering how these problems can be overcome. The following chapter will then show a number of examples of the technique in action.

5.1.1 USE OF REFLECTIVITY AND DIFFERENTIAL REFLECTIVITY FOR ESTIMATING $Z - R$ RELATIONS

If the observed values of Z and Z_{DR} over a small region are used to characterise the rain drop spectra over that region, better rainfall rate estimates will be a reality. Recall the normalised gamma distribution of raindrops of section 1.3:

$$N(D) = N_w f(\mu) \left(\frac{D}{D_o}\right)^{\mu} \exp\left(-\frac{(3.67+\mu)D}{D_o}\right) \tag{5.1}$$

$$f(\mu) = \frac{6}{(3.67)^4} \frac{(3.67+\mu)^{\mu+4}}{\Gamma(\mu+4)},$$

which represents natural rainfall well (Ulbrich, 1983). By following the work of Bringi and Chandrasekar (2001), this leads to $Z - R$ relationships of the form:

$$Z = aR^{1.5}, \tag{5.2}$$

with a dependent on N_w and μ. Integration of the suitably weighted normalised gamma function produces the expression:

$$Z = F_Z(\mu)N_w D_o^7. \tag{5.3}$$

Making the assumption that the terminal velocity is proportional to $D^{0.67}$,

$$R = F_R(\mu)N_w D_o^{4.67}; \tag{5.4}$$

and by removing D_o this becomes:

$$\frac{Z}{N_W} = H(\mu)\left(\frac{R}{N_W}\right)^{\frac{7}{4.67}} = H(\mu)\left(\frac{R}{N_W}\right)^{1.5} \tag{5.5}$$

where $H(\mu) = f_Z(\mu)f_R(\mu)^{1.5}$. Hence

$$Z = H(\mu)N_W^{-0.5}R^{1.5} = \frac{H(\mu)R^{1.5}}{\sqrt{N_W}}, \tag{5.6}$$

so using equation 5.2 this leads to,

$$a = \frac{H(\mu)}{\sqrt{N_W}}. \tag{5.7}$$

So over the chosen region of data, if the drop spectrum can be characterised to estimate N_w, it will be possible to derive the values of 'a' in equation 5.2 (assuming a value of μ).

Next consider the physical drop spectrum cause of variations in b. Initially consider the case where N_w remains constant. Increased rainfall rate is caused simply by an increase drop size, D_o. The assumption that this behaviour is standard within rainfall events is used elsewhere, for example in the work of Testud *et al.* (2000) for the ZPHI technique. Equation 5.3 shows Z varies as D_o^7 and 5.4 demonstrates R varies as $D_o^{4.67}$. So, substituting into equation 5.2 gives $b = 7/4.67 = 1.5$.

However, it is possible that N_w is a function of D_o, and this possibility will result in different values of b. Consider the case where N_w rises as D_o^2, so as rainfall rates increase there are both more and larger raindrops. This implies, via equations 5.3 and 5.4, that Z and R vary as D_o^9 and $D_o^{6.67}$, leading to a b of 1.35. Now consider the case where N_w varies as $1/D_o$, a case where as the drops get larger, their numbers decrease, suggesting Z and R vary as D_o^6 and $D_o^{3.67}$ so $b = 1.63$.

Now consider a more extreme example. If, rather than N_w being constant, D_o remains constant and as rainfall rate increases it is a result of more drops of the same size, Z and R scale together with N_w, so $b = 1$, this value was suggested for tropical convection by List (1988). Now consider the case with high aggregation of snowflakes leading to N_w scaling with $1/D_o^2$. Now Z and R vary as D_o^5 and $D_o^{2.67}$ resulting in a b of 1.87.

It was shown in chapter 2 that Z_{DR} can give the additional information required for more accurate rainfall rates from Z alone, although it was shown in section 2.4.4 that the signal is too noisy for use at each point. In chapter 3 the natural spread in Z_{DR} was examined. The suggestion is a method that uses the $Z - R$ derived from the region to calculate the rainfall rate of the individual pixels, without suffering as a result of the noisy (and possibly negative) observed gate-by-gate Z_{DR}. The noisy Z_{DR} remains utilised, however, by altering 'a' (and potentially 'b') from detected changes in the drop spectra,

which a simple default $Z - R$ cannot be expected to detect (chapter 2).

5.2 DATA REJECTION DUE TO NON-RAIN TARGETS

The technique described above relies on solely rain targets as the equations for calculation of R. Z and Z_{DR} given N_{w} (for example equations 2.13, 5.8, 5.10) all use drop shapes that are only appropriate for liquid water hydrometeors. Therefore any data points which are not the returns from liquid water must be carefully removed.

(a) dBZ

(c) Z_{DR} (dB)

(b) L_{DR} (dB)

(d) v m s^{-1}
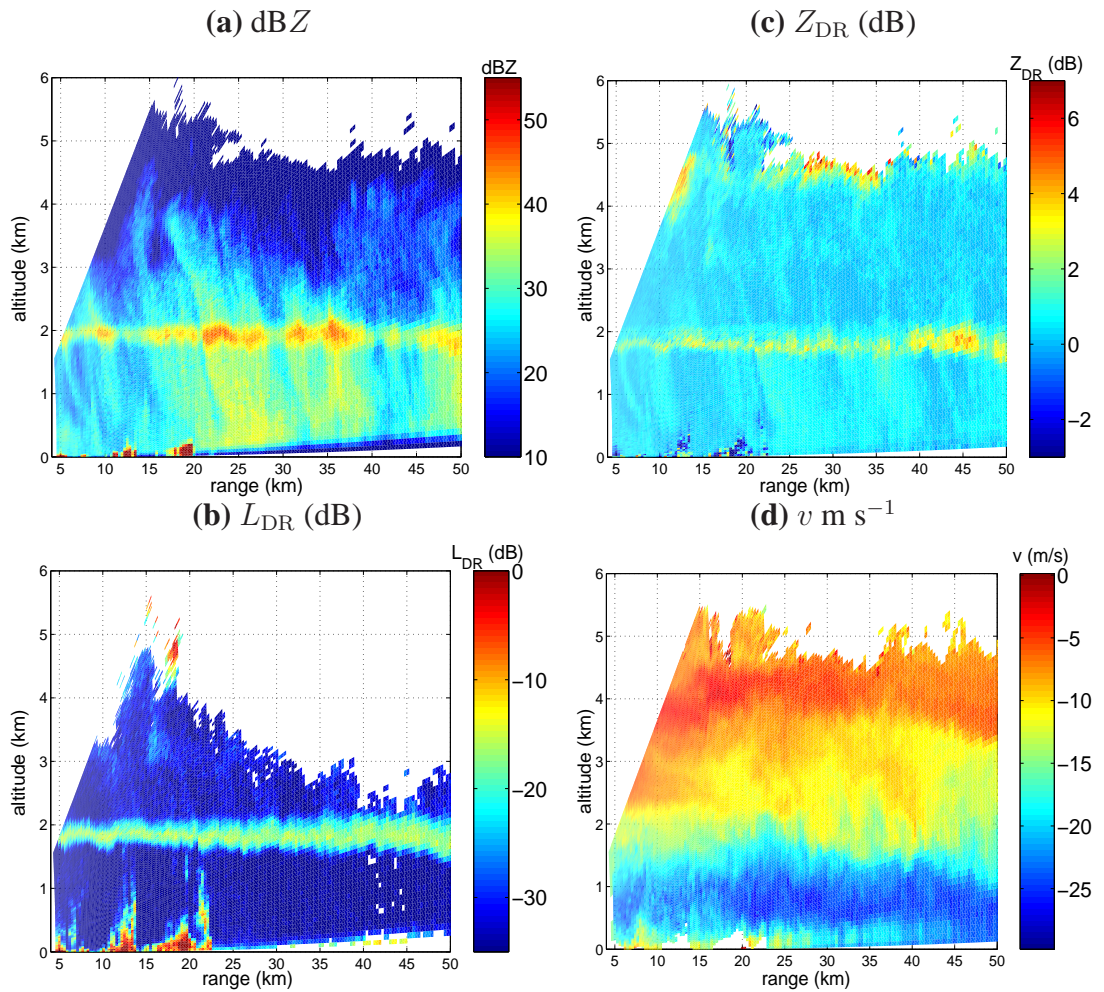
Figure 5.1 *A Range Height Indicator (RHI) showing the "bright band" and ground clutter. We can see at a height of near 2 km the clear bright band signature. Ground clutter is also observed at ranges of 12 km and 19 km, with its clear signature in L_{DR} (high values).*

5.2.1 GROUND CLUTTER AND ANAPROP

First consider the problem of "ground clutter" and "anomalous propagation". "Clutter" is a result of reflection of the radar beam from non-hydrometeor targets; for example the ground surface, tall buildings or trees. This can be seen in figure 5.1 (at 12 km and 19 km ranges). "Anaprop" (anomalous propagation) is a result of strong temperature and humidity gradients causing the radar beam to be refracted back to the surface, where non-meteorological targets reflect the beam. Anaprop can be especially difficult to distinguish with conventional radar (for example Pamment and Conway, 1998). However, both clutter and anaprop give rise to non-Rayleigh scattering so the amplitude and phase of horizontally and vertically polarised returns are uncorrelated. This means that these non-meteorological targets can be detected by use of L_{DR}. They have higher L_{DR} than occurs in natural precipitation Hagen (1997), as the opposite polarisation's reflectivity has similar size to that at the transmitted polarisation. Echoes from non-meteorological targets also have $\rho_{hh,vv}$ of near zero, where it is > 0.95 in rain, and this change is a result of the random nature of the returns from clutter targets. The problems of ground clutter are that these targets have an increased Z (leading to overestimates of the rainfall rate) and increased noise in Z_{DR}, fluctuating ± 3 dB from one gate to the next (effectively negating all information available about the target shape), so a simple L_{DR} threshold (for accepted data, $L_{DR} < -10$dB; this "catches" $\sim 90\%$ of clutter) is used to remove ground clutter points (see figure 5.2).

5.2.2 MELTING LEVEL

The next problem is that of the "bright band". This is the area where the snow flakes falling from a stratiform cloud melt (this explains an alternative name, the "melting layer") and occurs just below the 0°C isotherm. The bright band has an increased reflectivity relative to the rain below and ice above as the snow flakes have large diameters which, when melting, are covered in a "film" of water making them reflect like rain (water gives larger reflections than ice as the $|K^2|$ (dielectric factor) of ice is up to five times
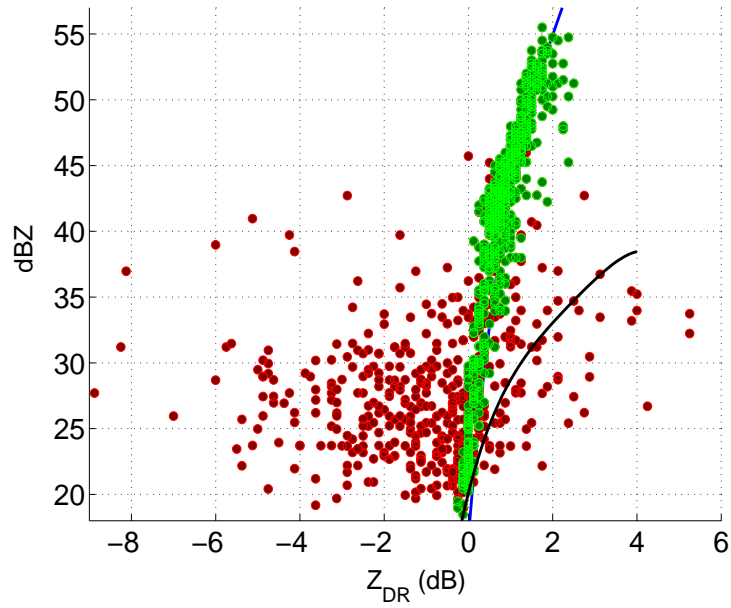
Figure 5.2 *Z-Z_{DR} plot from an area of rainfall data which is infected by clutter. The combined red and green pixels show the recorded data. The red pixels are those rejected by the L_{DR} thresholding, the green are those which are accepted. Also plotted for reference are the blue line of $N_{\mathrm{w}} = 8000$ mm^{-1} m^{-3} and the $Z_{\mathrm{1mm/hr}}$ line is shown in black.*

lower than that of water (1.4). The L_{DR} can be used to identify the melting snow flakes associated with the bright band (Frost *et al.*, 1991 and Straka *et al.*, 2000). This region is unsuitable for the Z/Z_{DR} technique as the melting flakes result in high Z (as much as 13 dB higher than the rain it melts into) and also an increase in Z_{DR}. Again the L_{DR} threshold (for accepted data, $L_{\mathrm{DR}} < -20$dB) is used to remove these points and points above the detected bright band are removed to avoid measurement in the ice, as shown in figure 5.3.

5.2.3 HAIL

Particularly during the summer time, hail can occur in convective events resulting in ice particles below the freezing level. Hail cannot be unambiguously identified using Z, Z_{DR} and L_{DR}, although, its presence will raise Z (due to larger particles). There will also be a reduction in the Z_{DR} recorded in the location of the hail (due to tumbling particles so
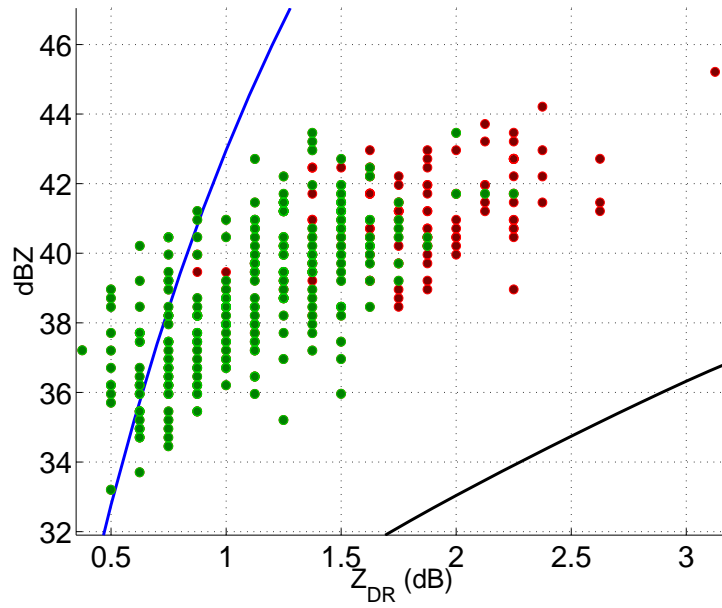
Figure 5.3 *Z-Z_{DR} plot from an area of rainfall data which is infected by melting snow from the "bright band". The combined red and green pixels show the recorded data. The red pixels are those rejected by the L_{DR} thresholding, the green are those which are accepted. Also plotted for reference is the blue line of $N_{\mathrm{w}} = 8000$ mm^{-1} m^{-3} and the $Z_{1\mathrm{mm/hr}}$ line is shown in black.*

no mean alignment), but larger positive values are observed in the area surrounding the hail (Bringi *et al.*, 1984). Smyth and Blackman (1999) suggested the best technique for identification of hail is the loss of consistency of the three variables, Z, Z_{DR} and ϕ_{DP} along a ray. Hail should be removed before an integrated Z/Z_{DR} technique is used.

Options to determine the appropriate N_{w} or a will now be considered.

5.3   AVERAGE POINT-BY-POINT RAINFALL RATES

This method would involve calculating the rainfall rate at each point from its individual Z and Z_{DR}, as per section 2.4.2. The data points are then plotted as $\log R$ against Z (figure 5.4). From this the best fit line to this data is calculated, but this poses a significant problem of how to determine this best fit. The very noisy nature of the data (especially in Z_{DR}) means that the data is not very highly correlated, meaning that the fit of Z against

R is rather different to a fit of R against Z. The solution is an "SD-fit", with slope given by the ratio of the standard deviation of Z and standard deviation of R, which passes through the mean of both data sets. See figure 5.4 for an example of this problem; the three lines show the two possibilities from correlation and the "SD-fit".
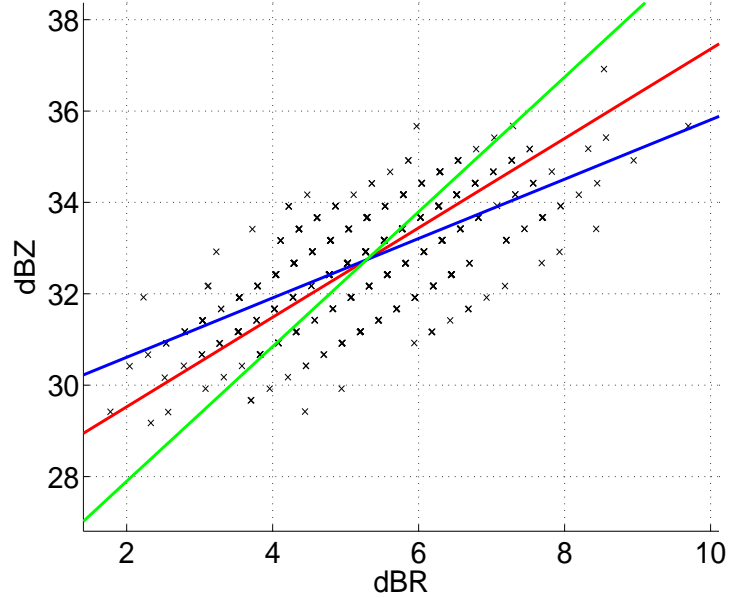
Figure 5.4 *An example of use of the average point-by-point rainfall rate method. This data is quite well correlated, although the lines showing the results from the 3 possible fits, (blue) for the fit of dBZ given $\log R$ [result: a=853, b=0.65], (red) the SD-line [result: a=572, b=0.98] and (green) the fit of $\log R$ given dBZ [result: 313, b=1.47], are quite different. When the correlation is lower (usually from small dynamic range) the differences in the three lines will be larger.*

Apart from issues with calculating R that will plague later possibilities, this method has a serious problem: for a given Z_{DR} both R and Z scale with N_{w}. This means that the result is biased, towards $b = 1$. This bias must be removed.

5.3.1 USING THE REFLECTIVITY FOR 1 MM HR^{-1}

The bias can be removed if Z_{DR} is converted to a variable that is not dependent on Z but can easily give the result of a and b. The answer to this problem is to use $Z_{1\mathrm{mm/hr}}$, which is defined as the reflectivity that would have a rainfall rate of 1 mm hr^{-1}. This is

dependent on Z_{DR} and is calculated by the formula given by Illingworth and Blackman (2002):

$$Z_{\text{1mm/hr}} = \frac{Z}{R} = 21.48 + 8.14\, Z_{\text{DR}} - 1.385\, (Z_{\text{DR}})^2 + 0.1039\, (Z_{\text{DR}})^3. \tag{5.8}$$

From $Z_{\text{1mm/hr}}$ it is trivial to calculate the rainfall rate,

$$dBR = dBZ - dBZ_{\text{1mm/hr}} \tag{5.9}$$

noting that $R = 10^{dBR/10}$. It was noted in section 2.4.2 that the calculation could be improved by use of $Z_{\text{1mm/hr}} = f(\log_{10} Z_{\text{DR}})$. This is formulated as

$$Z_{\text{1mm/hr}} = \frac{Z}{R} = 1.3910\, (\log Z_{\text{DR}})^3 + 6.3556\, (\log Z_{\text{DR}})^2 + 12.6032\, (\log Z_{\text{DR}}) + 28.6576. \tag{5.10}$$

Once $Z_{\text{1mm/hr}}$ is calculated this is plotted against dBZ (figure 5.5), and this data fitted. This plot does not have the scaling dependence the $\log R$ against dBZ plot has, as $Z_{\text{1mm/hr}}$ is effectively a rescaling of the Z_{DR} data. The fit obtained has the form

$$dBZ = m Z_{\text{1mm/hr}} + c. \tag{5.11}$$

From this the a and b must be derived. Starting from

$$Z = aR^b;$$

convert into decibels,

$$dBZ = 10 \log a + b\, dBR. \tag{5.12}$$

From combination with equation 5.9 this leads to

$$dBZ = 10 \log a + b\, dBR + b\, dBZ_{\text{1mm/hr}},$$

therefore;

$$dBZ(1 - b) = 10 \log a + b\, dBZ_{\text{1mm/hr}},$$

hence;

$$dBZ = \left(\frac{-b}{1-b}\right) dBZ_{\text{1mm/hr}} + \frac{10 \log a}{1-b}. \tag{5.13}$$

Compare this with equation 5.11, resulting in:

$$m = \frac{-b}{1-b} \tag{5.14}$$

and

$$c = \frac{10 \log a}{1-b}. \tag{5.15}$$

Equation 5.14 leads to

$$b = \frac{m}{m-1} \tag{5.16}$$

and equation 5.15 gives

$$10 \log a = c(1-b).$$

Using equation 5.16 this leads to

$$1 - b = 1 - \frac{m}{m-1} = \frac{m-1}{m-1} - \frac{m}{m-1} = \frac{m-1-m}{m-1} = \frac{-1}{m-1} = \frac{1}{1-m}$$

so

$$10 \log a = \frac{c}{1-m}. \tag{5.17}$$

So from the fit in $Z/Z_{\text{1mm/hr}}$ space, equations 5.17 and 5.16 can be used to calculate the $Z\text{-}R$ relationship parameters a and b.

This method is an improvement in that the bias caused by scaling of Z and R has been removed, and the two axes being fitted are now genuinely independent. There does however remain a rather serious problem, and one that will be yet more serious in the operational environment, negative Z_{DR}. This was discussed in section 2.4.4, and would mean any points of negative Z_{DR} must be "left out" as a $Z_{\text{1mm/hr}}$ would not be calculable for negative values of Z_{DR}. Leaving out the points will non-uniformly remove some data points, removing one side of the distribution of data, but not removing the opposite (positive) extreme. This will bias derived results, which will be serious especially in low rain.

5.4 BANDING THE DATA

An option to counter negative Z_{DR} is to "band" the data to create averaged points with far reduced errors, hence considerably less likely to give a negative Z_{DR}. It is important
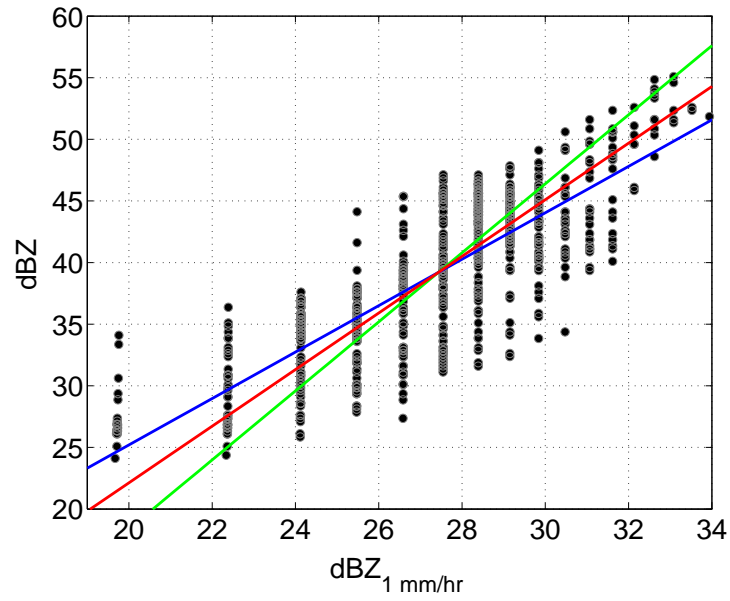
Figure 5.5 *An example of use of point-by-point $Z_{1\text{mm/hr}}$ rainfall rate method. The lines show the results from the 3 possible fits, (blue) for the fit of dBZ given $Z_{1\text{mm/hr}}$ [result: a=24, b=2.1], (red) the SD-line [result: a=80, b=1.8] and (green) the fit of $Z_{1\text{mm/hr}}$ given dBZ [result: 181, b=1.6].*

to remember that most of the error is in Z_{DR} and not Z. To maintain information on the distribution of the data it is best to band by number of points rather than Z value; to demonstrate this see figure 5.6. The banding is performed by sorting the data by Z, and the first 20 points are selected, averaged in Z and Z_{DR} to create the new data point which is saved. Then the process is repeated for each group of 20 consecutive points to create banded data to be used for calculation. The chosen value of 20 points is variable, chosen to maximise the number of data points remaining, but making negative Z_{DR} in the newly created data uncommon.

The banded data is then used to calculate $Z_{1\text{mm/hr}}$ and calculate the Z-R relationship to be used as in the previous section (5.3.1). The rare banded points with negative Z_{DR} will no longer cause the bias problem; these points incorporate an average and hence both extremes of the data are ignored. There does still remain a problem: by averaging both Z and Z_{DR} the variation in the two is not being fully implemented where the data density is low. Where there is a large spread of Z within a band, the Z_{DR} spread will
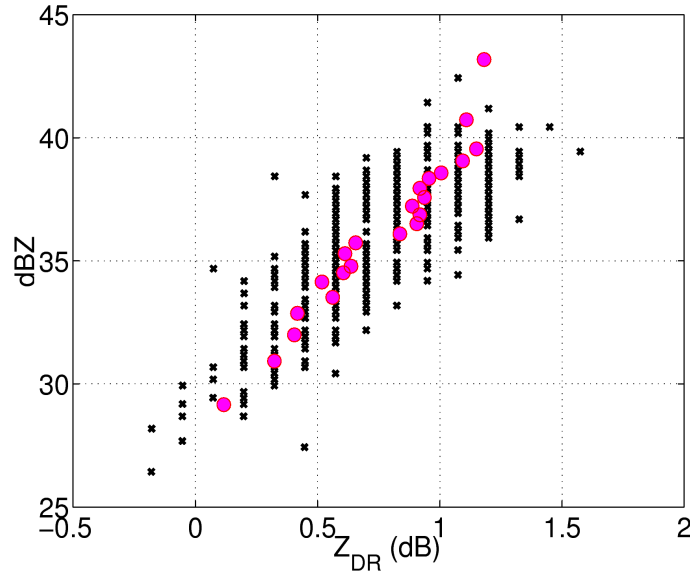
Figure 5.6   *An example of Z_{DR} against Z, demonstrating the banding technique. Every 20 data points (black x) are averaged to create the smaller, less error prone, data (pink o). It can be seen that banding has removed the points of negative Z_{DR}. This reduced data is then used for calculation of a and b.*

inevitably be increased and biased due to the curvature of constant N_{w} lines. Where the changing curvature of the Z/Z_{DR} line is high, this will have the largest effect of biasing the averaged point.

5.4.1   CONSISTENCY

The methods described thus far all calculate values of a and b, and often the derived values vary in an unphysical way. This is caused by there not being sufficient dynamic range in the data to determine both variables, as b is essentially a slope and a essentially an intercept parameter, and changing b changes a, but the effect of the change in the derived rainfall rate is small. The highly varying a will give us no physical interpretation of the underlying processes, being masked by the variations in b resulting from the small dynamic range in available data. Section 5.1.1 demonstrated that b changes represent the relationship between drop size distribution parameters N_{w} and D_{o}.

The noise in the Z_{DR} data and common lack of dynamic range of data mean there

is little signal to detect the second mode of variation (b). The difficulty of detecting the signal of the variations in b mean that an assumption of b must be made. Hence it will be assumed that N_{w} remains constant over small areas, and the technique considered will calculate what the N_{w} is over the small region. This is a very similar to the assumption of Testud *et al.* (2000), although in that paper the assumption is made over long radial sectors (see figure 4 of Le Bouar *et al.*, 2001), and physically it is less likely that N_{w} remains constant over these large radial regions than more square regions of similar area.

Using the normalised gamma distribution of raindrop sizes and drop shape functions (section 2.3), expected values of Z and Z_{DR} can be derived for any combination of drop spectrum parameters. This means that the expected position of points in Z/Z_{DR} space for rainfall of constant N_{w} can be calculated, figure 5.7. The figure shows clearly that Z scales with N_{w} and that N_{w} changes do not effect Z_{DR}. To estimate N_{w} over a region (and hence a) the most appropriate curve similar to the red curves of figure 5.7 must be found.
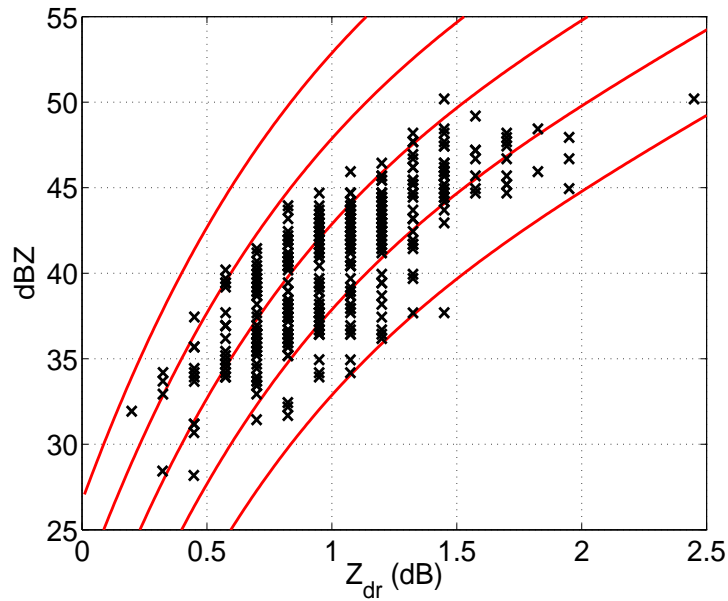
Figure 5.7 *An example of an area of data Z/Z_{DR} points (x) with lines of constant N_{w} (red line) these are for 800, $2\,500$, $8\,000$, $25\,000$, $80\,000$ mm^{-1} m^{-3}, lowest values to the lower right, higher to the upper left. A method to determine which of these lines is most appropriate for this data is needed.*

All the suggested methods to this point could work to only calculate the value of a. However these would be functioning simply as a large scale average of the Z_{DR} over the region, losing some of the possible benefits of the Z_{DR} data. A method to utilise the individual data points to find the most appropriate N_{w} value is used, hence a to use over the region.

5.5   OPTIMISED Z/Z_{DR} FIT

All of the previous methods could have the restriction in the value of b incorporated, although the assumption that N_{w} remains constant over the small regions considered means that the calculation of a can be made directly from the Z and Z_{DR} data. Given the relationship between D_{o} and N_{w} (b) the position of "true" (having no sampling error) points in Z/Z_{DR} space can be calculated for any chosen value of N_{w} (using assumed drop shapes and fall velocities) or a. This means the measured data (which has the large sampling noise) can be compared to lines of constant N_{w} (see figure 5.7) to find the line which is most appropriate to the data of the selected region. The chosen line will have the smallest residuals assuming the error is all in Z_{DR}, so Z error is negligible. This technique will give equal weight to data with negative Z_{DR}, yet remain stable. It will be described in far more detail in the remainder of this chapter.

5.5.1   REFLECTIVITY/DIFFERENTIAL REFLECTIVITY SPACE

The values of data Z and Z_{DR} observed within the chosen region (Z and Z_{DR} data shown in figure 5.8 show an example of such data; in this case it is a 5×5 km box containing vigorous cold frontal rain) can be plotted in Z-Z_{DR} space (this is shown in figure 5.9).

In figure 5.9 the line plotted for a drop spectrum of constant $N_{\text{w}} = 8000 \text{ mm}^{-1}\text{m}^{-3}$ and $\mu = 5$ is shown, allowing only the median drop diameter (D_{o}) to increase for higher rainfall rates. This line is calculated from the raindrop sizes of Andsager *et al.* (1999) and the normalised gamma spectrum to calculate theoretical radar returns.

(a) dBZ **(b)** Z_{DR} (dB)
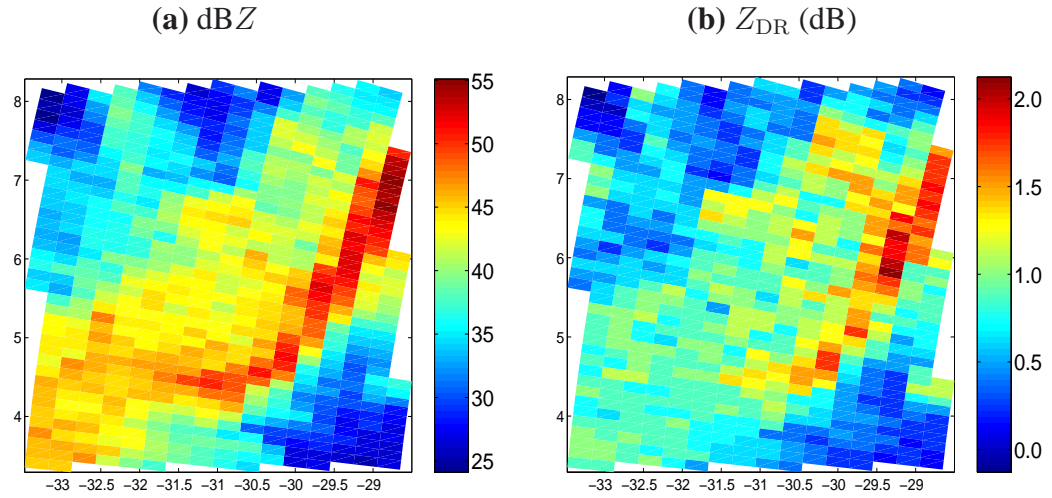
Figure 5.8 *A 5×5 km box of (a) reflectivity (dBZ) and (b) differential reflectivity (Z_{DR}) data. This box is located in an area of vigorous frontal rain approximately 35 km from the antenna. Axis numbering is in km from the radar.*
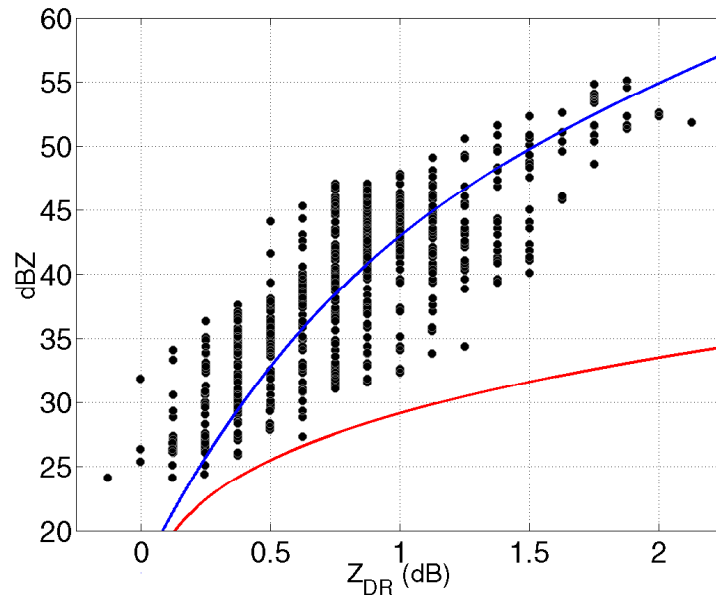
Figure 5.9 *dBZ plotted against Z_{DR} for the data in figure 5.8. The blue line shows the line of constant N_{w} of 8000 mm^{-1}m^{-3} and constant μ of 5. This data shows that N_{w}=8000 mm^{-1}m^{-3} is a good fit to this particular data. The red line shows the line for 1 mm hr^{-1} rainfall rate, assuming $\mu = 5$.*

Points moving vertically in Z-Z_{DR} space are altering the drop concentration, N_{w}. Movement upwards implies higher concentrations (hence larger rainfall rates); downwards is for reducing concentration (lower rainfall rates). Horizontal motion is for changes

in the median drop size: higher Z_{DR} implies larger drops; smaller Z_{DR}, smaller drops. The figure also shows the spread of data as a result of the Z_{DR} sampling errors.

5.5.2   OPTIMISING TO FIT DATA

Chapter 2 discussed the problems that occur as a result of noisy Z_{DR} in section 2.4.3. Our method of overcoming the high noise levels is to assume that the natural drop spectra properties do not change over the small areas which are being considered. This clearly leads to a compromise, as the area must be large enough to reduce the noisy Z_{DR} signal sufficiently for an accurate estimate of the drop concentration, but keep the area considered to a minimum to reduce the magnitude of natural variations. The size of the boxes to be used will be discussed later in this chapter in section 5.6.2.1.

To describe the method of estimating the drop concentration of the rainfall in the selected region, a graphical approach will be used, as shown in figure 5.10, on page 97. After selecting the data from the chosen region, the scatter of Z and Z_{DR} is examined; see plot (a). The estimate of N_{w} required is gained from the position of this data relative to lines of constant N_{w}. A line of constant N_{w} has the form of the red line in plot (b); the optimum line of this form to fit the data is to be found. As the error in Z_{DR} is high relative to the signal, Z_{DR} error will almost exclusively be dominant over Z error, therefore the errors in Z will be neglected. The horizontal residuals from the attempted fit (red line) are calculated as shown (in blue) in plot (c). The mean square residual is used to measure how well the curve matches the data. Hence, by allowing only N_{w} to vary, to calculate the best fit to the data the minimum mean square residual is found. Increasing the drop concentration does not alter Z_{DR}, although reflectivity scales with the change. This means that doubling the drop concentration moves the curve in Z/Z_{DR} space only by doubling in the Z direction (a gain of 3 dB). Plot (d) shows some examples of lines of different drop concentrations. An iterative approach is used to find the best N_{w} (with lowest mean square residual), $N_{\text{w}}^{\star}$ for the data (plot [e]). This assumes that the raindrop size spectrum shape parameter, μ, is constant. Changes in μ have a similar effect in Z/Z_{DR} space to changes in concentration, so μ variation may be mistaken as a drop

concentration change, this was seen in section 3.2.3. This means that the true spectrum concentration is equal to $N_w^\star$ only when $\mu = 5$. The derived $N_w^\star$ is then passed to the equation

$$a = 138\sqrt{\frac{8000}{N_w^\star}}, \tag{5.18}$$

for $\mu = 5$. Or

$$a = 218\sqrt{\frac{8000}{N_w^\star}}, \tag{5.19}$$

when $\mu = 0$ to calculate a of the chosen area. The rainfall rates of individual pixels are then calculated using $Z = aR^{1.55}$.

5.6 THE INTEGRATED REFLECTIVITY/DIFFERENTIAL REFLECTIVITY TECHNIQUE: ALGORITHM

Before passing to the integrated Z/Z_{DR} technique the area of data to be analysed must be selected. The selected data has thresholds applied to remove data from non-rain targets. At this point it must be decided if enough data from rain is present, assuming enough rain pixels N_w and a are estimated, else the region is defined as unsuitable and passed to the categorisation for the reason for rejection. These basic steps are shown in the form of a flowchart in figure 5.11.

This section will consider the implementation of each of these steps in more detail.

5.6.1 APPLYING THRESHOLDS

The fits to Z/Z_{DR} data rely on the use of data only from rain, as was examined in section 5.2. Data passed to this point of the algorithm will contain points with non-rain origin which must be removed. For data from the Chilbolton radar this removal is done by clearing all data with L_{DR} greater than -20 dB, hence removing clutter, anaprop and melting snow. Data beyond the detected bright band is also removed as ice (which will not have the same drop shapes as liquid water). At low rainfall rates Z_{DR} will have no
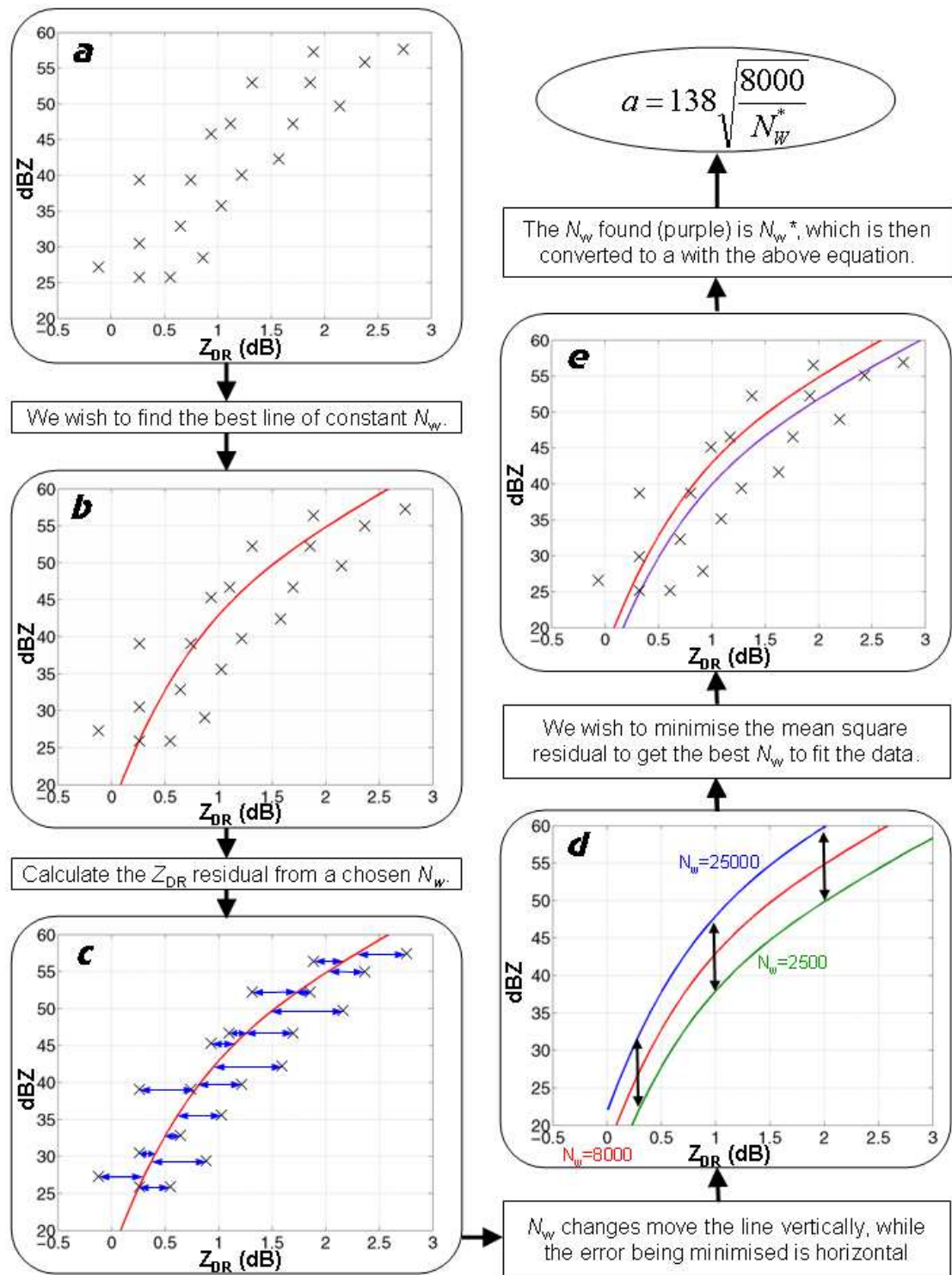
Figure 5.10   *Flowchart of the steps to estimate N_w and a.*
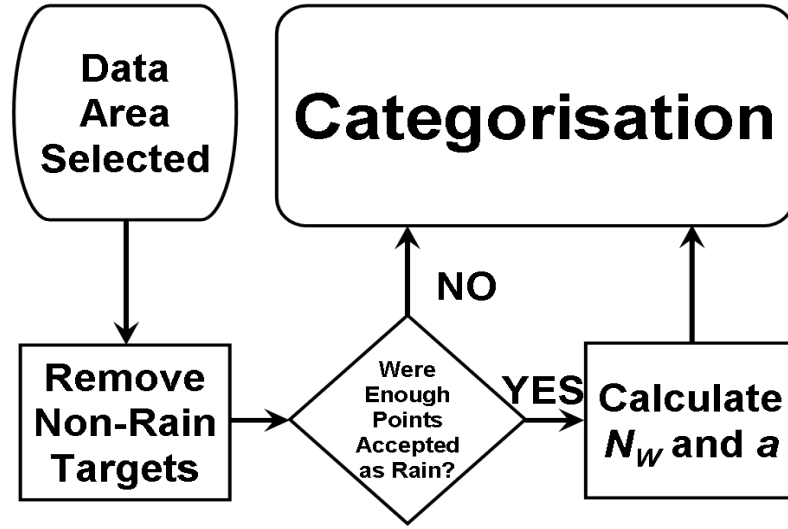
Figure 5.11 *Flowchart of the basic steps of the integrated Z/Z_{DR} technique .*

signal and begin to suffer from problems related to the signal to noise ratio. Rain too light for this technique is removed by accepting only data of greater than 20 dBZ (this is too low, so Z_{DR} will be 0 dB or very close to it for all but the most extreme DSDs). The data that was accepted as moderate to heavy rain is then passed on.

5.6.2 CALCULATING 'a'

5.6.2.1 HOW MUCH DATA IS NEEDED?

For accurate (25%) rainfall rates at $3-10$ mm/hr Z_{DR} must be accurate to 0.1 dB. Assume an error in Z_{DR} of σ_{point} and that N points are to be considered. This means that these points have total error:

$$\sigma_{total} = \frac{\sigma_{point}}{\sqrt{N_{samp}}}. \tag{5.20}$$

Hence the number of points required for 0.1 dB accuracy is

$$N_{req} = \left(\frac{\sigma_{point}}{0.1}\right)^2. \tag{5.21}$$

So when considering the CAMRa radar (where $\sigma_{point} \approx 0.2$ dB), to achieve the required accuracy, the average of 4 points is required (for an operational radar this number is much larger, ~ 25, depending on accuracy). The plot showing the required points for different values of the error is shown in figure 5.12. Unless this required number of points is met, accurate estimates of N_{w} and a are not possible and the chosen region must be rejected for the technique.
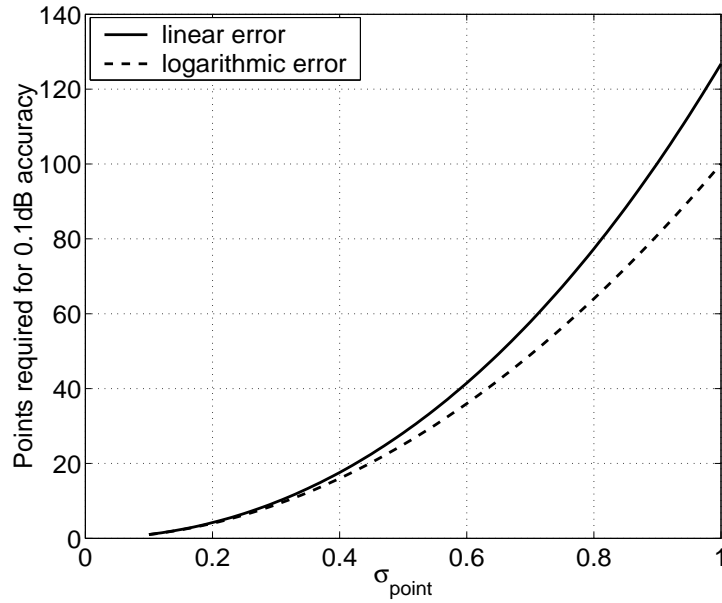
Figure 5.12   *The required number of points for different errors in Z_{DR}.*

To demonstrate this, real radar data is used. For this a section of data points of extent with 64 pixels in range and azimuth is selected. This sector of data is then used to calculate a and N_{w} with grid resolutions from 4096 pixels to just 4 pixels. The resultant values of N_{w} are shown in figure 5.13. The figure shows that at lower resolutions the reduced resolution simply averages out any underlying signal present with averaging. The highest resolution plotted is on the limit of accuracy suggested numerically, and it can be seen that this data predominantly shows signal, possibly with small amounts of noise present. This shows that very small grid resolutions can be used with Chilbolton data as expected since the Z_{DR} is very accurate. However, it would be interesting to see the result when noise is added to the data to simulate an operational radar. To do this
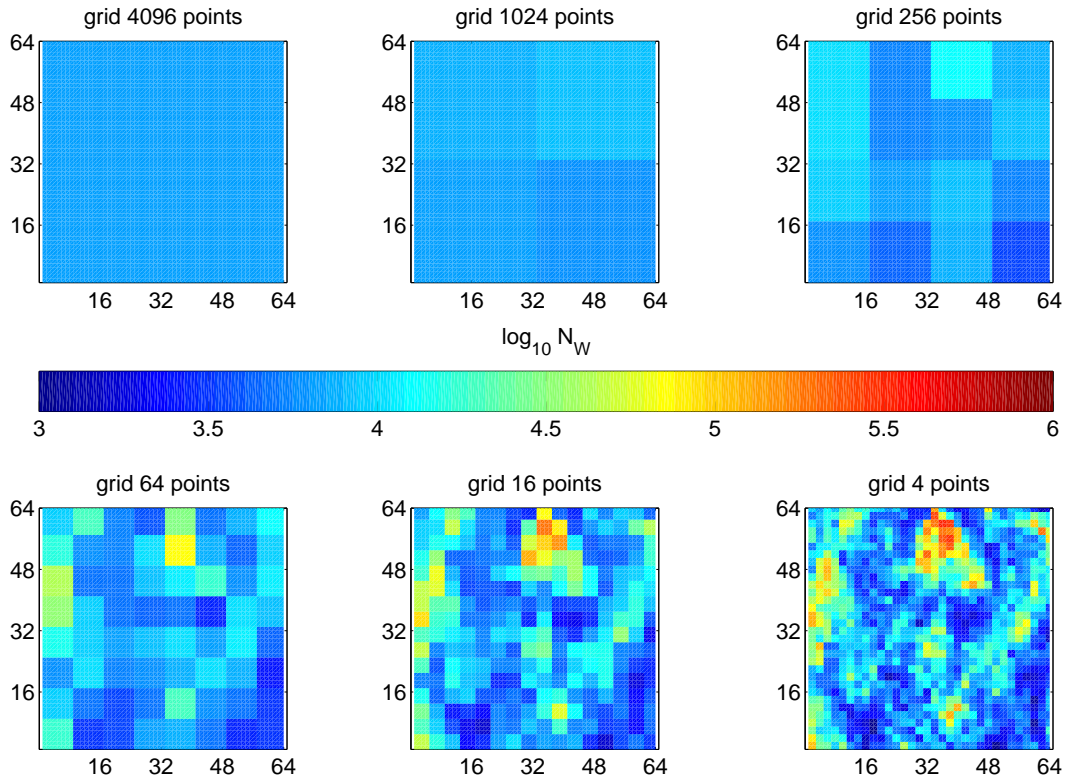
Figure 5.13 *Colour plots showing the N_w calculated from grid of various sizes. The data used was taken with the accurate CAMRa radar, where each pixel has range of 300 m and has $0.28\,^{\circ}$ in azimuth at a range of 50 km (so pixels are near square). The grid scales are [top left] ~ 20 km, [top centre] ~ 10 km, [top right] ~ 5km, [lower left] ~ 2.5 km, [lower centre] ~ 1.2 km, [lower right] ~ 0.6 km.*

Gaussian noise of 0.5 dB is added to the Z_{DR} data of figure 5.13. The procedure is then repeated to yield figure 5.14. This figure shows similar values to that without noise for the top plots and lower left. However as would be expected, the noise in Z_{DR} has generated large noise levels in estimated N_{w} when 4 points are used and is still noisy at 16 points. This shows that to achieve good accuracy, but to avoid unnecessary smearing of the data, with a 0.5 dB Z_{DR} error one must estimate N_{w} over a grid size of ~ 64 points. It is worth noting that the area this many points covers would be dependent on radar resolution.
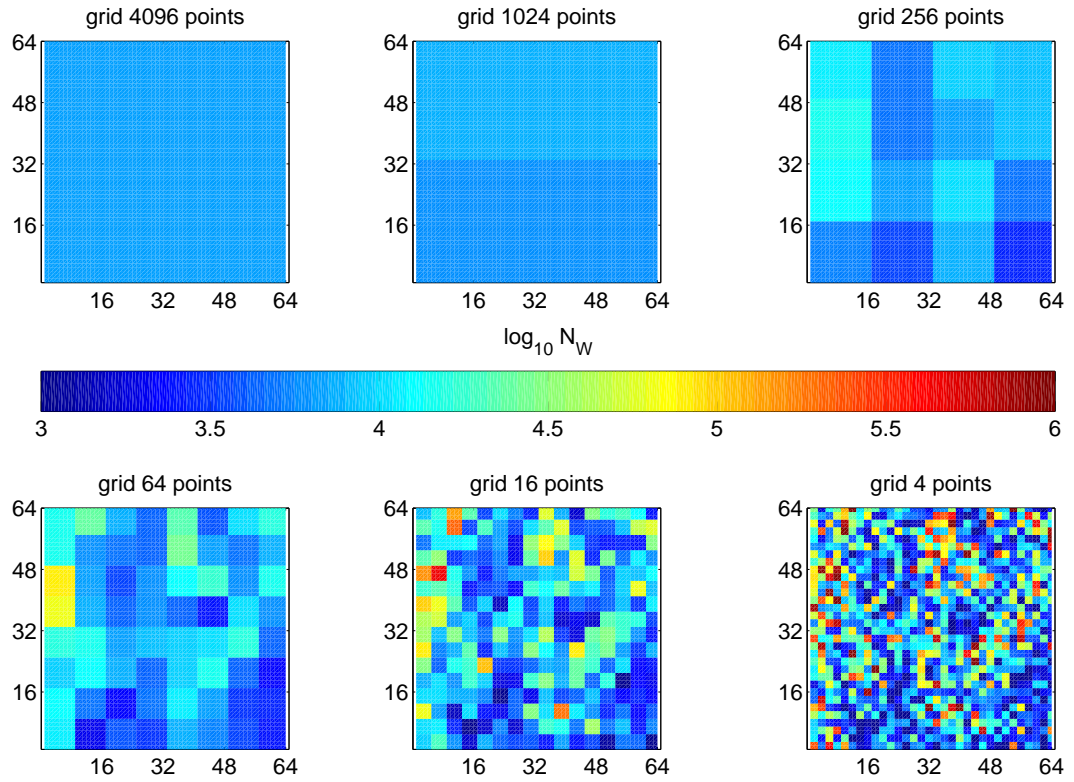
Figure 5.14 *Colour plots showing the N_w calculated from grid of various sizes. The data used was taken with the accurate CAMRa radar but with 0.5 dB Gaussian noise added to Z_DR, where each pixel has range of 300 m and has $0.28\,^\circ$ in azimuth at a range of 50 km (so pixels are near square). The grid scales are [top left] ~ 20 km, [top centre] ~ 10 km, [top right] ~ 5km, [lower left] ~ 2.5 km, [lower centre] ~ 1.2 km, [lower right] ~ 0.6 km.*

5.6.2.2 ITERATING TO FIND DROP CONCENTRATION

Section 5.5.2 and figure 5.10 described the theory behind estimating N_w but not how this is achieved algorithmically. N_w is estimated iteratively, starting with wide bounds on the possible values of N_w. These are reduced until the best N_w is achieved. At each stage of the iteration the bounds are evenly divided into N values of T, where T is a value related to N_w via the equation:

$$N_W = 8000 \left(10^{\left(\frac{T-16.67}{10} \right)} \right);$$ (5.22)

the first and last T corresponding to the maximum and minimum N_w (T is used for speed of the algorithm, but is essentially a scaling of N_w). For each value the theoretical curve

of constant N_{w} is calculated, using the polynomial:

$$dBZ = -0.472 \left(\log Z_{\mathrm{DR}}\right)^4 + 4.65 \left(\log Z_{\mathrm{DR}}\right)^3 - 17.79 \left(\log Z_{\mathrm{DR}}\right)^2 + 39.81 \left(\log Z_{\mathrm{DR}}\right) + T,$$

(5.23)

applicable at S-band (the effect of T is a displacement only in the Z direction), so as to calculate the root mean square error in the Z_{DR} direction. The minimum root mean square is found and maximum and minimum points are set to the values of N_{w} either side of that with lowest least square; see figure 5.15. The same process is repeated until N_{w}
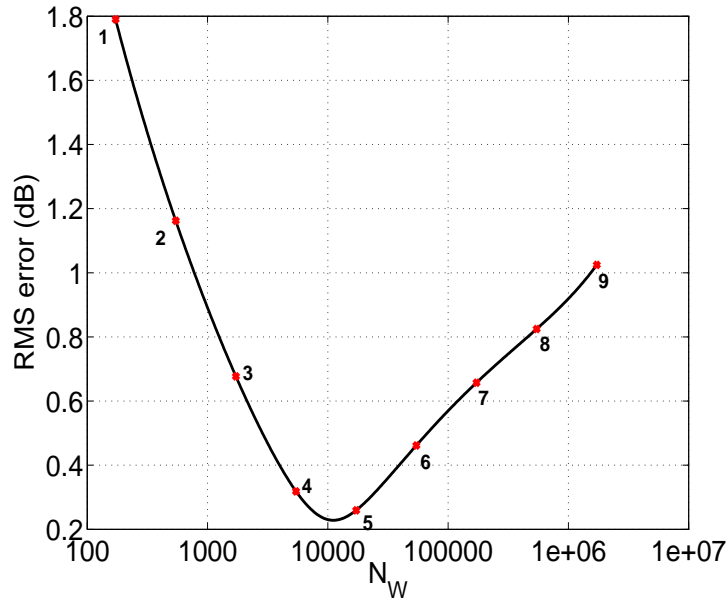
Figure 5.15 *The curve showing the method of estimating the optimal N_{w}. This case is the first iteration showing the 9 trial points. The best of the nine is **5**, so the algorithm is reset with minimum at **4** and maximum at **6**.*

is found to a suitable accuracy. The whole method is described in the flowchart of figure 5.16. For optimal speed 9 values of T are chosen per iteration (this number performs the least calculations of RMS error to achieve required accuracy in T, N_{w} or a).

5.6.3 REJECTION

It is important to know whether the output from the integrated Z/Z_{DR} technique was reliable for each point and the causes of any unreliability. A number of problems will
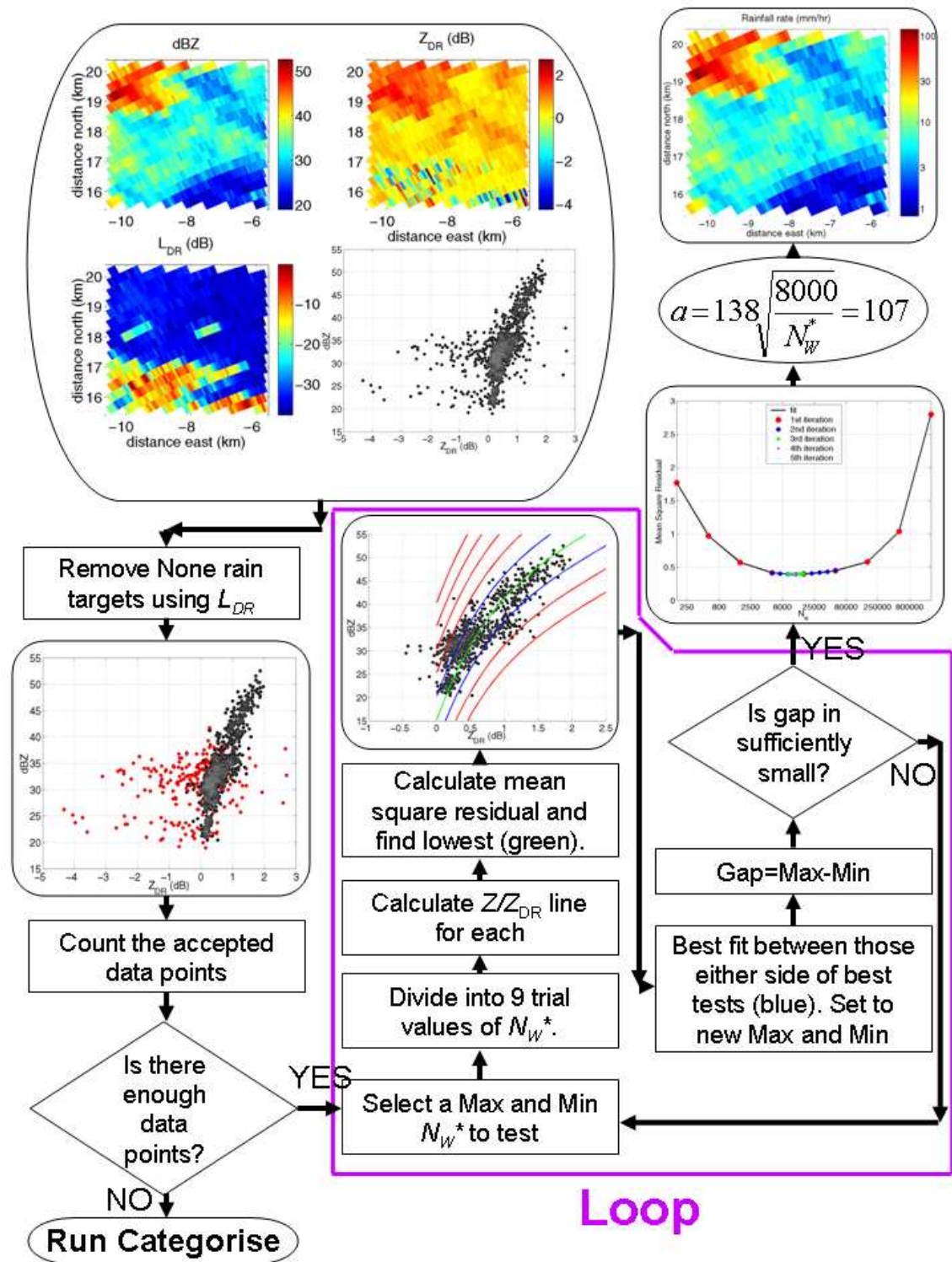
Figure 5.16 *Flowchart of the integrated Z/Z_{DR} technique.*

lead to an unreliable result; most importantly will be a lack of data points confirmed as from rain. However a rejected result may be able to indicate the cause of the failure and hence suggest other methods for rainfall calculation (for instance areas of attenuation would be suitable for the ZPHI technique of Testud *et al.*, 2000). The rejections and possible responses are shown in table 5.1.

No rain	areas with no signal	No rainfall calculation is needed
Clutter	$> 50\%$ clutter/anaprop	A correction scheme should be applied
Bright band	Area in the melting snow	VPR correction
Light rain	$Z < 25$ dBZ	Use default Z-R method.
Attenuated	Where ϕ_{DP} is significant	Apply the ZPHI technique
Not enough data	< 25 good pixels	Use a standard method.

Table 5.1 *The options for rejection of the result of the ZPHI technique, the causes of the rejections and possible responses.*

It is important to recognise what options can be taken from a rejected result. Areas without rain need to be examined to determine whether this was caused by no precipitation, or data rejected as clutter or above the bright-band for example. In areas of light rain the Z_{DR} signal will be too small for reliable use, so a more basic Z formulation is needed. Where the technique identifies that the signal has suffered from attenuation, a phase shift should have occurred. In this case the alternative methods are used.

5.6.4   USE OVER SCANS

When run, the technique returns values of a and also returns a rejection number, indicating whether the data was rejected and the reason if it was. When run repeatedly over a PPI scan, a plot as in figure 5.17 can be made showing the changing a, calculated rainfall rates and rejections.
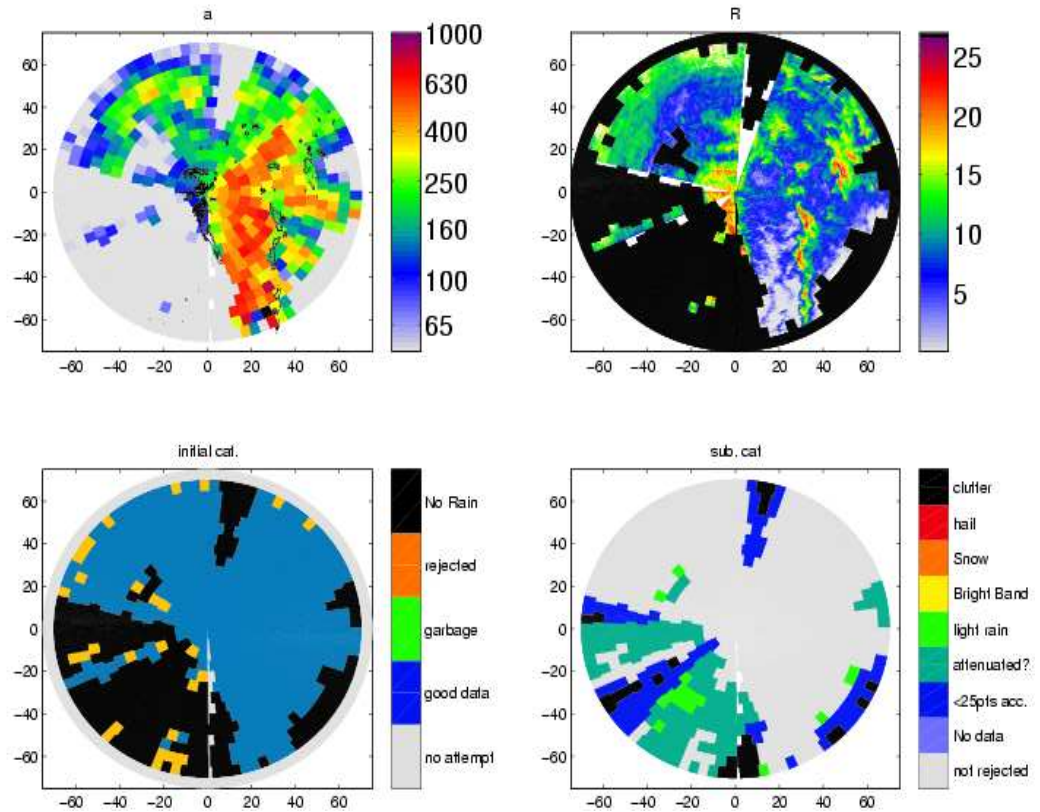
Figure 5.17 *The final output from running the Integrated $Z/Z_{\mathrm{DR}}/$ Technique with 5 km resolution from a PPI. The top-left shows a, top-right R calculated from the technique, with areas rejected blanked out. The bottom panels show rejection and the reasoning in two plots.*

5.7 RETURNING b VARIATION

As was explained in section 5.4.1, b has been set as constant for the calculation of a, but naturally b may vary. However there is often too small a dynamic range of data to adequately measure b, resulting in undesirable unphysical b despite the calculated rainfall rates being reasonable. It is possible to allow b variation into the optimised technique, as changing b changes the N_{w} to D_{o} relationship and hence the Z/Z_{DR} curve, although the effect of a remains only a change in Z (no Z_{DR} change), so the best a can be calculated for any b. To determine b, the best a is calculated for several reasonable values of b, noting the RMS residual of each optimal a. The optimal relation is then the a and b

combination with lowest RMS residual, selecting the optimal b if significantly different from 1.5. Some examples of this are shown in figure 5.18.
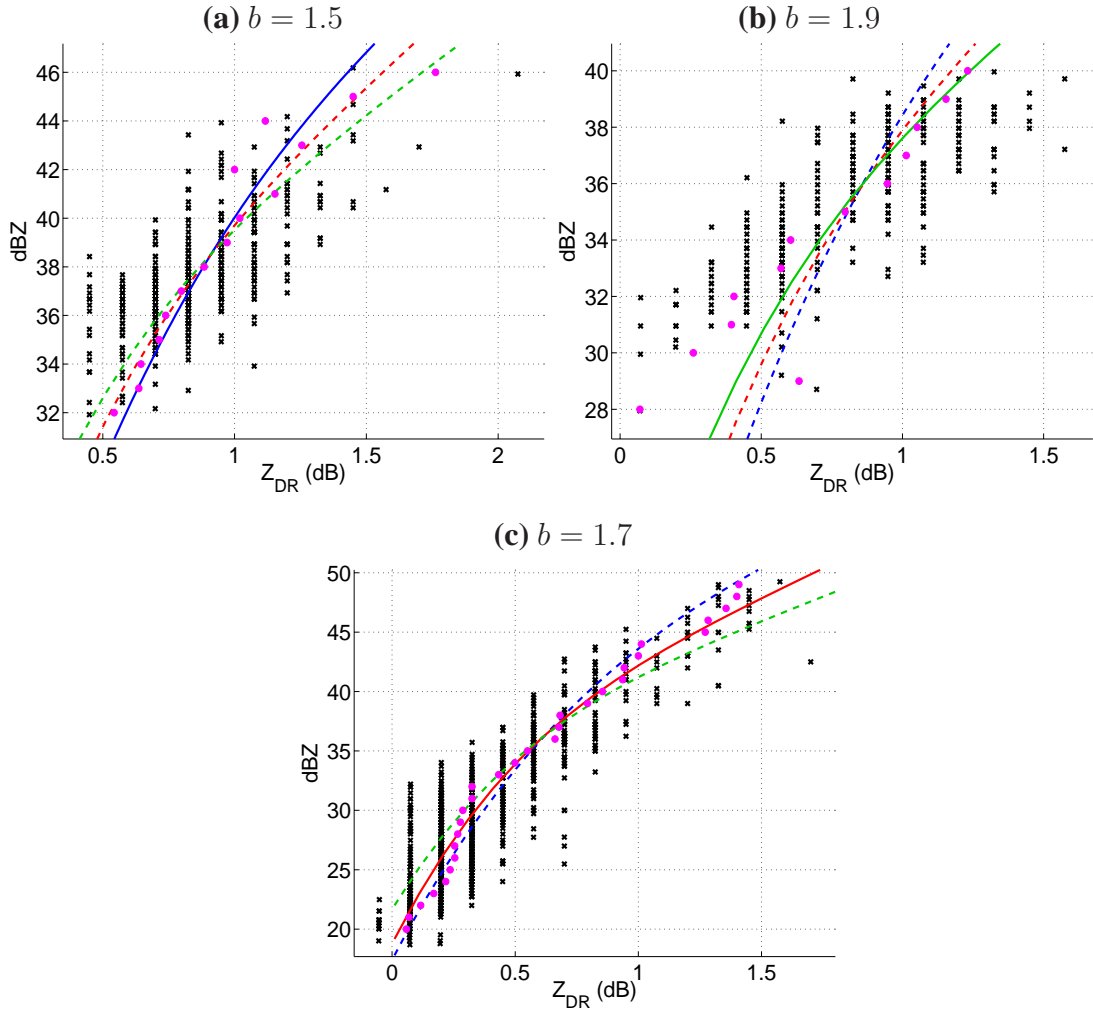
Figure 5.18 *Examples of the optimised selection of b. The black crosses show the data, pink circles show banded Z for ease of comparison to the lines (note these are not used by the algorithm and are purely a visual aid). The coloured lines show the best fit for the respective value of b, blue $b = 1.5$, red $b = 1.7$ and green $b = 1.9$.*

5.8 SUMMARY

This chapter has examined the potential of using Z and Z_{DR} over an area to estimate the rainfall rates, hence utilising the signal available from Z_{DR}, but not greatly suffer-

ing from the high noise levels in its measurement. The chapter started with a return to the normalised gamma distribution of raindrops, where it was shown that, assuming N_{w} remains constant the rainfall is calculated using $Z = aR^{1.5}$, where a is inversely proportional to the square root of drop concentration. This means that if the data within the chosen area can be used to estimate N_{w} (assuming μ remains constant), the value of a can be estimated for use in calculating rainfall rates. When the rain does not have constant N_{w}, but N_{w} is related to D_{o}, the exponent of equation 5.2 deviates from 1.5. When concentration increases with median drop diameter the value of b is lowered (as suggested for convective rain), and when concentration decreases as drop sizes increase, b is raised (as often used for stratiform rain).

It is important to remove data points that come from non-rain targets as the data will have unexpected and potentially extreme values of either Z or Z_{DR} (depending on what the scattering targets are). The problems of various non-rain targets were discussed in terms of the effect on Z and Z_{DR}. The removal of these non-rain points is considered, most being removed by a strict L_{DR} threshold of -20 dB. Hail can be removed by identification of regions where Z, Z_{DR} and ϕ_{DP} lose their consistency.

Given that the aim is to find a (or N_{w} which is related to a) from the data of the chosen area, a number of possibilities are considered. The first method examined was that where the rainfall rate is estimated from each point individually, then the fit of $\log R$ against Z is used to estimate a and b. Unfortunately, there are several problems, such as the poor correlation of the plot making the fit difficult to justify and the result is biased toward $b = 1$. To remove the bias, a fit between Z and $Z_{\mathrm{1mm/hr}}$ (the reflectivity that would correspond to 1 mm/hr rainfall given the observed Z_{DR}) is considered. Fits in Z and $Z_{\mathrm{1mm/hr}}$ space are shown to be related to a and b and do not have the bias, but retain problems from the low correlation. Both of these methods had issues when Z_{DR} is negative, as the unphysical Z_{DR} cannot be used as $Z_{\mathrm{1mm/hr}}$ cannot be calculated. However the negative values form part of the distribution of Z_{DR}, so their removal will introduce a bias.

To remove the bias caused by negatively observed Z_{DR}, the data may be "banded", creating averaged data from the true underlying data, with reduced noise in Z_{DR}, which

is hence less likely to be negative and, if it is, will remove both ends of the Z_{DR} spread. This data that results from banding is used as true data in the $Z_{\mathrm{1mm/hr}}$ method. This method suffers when the variation in Z is large: any band will contain a spread of Z values; the larger the spread the larger the variation in the true Z_{DR} (the value before the sampling noise).

All of these methods generate unphysical variations in a and b when the dynamic range of data is small (although retain good estimates of rainfall). It would be preferable for the values to be more meaningful before rainfall calculation. The large noise in Z_{DR} means the signal corresponding to the second mode of variation (b) is often too small to detect. It is therefore assumed that b remains constant at 1.5, the same assumption as in the ZPHI technique of Testud *et al.* (2000) but the assumption in this work is less strict as the distances with no variation are smaller. This assumption leads to the method of an optimised Z/Z_{DR} fit. Given a constant N_{w} (and assuming μ remains constant), values of Z and corresponding Z_{DR} can be calculated. The optimised Z/Z_{DR} fit will be a line of constant N_{w}, which has the minimal deviation from the data. The method introduced the effective drop concentration, $N_{\mathrm{w}}{}^{*}$, which is derived (it is effective as μ changes are disguised within). $N_{\mathrm{w}}{}^{*}$ is then utilised to estimate R. The algorithm was described and amount of data required for suitable accuracy is considered. Rejection of unreliable results is important, so a rejection method is considered, which not only indicates an unreliable result, but indicates possible other methods for calculating rainfall.

The chapter concludes with a brief discussion of the possible return to allowing b to vary, but within the optimised Z/Z_{DR} method, adjusting when the evidence for the change is available. The following chapter will discuss use of this optimised Z/Z_{DR} method and the results it yields.

CHAPTER 6:
THE INTEGRATED
REFLECTIVITY/DIFFERENTIAL
REFLECTIVITY TECHNIQUE:
RESULTS

6.1 EXAMPLES AND DEMONSTRATIONS

In this chapter the use of the integrated Z/Z_{DR} technique will be studied via a number of examples of its use.

6.1.1 EXAMPLE 1: FULL RUN-THROUGH

First a region of data of size 25 km^2 is selected; for this example the Z and Z_{DR} data is shown in figure 6.1. The first step will be to check for non-rain targets in this area with an L_{DR} threshold of -20 dB. For this example all points pass and are accepted as rain.

Now this data will be used to find the optimal drop concentration via iteration. For each value of N_{w} to be tested the Z and Z_{DR} values expected are calculated. Each point is then considered to be measured correctly in Z, hence the residuals from our calculated line and each point are calculated by the difference in the point's Z_{DR} and the expected Z_{DR} for that Z. The mean square residual is calculated for comparison with other chosen N_{w} values.

The steps of the iteration are shown in table 6.1 closing on to a value of $N_{\mathrm{w}} = 10000 \text{ mm}^{-1} \text{ m}^{-3}$. The Z/Z_{DR} line for this drop concentration is plotted over the data

(a) dBZ **(b)** Z_{DR} (dB)
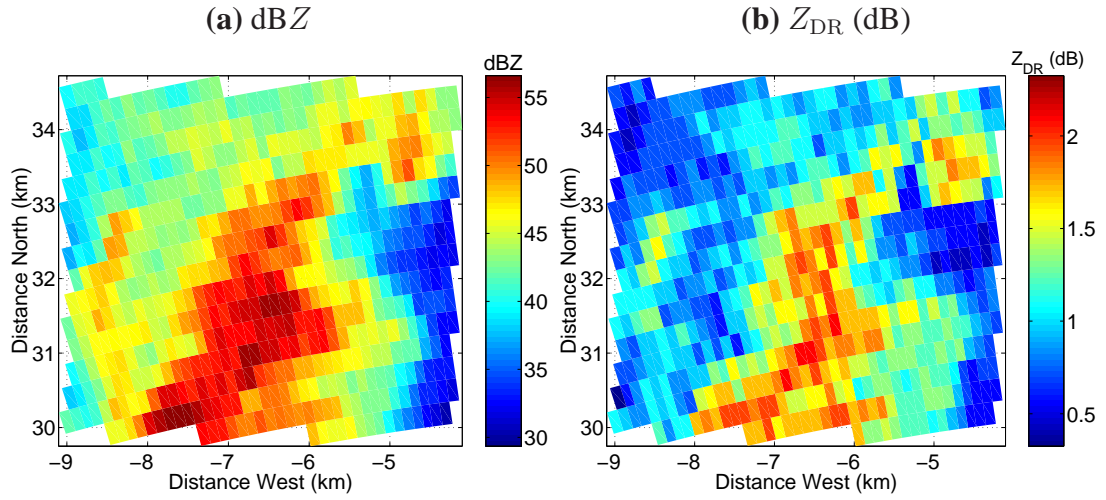
Figure 6.1 *A 5x5 km box of (a) reflectivity (dBZ) and (b) differential reflectivity (Z_{DR}) data . This box is located in an area of vigorous frontal rain approximately 35 km from the antenna.*

points in figure 6.2. This N_{w} is converted to a with equation 5.19 to give a value of $a = 123.5$ when assuming $\mu = 5$ (or 195 if $\mu = 0$). This value is then used on each Z value used within the chosen region for rainfall rates.
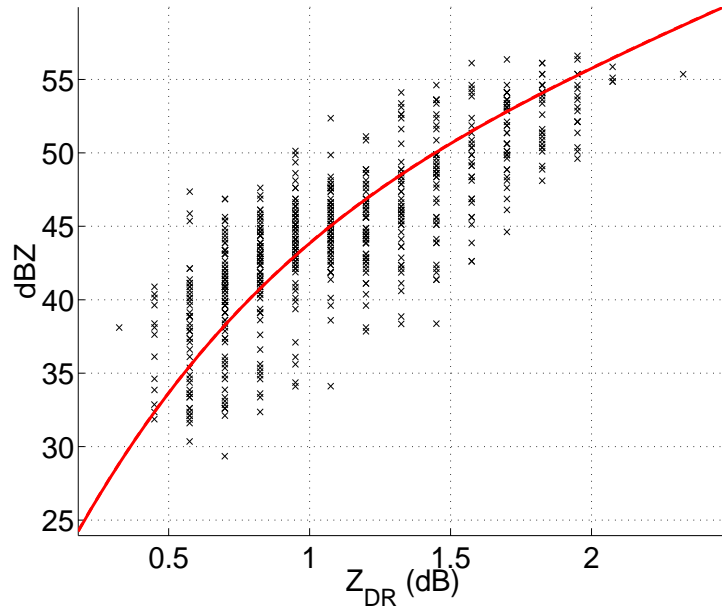
Figure 6.2 *The plot of Z_{DR} and dBZ of the data and the line of best fit.*

step	**1**								
T	0	5	10	**15**	20	**25**	30	35	40
N_w (m^{-3} mm^{-1})	172	545	1722	**5446**	17222	**54462**	172220	544620	1722200
a	941	528	297	**167**	94	**53**	30	17	9.4
RMS	1.8026	1.1541	0.6595	0.3046	**0.2822**	0.4993	0.7030	0.8778	1.0845
step	**2**								
T	15.00	**16.25**	17.50	**18.75**	20.00	21.25	22.50	23.75	25.00
N_w (m^{-3} mm^{-1})	5446	**7263**	9685	**12915**	17222	22966	30626	40840	54462
a	167	**145**	125	**109**	94	81	71	61	53
RMS	0.3046	0.2551	**0.2349**	0.2465	0.2822	0.3314	0.3864	0.4431	0.4993
step	**3**								
T	16.2500	16.5625	16.8750	**17.1875**	17.5000	**17.8125**	18.1250	18.4375	18.7500
N_w (m^{-3} mm^{-1})	7263	7804	8387	**9012**	9685	**10407**	11184	12018	12915
a	145	140	135	**130**	125	**121**	117	113	109
RMS	0.2551	0.2471	0.2410	0.2369	**0.2349**	0.2350	0.2370	0.2409	0.2465
step	**4**								
T	17.1875	17.2656	17.3438	17.4219	17.5000	**17.5781**	17.6562	**17.7344**	17.8125
N_w (m^{-3} mm^{-1})	9012	9176	9342	9512	9685	**9861**	10039	**10222**	10407
a	130	129	128	127	125	**124**	123	**122**	121
RMS	0.2369	0.2362	0.2357	0.2352	0.2349	0.2348	**0.2347**	0.2348	0.2350
step	**5**								
T	17.5781	17.5977	**17.6172**	17.6367	**17.6562**	17.6758	17.6953	17.7148	17.7344
N_w (m^{-3} mm^{-1})	9861	9905	**9950**	9995	**10040**	10086	10131	10177	10222
a	124.3	124.0	**123.7**	123.5	**123.2**	122.9	122.6	122.4	122.1
RMS	0.2348	0.2347	0.2347	**0.2347**	0.2347	0.2347	0.2347	0.2348	0.2348

Table 6.1 *The iteration steps of example 1. Red colours indicate the minimum RMS at this iteration, leading to the blue colours showing the bounds of the next iteration.*

6.1.2 EXAMPLE 2: VARIATIONS WITHIN EVENTS

For this example a single scan will be examined. The chosen scan is from $14\text{:}20$ GMT on the 9th Oct. 2000, taken from the Chilbolton radar. A selection of areas of this scan will be examined to show the differences that result. The reflectivity of this scan is shown in figure 6.3, also showing some important phenomenon effects in the data. The general weather conditions seen are a cold front approaching Chilbolton from the west, preceded by widespread moderate rainfall. Behind the front are some weak convective showers.
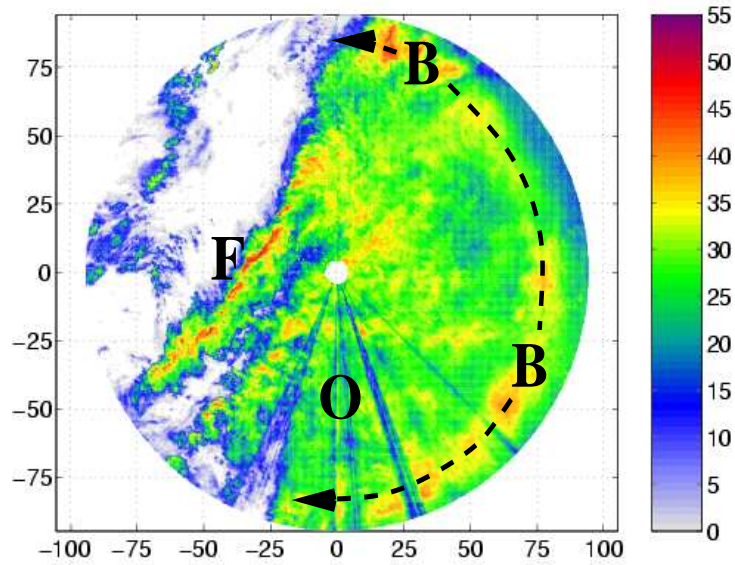
Figure 6.3 *False colour plot showing reflectivity of a single PPI performed on 9th Oct. 2000. The scale on x and y axes are in kilometres. The image is annotated as follows: B shows the location of the bright band on this scan; O shows a sector which contains a number of partially obscured beams, spotted by reduced reflectivity (for calculating N_{w} these rays have the data removed); F shows a cold front approaching Chilbolton.*

Firstly, data from the front will be examined. Data from a 5×5 km area centred about an area of the front is used and plotted in figure 6.4. This data has $a = 75$ and $N_{w} = 28000$ mm^{-3} mm^{-1}.

The next region to consider is the rain preceding the front; figure 6.5 shows an example of this data. This example shows $a = 133$ and $N_{w} = 8600$ mm^{-3} mm^{-1}. This means
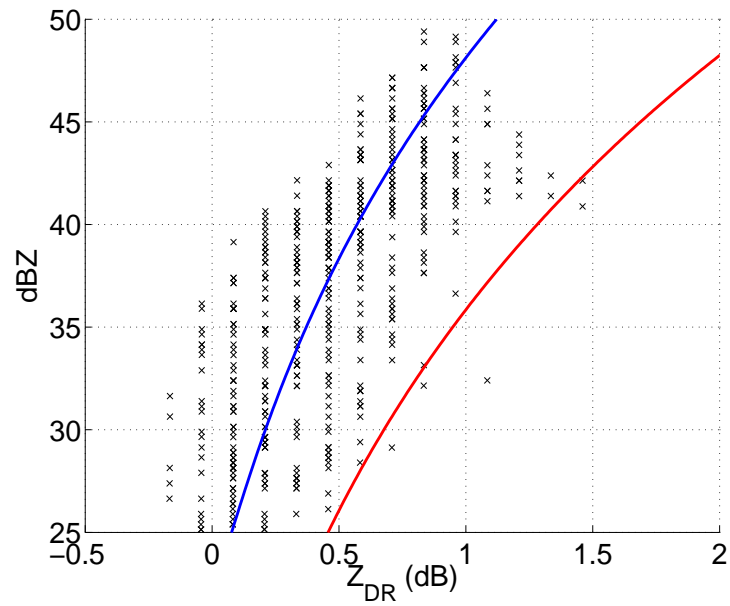
Figure 6.4 *Plot of Z and Z_{DR} for an area of rainfall based within the front. Also plotted are the fitted line of constant "a"s (hence N_{w}s) and of $a = 300$.*

that there are more drops in the frontal rain than the rain that precedes it.
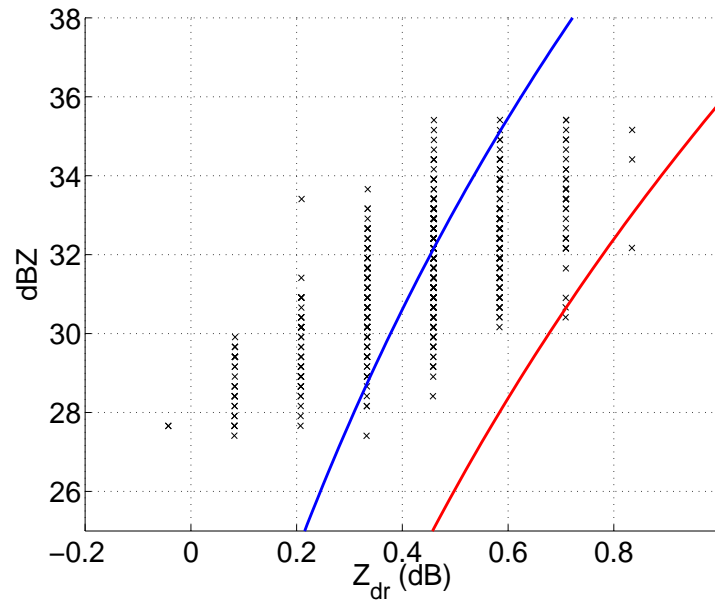
Figure 6.5 *Plot of Z and Z_{DR} for an area of rainfall to the east of Chilbolton. Also plotted are the fitted line of constant "a"s (hence N_{w}s) and of $a = 300$.*

Figures 6.6 and 6.7 show the values of a and effective drop concentration over the scan.
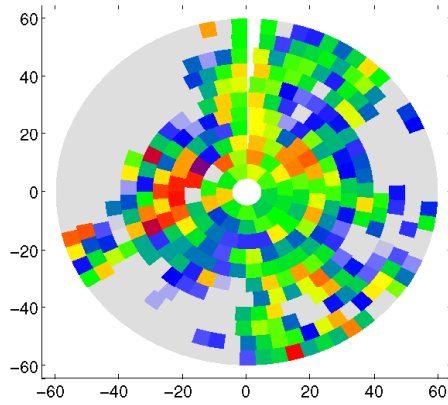
Figure 6.6 *A false colour plot showing the values of a over the scan shown in figure 6.3.*
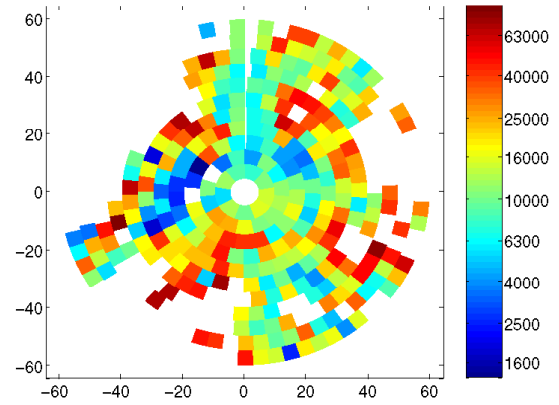
Figure 6.7 *A false colour plot showing the values of N_{w} over the scan shown in figure 6.3.*

6.1.3   EXAMPLE 3: TIME VARIATIONS

In this example the time variations that are detected by the integrated Z/Z_{DR} technique are examined. The data for this example was taken during the early afternoon of the 21st of April, 2004. During the time to be examined in this example the radar performed a scanning procedure where a $45°$ sector was scanned back and forth, with RHIs performed occasionally to confirm the location of the bright band. This means that 59 scans are performed within the 72 minutes that are examined. The weather during the scanning procedure was dominated by widespread moderate rainfall from a passing frontal system. During the time this example considers the rain shows very little variation. This can be seen in figure 6.8. This lack of variation in reflectivity suggests that there is little variation within character of the rainfall.

To examine the use of the integrated Z/Z_{DR} technique over this period the data chosen to examine for each scan will be from a square of size 5×5 km centred on the point selected for figure 6.8. This yields the variations in a throughout the period, as plotted in figure 6.9.
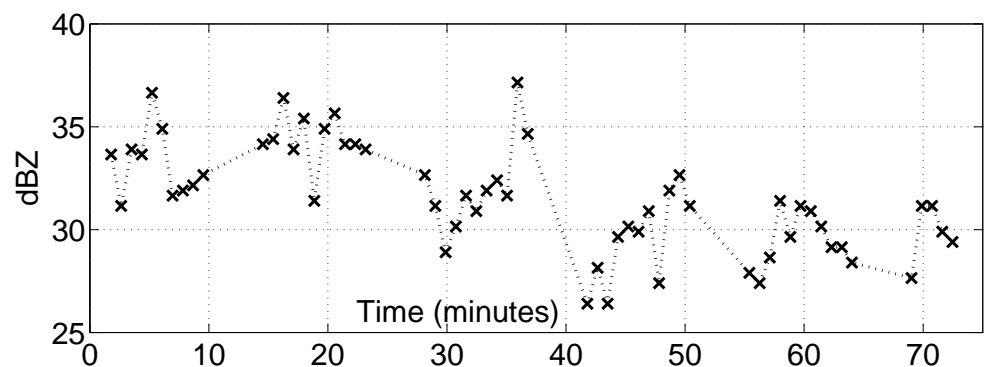
Figure 6.8 *A plot showing how the reflectivity changes over an hour. The reflectivity is recorded at a single point.*
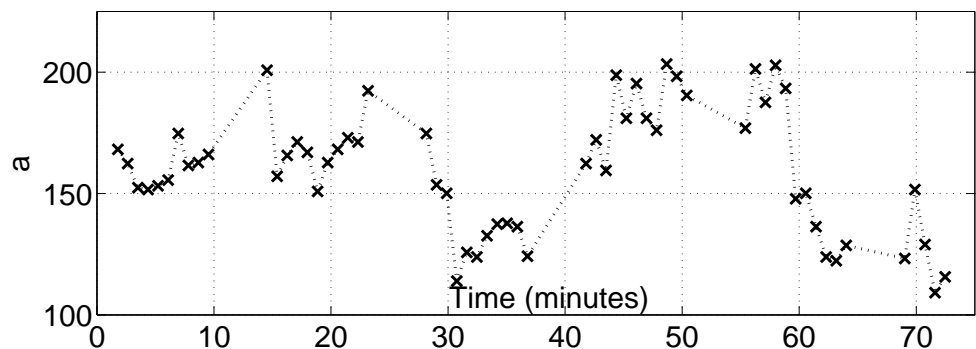
Figure 6.9 *A plot of the variation of a over an hour while scanning a $45°$ sector repeatedly. The plot shows crosses for the a calculated from each scan.*

Given the value of a and the reflectivity of the point, the rainfall rate variation over the period can be calculated, as shown in figure 6.10. This shows that the rain rate is under-estimated throughout the period by both of the demonstrated standard algorithms.

6.1.4 FURTHER EXAMPLES

A number of other examples are shown in table 6.2. This table shows the date and rain type that the data was taken from, a plot of Z/Z_{DR} space showing the region's data and the best fit line (note these plots have identical axis sizing), the resultant drop concentration and a for each region.
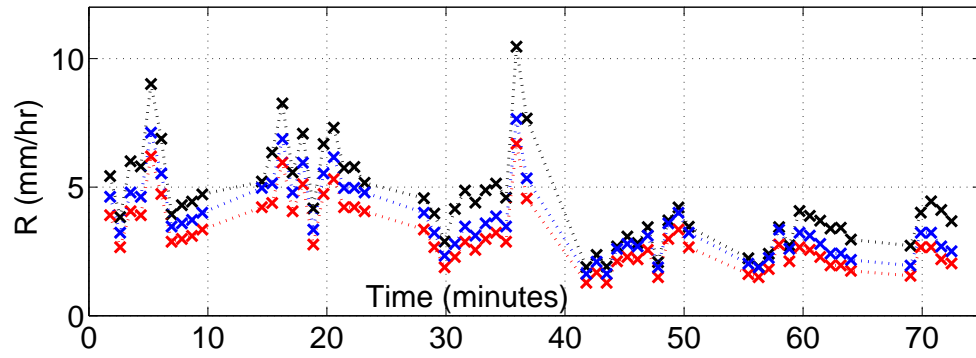
Figure 6.10 *A plot of the variation of rainfall rate over an hour while scanning a $45°$ sector repeatedly. The plot shows in black, crosses for the R calculated using the integrated Z/Z_{DR} technique on each scan. The crosses in red shows the rainfall rate calculated from a traditional $Z - R$, $Z = 300R^{1.5}$; the blue shows the rainfall rate calculated form the UK Met Office standard $Z - R$, $Z = 200R^{1.6}$.*

6.2   THE PHYSICAL BASIS OF RESULTS

This section will examine how results from the integrated Z/Z_{DR} technique are explained from the physical processes that underlie the observations.

6.2.1   VARIATIONS OF DROP CONCENTRATION WITH Z

It has been shown previously that, assuming μ remains constant, changes in drop concentration (N_{w}) correspond to changes in reflectivity, but not Z_{DR}. In Marshall and Palmer (1948) rain, N_{w} is effectively constant.

It is quite possible that the integrated Z/Z_{DR} technique will give results which show a relationship between Z and N_{w}. Figure 6.11 shows two examples of the comparison. The line plotted showing the average, which in plot (a) demonstrates a shallow positive gradient, suggesting that N_{w} increases with reflectivity. This pattern is analogous with a lower value of 'b' (high N_{w} suggests low a, which in turn implies high rainfall rates, the same applies in reverse). This is likely to change from event to event. It has been shown previously that this b alteration is caused by N_{w} changing with D_{o}. Plot (b) shows the gradient at low reflectivity to be negative, becoming positive at 35 dBZ.
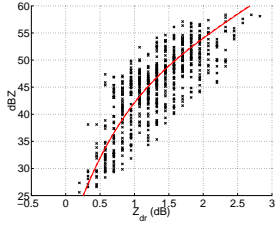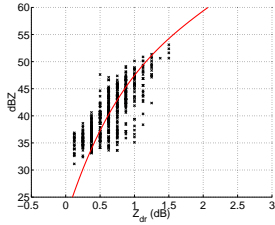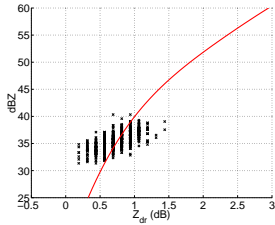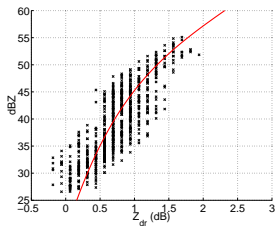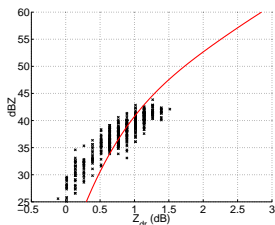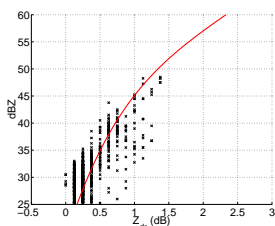
Case	Plot	N_{w} (m^{-3} mm^{-1})	a
Frontal rain 18/08/2000		6700	151
Heavy Storm 15/09/2000		23000	81
Stratiform rain 09/10/2000		4060	194
Cold Front 09/10/2000		13900	105
Showers 19/03/2004		4910	176
Showers 19/03/2004		13400	107

Table 6.2   *A table of examples of the integrated Z/Z_{DR} technique on different rains.*
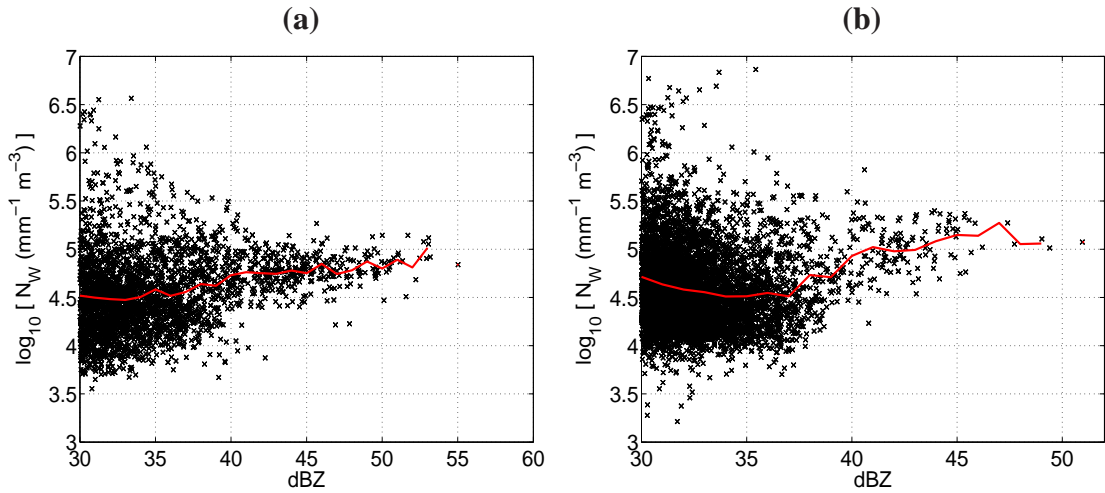
Figure 6.11 *A plot of the drop concentration ($N_{\rm w}$) against mean reflectivity from 16 point Chilbolton boxes. Also plotted is a line showing how the mean varies from bands of Z. This data was derived from data taken by CAMRa radar, for (a) on 18 August 2000, for (b) the data is from 9 October 2000.*

6.2.2 THE DIFFERENCES BETWEEN CONVECTIVE AND STRATIFORM RAIN

The physical processes involved when forming the drop size distributions of rain are dependent on the method of formation of the rain and the conditions that lead to them. In section 1.1 it was mentioned that the principal rain "type" dictates the $Z - R$ relationship used when polarisation diversity information is not available. This is seen in the use of $Z = 300R^{1.4}$ in the USA, while in Britain $Z = 200R^{1.6}$ is used. This is because in the UK stratiform rain is dominant, whereas in the USA convective rain is more important, this change has been known for many years, e.g. Battan (1973). The different $Z - R$ relations show the pattern of change of $N_{\rm w}$ with $D_{\rm o}$ in the different b, but also different drop concentrations are shown in the a. Stratiform rain tends to leave the cloud in the form of snow, which falls and melts once it passes the $0\,^{\circ}$C isotherm. This melting snow may explain the $Z - R$ relation in stratiform conditions: as the snow flakes get larger (and hence become larger raindrops upon melting) collisions become more frequent, so accretion and aggregation occur at faster rates. This will mean that the drop concentration becomes lower as the drops grow. This type of situation was considered in section 5.1.1, where the effect of $N_{\rm w}$ falling as $1/D_{\rm o}$ was shown to result in b close to the 1.6 widely

used in Europe. In convective precipitation the snow phase is not present, so the large flakes are not a factor in the development of the rain beneath. In convection the b is lower. This would be explained by a relation such as N_{w} rising as $D_{\mathrm{o}}{}^2$, which in section 5.1.1 was shown to give rise to a b of 1.34. This would mean that the drops are bigger as they become more numerous.

To examine how different types of rain are picked up by the integrated Z/Z_{DR} technique first a scan will be considered. This will be the same as the scan of example 6.1.2. For ease of understanding the a calculated for this scan will be shown, zoomed into the front, with contours of reflectivity (figure 6.12). The noise in reflectivity means that contours of Z without any additional averaging are noisy, so for the contours, reflectivity is averaged with its neighbouring points (note this averaging is only used for the contours). Calculation using the integrated Z/Z_{DR} technique used unaveraged data. The solid contours show the location of the heavier rain falling from the front. It can be seen that the a calculated in the heavy rain is generally lower than the surrounding areas. During the approach of the front, the value of a is higher than average. To demonstrate this more clearly a plot showing how a and Z change along a ray is shown in figure 6.13. This ray is chosen to cross the front. The maximum rain from the front occurs at a range of approximately 45 km, which coincides with the low a. This suggests in the frontal rain, as the rainfall rate increases, the drop concentration rises, similar to the convective example above where $N_{\mathrm{w}} \propto D_{\mathrm{o}}^2$. The more consistent stratiform rain to the east of Chilbolton shows less variation in a as well as Z. The heavier rain in this region (> 35 dBZ) shows a possible increase in a, which suggests higher rainfall rates have lower drop concentrations, and therefore larger drop sizes. This follows the suggestion of a relationship similar to $N_{\mathrm{w}} \propto 1/D_{\mathrm{o}}$.

To examine the relationships of how a changes with Z they are plotted in figure 6.14. The previous paragraph suggested the two rain "types" had different characteristics so these are differentiated in the plot. First consider the frontal rain (the red circles). This is positively correlated, with coefficient 0.41. This is from a total of 93 points, and using a student-t test this is significant at the 99% level, confirming the suggested relationship that
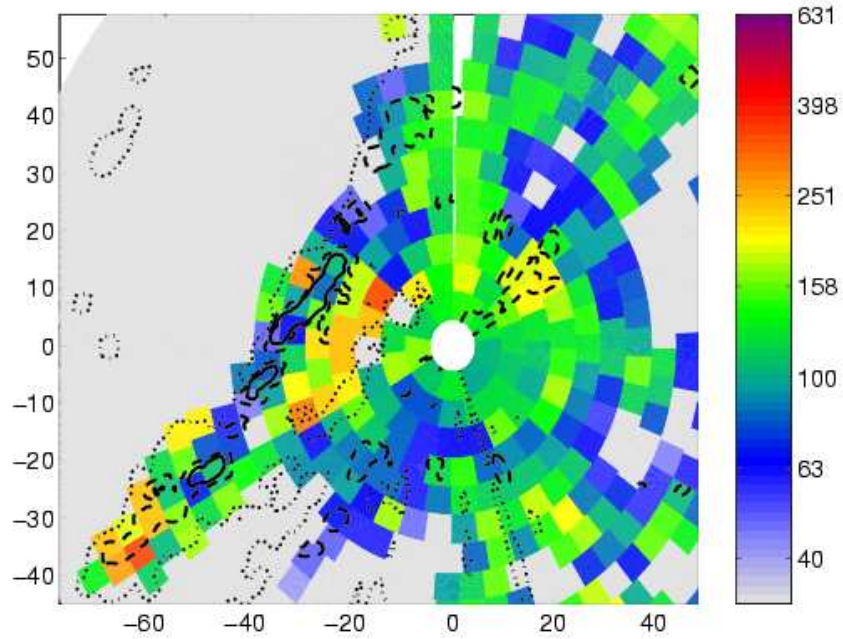
Figure 6.12 *Plot of the a from a scan. Overlaid are contours of reflectivity (this is averaged to make contours less noisy and hence more meaningful). The contours are for: solid line 40 dBZ, dashed line 35 dBZ and dotted line 20 dBZ. This shows where the rain and heavy rain is occurring.*
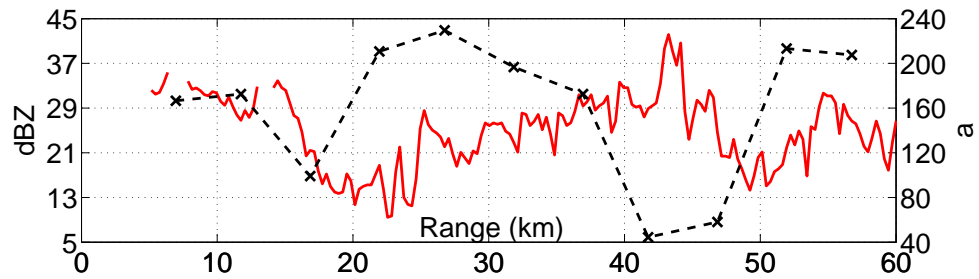
Figure 6.13 *Plot of a and reflectivity along a ray through the front from figure 6.12. Reflectivity is shown in red (axis to the left), with the black showing a (axis to the right).*

effective drop concentration increases with rainfall rate. When considering the stratiform rain (blue crosses) the expected correlation is not seen. From 254 points available a correlation of -0.042 is obtained, this is not significant even at the 95% level.

Finally this will be examined in terms of drop size distribution parameters, N_w and D_o, which will give the physical backing to the results obtained. The results are shown
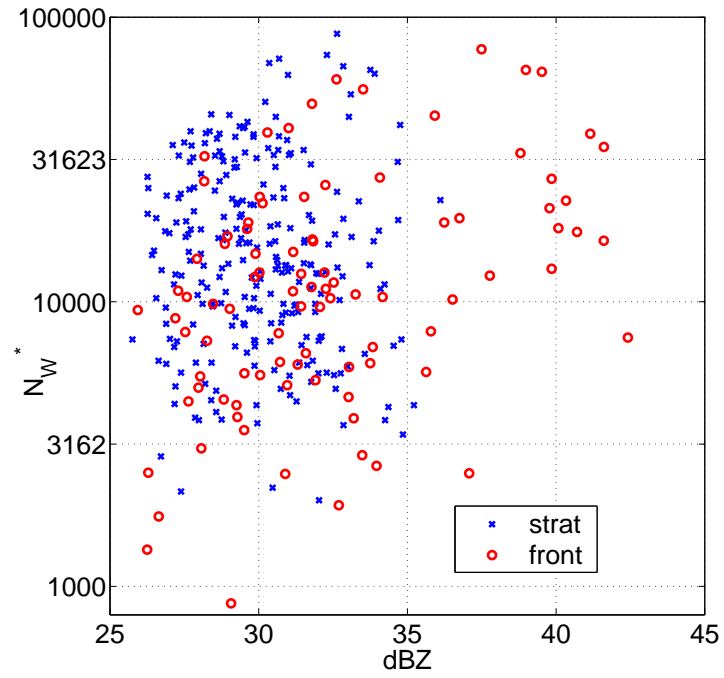
Figure 6.14 *Plot of $N_{\mathrm{w}}^{\star}$ against the mean Z of the box for the data in figure 6.13. For this figure the data has been separated by azimuth into rain from the front (red 'o's) and rain from the preceding stratiform rain (blue 'x's).*

in figure 6.15. $N_{\mathrm{w}}^{\star}$ has been calculated via the integrated Z/Z_{DR} technique, remember that this is $N_{\mathrm{w}}^{\star}$, not N_{w}, as changes in μ occur are not detected and appear through the method simply as a change in $N_{\mathrm{w}}^{\star}$. The calculation of D_{o} is from the equation of Bringi and Chandrasekar (2001),

$$D_{\mathrm{o}} = 1.529 Z_{\mathrm{DR}}^{0.467}, \tag{6.1}$$

appropriate for S-band. The Z_{DR} used was the average Z_{DR} of box, to limit the effect of noise in Z_{DR}. Here it is clear that for this rain the drop concentration decreases with increasing drop size.
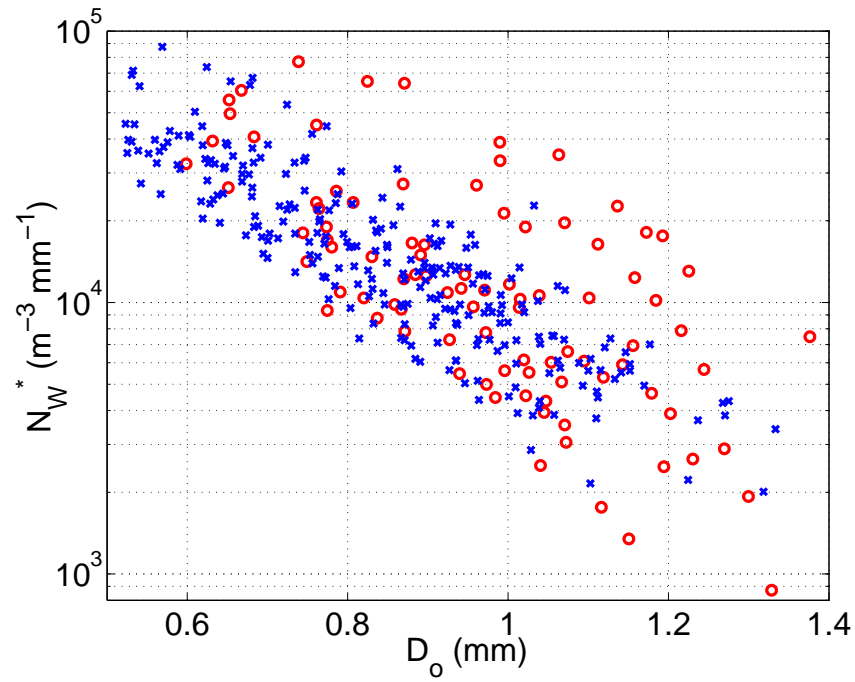
Figure 6.15   *Plot of $N_{\mathrm{w}}^{\star}$ against D_{o} (calculated from Z_{DR}) of the box for the data in figure 6.13. For this figure the data has been separated by azimuth into rain from the front (red 'o's) and rain from the preceding stratiform rain (blue 'x's).*

6.3   COMPARISON WITH RAIN GAUGES

6.3.1   GAUGE COMPARISON PROBLEMS

Rain gauges suffer from a number of problems that cause errors in the measured rainfall rates. These work alongside problems with the comparison of radar derived rainfall rates with the measurement of a rain gauge.

Possibly the biggest problem comes from rain-gauges measuring rain falling through a small area (~ 0.01 m^2), whereas the radar measures the integrated rain over a large volume (~ 4000000 m^3). The very small scales of variation (both temporal and spatial) in rain mean that this comparison is not perfect.

Another problem comes from the positions of the measurements. The rain-gauge is at ground level, whereas the radar sampling volume is above the rain-gauge by ~ 250 m.

This means that the rain measured by the radar still has to fall to the rain-gauge leading to several possibilities and inevitabilities.

A raindrop that falls into the rain-gauge must have passed through the radar sampling volume previously, meaning that the rain-gauge lags behind the radar.

If a horizontal wind is blowing the raindrops will drift, which means that the drops falling into the rain-gauge will not necessarily have passed the radar sampling volume directly over the gauge, but have been blown into the gauge from other radar pixels.

The raindrops may undergo a change during the fall from radar volume to the rain-gauge. Mostly this will be evaporation of the drops, reducing the rain intensity. However the radar beam may "over-shoot" the rain, and measure rain before the rain falls through saturated air, hence condensing to the drops and increasing the rainfall intensity (this effect is common in mountainous areas where "seeder-feeder" rain is commonplace). Figure 6.16 shows this effect, on the left the rain falls through a region of saturated air, so the drops grow, to the right no such saturated region is encountered, hence the drops evaporate.
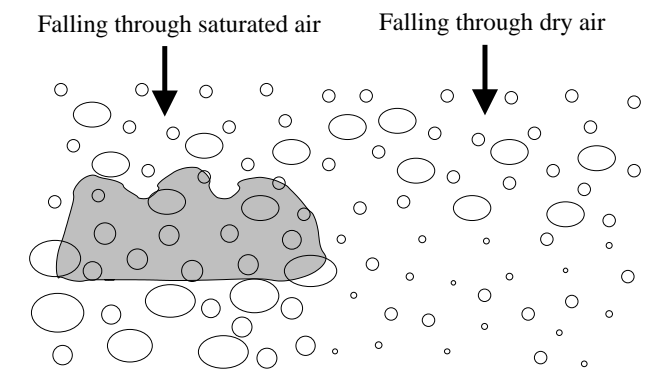
Figure 6.16 *Schematic diagram of rainfall spectra changing as the drops fall. The grey shaded area is a cloud where the air is saturated.*

These various effects all act to make radar rain-gauge comparisons especially difficult.

6.3.2 CASE STUDY - 21 APRIL, 2004

To compare the use of the integrated Z/Z_{DR} technique with the data recorded by rain-gauges a single case will first be examined. The case examined is that of the day described in section 6.1.3, which involved moderate rainfall for several hours. During this time the CAMRa radar was performing a scan routine which involved PPI scans over a sector to the west of Chilbolton. In this region 5 rain gauges operated by the Environment Agency are located. These raingauges are of tipping bucket type, with bucket size of 0.2 mm, recording the time of each tip to an accuracy of 1 second or 1 minute, depending on which gauge is being considered. These gauges are described in table 6.3.

Location Name	Range from Chilbolton	Time Resolution
Easterton	40 km	1 minute
Harestock	26 km	1 second
Tidworth	18 km	1 second
Tisbury	44 km	1 second
Winterbourne Stoke	32 km	1 second

Table 6.3 *Environment Agency raingauges to the west of Chilbolton.*

Having rain gauge tip times is powerful and allows for greater detail of rainfall rates than is available from accumulations that are frequently considered. However there remains a lack of sampling even at light rainfall rates: a rate of 12 mm/hr corresponds to 60 bucket tips per hour, which is a tip once per minute. At 3 mm/hr the bucket tips at a rate of just 15 per hour, or a tip every 4 minutes. This demonstrates an important factor in measurement of rain via raingauges: higher rainfall rates give better temporal resolution. The time resolution available for the moderate rainfall rates considered in this thesis are samples once every 1-4 minutes. It should also be noted that the raingauge records the time only when a 0.2 mm bucket is filled with rain. The rain distribution to fill this bucket is not in any way recorded, so a tip simply only supplies the time at which a 0.2 mm accumulation has built up. This may take one hour to happen, appearing to record a rate of 0.2 mm/hr, although this may occur from a period of 59 minutes with no rain followed by

one minute of 12 mm/hr rainfall. Hence it is important to remember the tipping bucket raingauge measures the rainfall accumulations, not the instantaneous rainfall rates.

Initially longer accumulations will be considered. To calculate the accumulations from the radar data the derived rate from each scan is considered to fall for the time centred on the scan. In practice the rain will change from the "snapshot" being viewed from the radar. However the scans repeat frequently (45 s with 5 minute breaks) for this case study so the variation between scans will be small, so error incorporated will be small (this effect is examined in detail in chapter 4). The PPI scans are taken at an elevation of $0.7°$, which is the lowest possible available elevation to avoid beam blocking within the scanned sector.

Figure 6.17 shows the accumulation at the Tisbury gauge. This gauge is at a range of 44 km west-south-west of the radar, and given the scan elevation of $0.7°$ this implies the radar beam is centred 685 m above the raingauge. This means that from falling from the centre of the beam to landing in the gauge takes a drop ~ 100 s. This lag will be corrected for, but will retain a small error.

This plot shows accumulations calculated by several different methods suggested in chapters 2 and 5. The plots have been shown for two options from the data. Plot (a) shows the accumulations with unaltered data from the CAMRa radar; plot (b) is calculated after adding extra noise to the Z_{DR} data to simulate data that would be available from an operational radar. In both cases the integrated Z/Z_{DR} technique is operated on a 5 km grid. The most important observations from plots (a) and (b) are that the point-by-point Z and Z_{DR} method suffers from the poor Z_{DR} data, shown by the accumulation being much lower than the other methods and raingauge predict. The trace from point by point Z and Z_{DR} is also noisier; the use of accumulations has the effect of disguising this. It is clear from the figures that the integrated Z/Z_{DR} technique shows very little difference in the results (hence a) with or without added Z_{DR} error, demonstrating that the technique can handle the noise well.

When considering the total accumulations predicted by the various methods the gauge shows a total of 9.4 mm, the simple $Z - R$ estimates this as 7.6 mm, and the Z and Z_{DR}
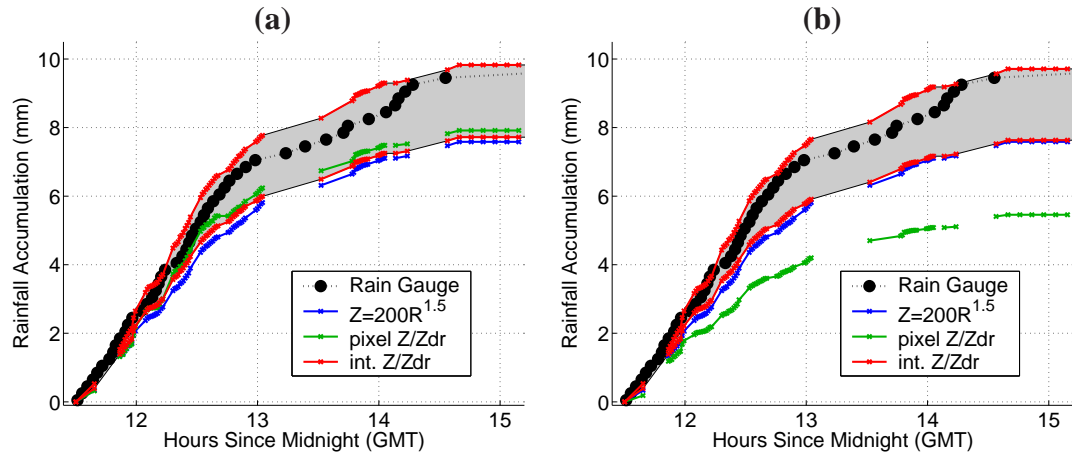
Figure 6.17 *Rainfall accumulation at the Tisbury raingauge. Plot (a) uses data as available from the CAMRa radar, so has very good Z_{DR}. Plot (b) gives the same result, but calculated having increased the noise on Z_{DR} to 0.5 dB, so at an operational level. The lines are as follows: large black circles show the rain gauge tips (note that these are connected by a dotted black line this will however not be how the rain proceeds between tips). The blue line shows the accumulation predicted by a simple Z–R of $Z = 200R^{1.5}$. The green line shows the accumulation predicted via the point by point Z and Z_{DR} using the equation 2.14 described in section 2.4.2. Finally the integrated Z/Z_{DR} technique is shown in red. This is shown with two lines, for different μ possibilities. The upper line is accumulation assuming $\mu = 5$, the lower for the assumption that $\mu = 0$.*

method estimates just 5.4 mm. The integrated technique assuming $\mu = 0$ suggests that the accumulation is 7.6 mm; when $\mu = 5$ this is 9.7 mm.

Figure 6.18 shows a similar plot to figure 6.17, only for the location of the Easterton rain gauge. This gauge lies 40 km to the west-north-west of Chilbolton, which is 30 km north of Tisbury. For this gauge the radar beam is centred 600 m above the gauge. A similar pattern is shown with this gauge, the addition of the Z_{DR} noise creating an underestimate in the Bringi and Chandrasekar (2001) method of the green line. Also the noise addition has very little effect on the results of the integrated Z/Z_{DR} technique , although this gauge shows a rain trace similar to the $\mu = 0$ line.

Comparing accumulations has the effect of averaging out any errors; the longer the period of accumulation the greater the averaging effect. This means that shorter accumulations (averaging periods) are a more strict test of any rainfall estimation algorithm. To that end the accumulations over smaller times will be considered. The problem here
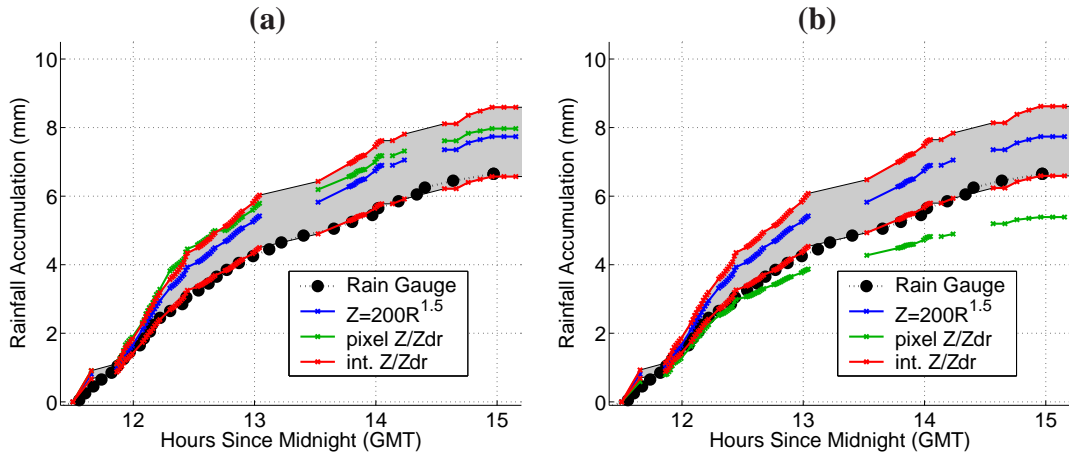
Figure 6.18 *Rainfall accumulation at the Easterton raingauge. Plot (a) uses data as available from the CAMRa radar, so has very good Z_{DR}. Plot (b) give the same result, but calculated having increased the noise on Z_{DR} to 0.5 dB, so at an operational level. The lines are as follows: large black circles show the raingauge tips (note that these are connected by a dotted black line this will however not be how the rain proceeds between tips). The blue line shows the accumulation predicted by a simple Z–R of $Z = 200R^{1.5}$. The green line shows the accumulation predicted via the point by point Z and Z_{DR} using the equation 2.14 described in section 2.4.2. Finally the integrated Z/Z_{DR} technique is shown in red. This is shown with two lines, for different μ possibilities. The upper line is accumulation assuming $\mu = 5$, the lower for the assumption that $\mu = 0$.*

is that the raingauge measures accumulation, so this limits how small a period can be used for accumulation. Another problem that is brought in when considering short accumulation period is the uncertainty of time lag between the radar and gauge. Some short accumulations are shown in figure 6.19. The first plot (a) shows a period of 6 minutes when the gauge detects 0.6 mm (three tips); a rate of 6 mm/hr. During this period nine scans were performed. There is a small discrepancy between the start points of radar (from first scan) and the gauge (first [starting] tip), the gauge being slightly after the radar. The time to reach 0.6 mm accumulation is shown in table 6.4. In this example the integrated Z/Z_{DR} technique shows excellent performance. The second plot of figure 6.19, (b), shows a similar plot, this time with just two tips (0.4 mm) occurring within 6.5 minutes. This time the initial tip is slightly before the first scan. On this occasion the traditional $Z - R$ overestimates the rainfall occurring. However the pointwise Z/Z_{DR} method performs well, but it must be remembered that the noise in Z_{DR} will limit the
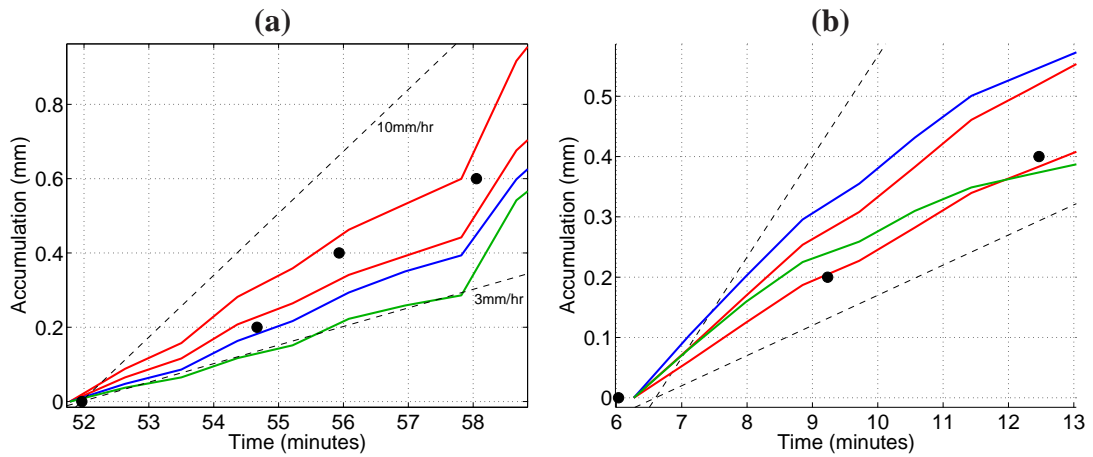
Figure 6.19 *Examination of small accumulations, (a) over the Tisbury gauge (b) over the Tidworth gauge. The colours are as in figure 6.17. This plot shows dashed lines of 3 and 10 mm/hr rainfall rates.*

Method	Time to 0.6 mm (mins)
Gauge	6.1
Int. Z/Z_{DR}	$6.0 - 6.6$
Pointwise Z/Z_{DR}	7.5
$Z = 200R^{1.5}$	6.9

Table 6.4 *Time to accumulate 0.6 mm for the lines of figure 6.19.*

usefulness of this method.

6.4 MODELLED RAINFALL

False radar data can be modelled, given the values of a and b. To do this the expected "true" values of Z and Z_{DR} are calculated. Z values can then be defined and random Gaussian noise of Z_{DR} with standard deviation as defined, depending on the data type being modelled. This allows the technique to be tested for consistency, and can be used to examine the accuracy of the method.

By setting a to be 300, b to 1.5 (with $\mu = 5$), the integrated Z/Z_{DR} technique will be examined. To model data from an operational radar, noise will be added: a Z noise of 0.7 dB, with Z_{DR} having 0.5 dB noise. The values of Z to be used are calculated based

on a random mean (with variations from 30 dBZ to 45 dBZ) with similarly randomly generated standard deviation (of 2 dBZ to 10 dBZ). With this setup the integrated Z/Z_{DR} technique will be tested, compared to the "truth" which is known from the setup. The integrated Z/Z_{DR} technique estimates rain, the mean being 100.16% of true rainfall. This shows there is no significant bias in the results, with a standard deviation of 3.97%, from 10000 runs. The histogram is shown in figure 6.20. The accuracy is dependent on
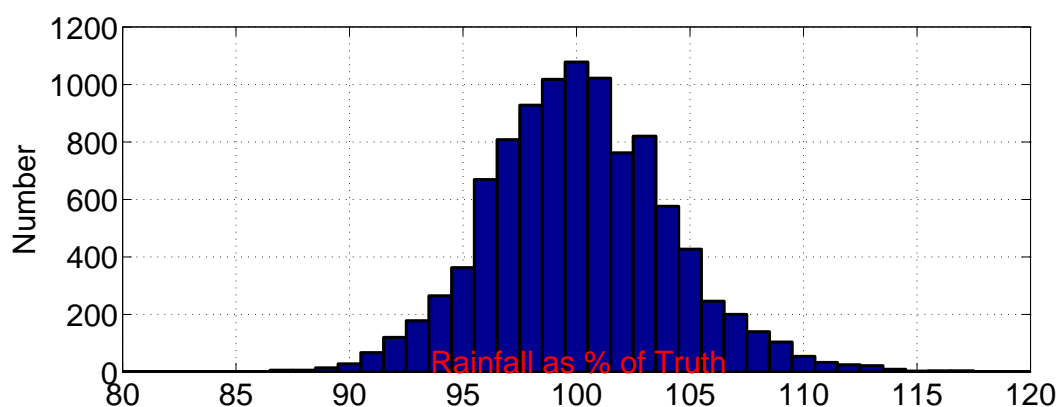
Figure 6.20   *Histogram of results of integrated Z/Z_{DR} technique from synthetic data to emulate an operational radar.*

the mean reflectivity: higher reflectivity areas provide better rainfall rate estimates than lower reflectivities. This is clear from the standard deviation variations across reflectivity: where only a reflectivity of 30-32 dBZ is used the standard deviation in rainfall error is 5.0% (from 1313 runs); for reflectivity of 43-45 dBZ that standard deviation is 3.0% (from 1325 runs). The cause of this is the shape of lines of constant N_{w}. At lower reflectivities, where the drops are more spherical, a line of constant N_{w} has higher gradient than when the reflectivity increases. The higher gradient means that a change in N_{w} has less effect in the Z_{DR} position of the line.

The accuracy of the technique is of course limited by the accuracy of the data. Since the principal noise (in relation to techniques to estimate rainfall) in radar data is likely to be in Z_{DR} the noise in its measurement is likely the determining factor in the accuracy of derived N_{w}, a and R. It has been shown that the technique described can estimate the nature of the underlying rainfall despite large errors in individual data points. To examine

the accuracy of the technique, Gaussian noise will be added to false data generated from known $Z - R$ relationship (see figure 6.21). Note that as would be expected the error
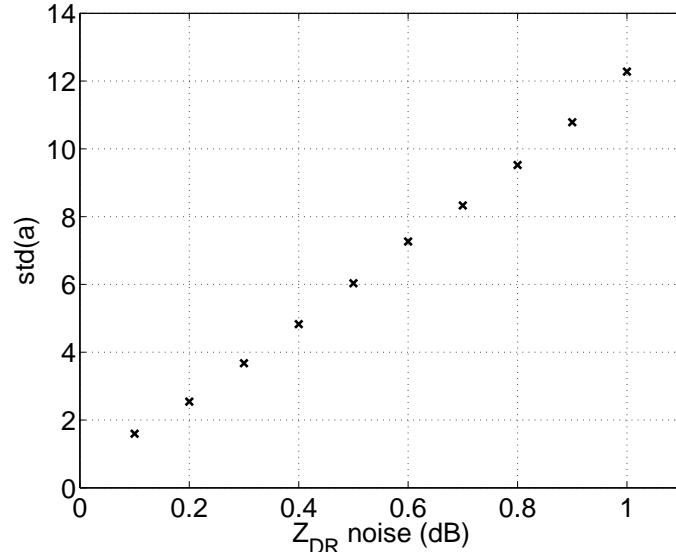
Figure 6.21 *Plot showing the error in derived a (from standard deviation) when Z_{DR} is given a Gaussian noise with standard deviation as shown on the horizontal axis. The "true" values are for $a = 300$ and $b = 1.5$. The reflectivities used in the estimation are from an area of radar data of 5×5 km of Chilbolton data, totalling 500 points. The statistics are generated from 1000 runs.*

is larger where the noise in Z_{DR} is high. These errors in a are translated into error in derived rainfall rates, but the errors remain small. Even at the level of 1 dB noise with the 500 points used for characterisation, rainfall rates have a standard deviation error of just 3%.

The 500 points used is a larger number than is needed for the 25% accuracy desired (this was seen in section 5.6.2.1). To investigate the error dependence on the number of points being used for characterising the data, one thousand examples of calculation are considered from number of points ranging from one (effectively a gate-by-gate method) to 512 points. The errors are expected to follow equation 5.20, so the error is halved when the number of points is squared. This is demonstrated in figure 6.22, showing the expected linear shape, passing through the origin (zero error when infinite points are used). It can be seen that the error does halve when comparing a calculation from four
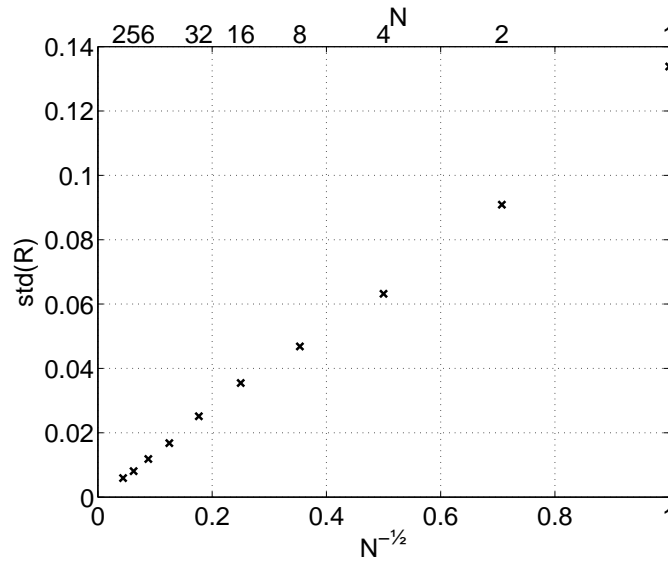
Figure 6.22   *Plot showing the error in derived R (from standard deviation when calculated using reflectivity of 39.8 dB [true $R = 10$ mm/hr]). The scale is of $\log R$ (hence factor errors), when Z_{DR} is given a Gaussian noise with standard deviation of 0.5 dB. The "true" values are for $a = 300$ and $b = 1.5$. The reflectivities used in the estimation are from an area of radar data of 5×5 km of Chilbolton data; the accuracy is shown compared to the number of points used for calculation. Equation 5.20 describes the expected relationship between error and number of points, which goes as $\frac{1}{\sqrt{N}}$ (lower horizontal axis). The number of points this corresponds to is shown on the upper horizontal axis. The statistics are generated from 1000 runs.*

points with one of 16.

This method does not allow for change in drop size distribution within the considered area. Although this will likely be small over the areas being considered, its effect may be problematic.

6.5   SUMMARY

This chapter has shown a number of examples of the use of the optimised integrated Z/Z_{DR} technique described in chapter 5 with real radar data. An example showing the use of the algorithm in full detail was shown in example 1, including a table showing the iterative approach. Example 2 demonstrated use of the optimised integrated Z/Z_{DR}

technique over a complete scan, showing variations in calculated drop concentrations. This example scan was considered further in terms of the types of rainfall occurring within the scanned rain.

Example 3 showed the temporal variations detected by the optimised integrated Z/Z_{DR} technique during a period of over one hour of rainfall. The example showed the variations in a detected, showing the rainfall rates from the optimised Z/Z_{DR} fit and simple $Z - R$ relationships.

The chapter continued to examine the results from the integrated Z/Z_{DR} technique, while attempting to explain the results physically. Differences between convective and stratiform rain were examined: increased large drop growth at the expense of the smaller drops in melting snow may cause the high b often found in studies of stratiform rain, whereas drops become larger, as less of them are present. The lack of melting level for convective rain means that low b has been reported widely, caused by more drops as they get larger. A scan was examined in terms of the characteristics of the rainfall being measured. A plot of a and Z showed that the higher reflectivities tend to have lower a for the frontal rain, hence higher N_{w}. The reverse occurs in the stratiform rain. The scan is considered to show the relationship between D_{o} and N_{w}.

The chapter continues into comparison with rain gauges. Comparing rainfall derived from radar with gauge values is fraught with difficulty. Errors arise from a number of possibilities, including differences in the scale of sampling region and changes in the rain between radar beam and gauge. However, despite these problems it is shown that the optimised integrated Z/Z_{DR} technique gives good results with the Chilbolton radar data, even when it is degraded to have the measurement accuracy of Z_{DR}. The comparison is shown to give good rates even down to very small accumulation times.

Finally the chapter examines the integrated Z/Z_{DR} technique with modelled data, where the rainfall rate is "known". The use of modelled rain allows large amounts of data to be simulated, making error statistics possible. Modelled data show that the integrated Z/Z_{DR} technique has no significant bias, with standard deviation error of $\sim 4\%$ and the expected lower error at higher rainfall rates caused by the curvature of the lines of

constant N_{w}.

CHAPTER 7:

OPERATIONAL INTEGRATED REFLECTIVITY/DIFFERENTIAL REFLECTIVITY

7.1 INTRODUCTION

Previous chapters have shown the potential of dual polarisation radar to improve rainfall estimation over the traditional non-polarisation diversity radars (chapter 2). However the noise that is inherent to the measurement of the polarisation parameters is very large, especially in the operational environment. This noise limits the use of the phase shift radar parameter for improved rainfall estimation to be viable only in very heavy rain. However, as discussed in chapter 3, the changes in drop size spectra are available in the Z and Z_{DR} data, and if this can be exploited, improved rain rates can be a reality, even with the noisy operational radars. Chapter 5 described a technique that uses the Z and Z_{DR} data within a small area, finding the optimal value of a (and hence N_{w}), to then be used in $Z = aR^{1.5}$ for rainfall calculation. Chapter 6 showed examples of the use of the integrated Z/Z_{DR} technique with the accurate Chilbolton radar. In this chapter the use of the integrated Z/Z_{DR} technique in the operational environment (especially in the UK) is considered. This will include the amendments to the technique that are needed because of the different radar wavelength, higher noise levels and reduced resolution.

7.1.1 WHAT IS DIFFERENT IN THE OPERATIONAL ENVIRONMENT?

One of the principal differences between research and operational radars is the wavelength of the radar beam. CAMRa operates at S-band ($\lambda \approx 10$ cm), which is the wave-

length of operational radars in the United States, whereas in the UK (as well as Japan and much of Europe) operational network radars operate at C-band ($\lambda \approx 5.6$ cm). This results in changes in the measured variables, affecting lines of constant drop concentration or rainfall; see figure 7.1. The smaller wavelength also means that non-Rayleigh scattering is more common due to particles of size with similar order of magnitude as the wavelength. Entering the Mie regime greatly changes the scattering characteristics, so ideally it should be avoided.
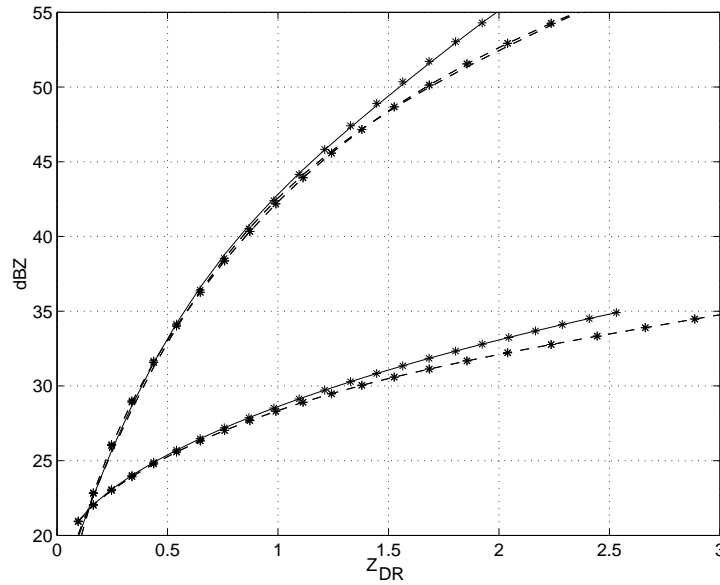
Figure 7.1 *Plot showing the lines of constant N_w and 1 mm/hr for S-band (solid lines) and C-bands (dashed lines). Here $\mu = 5$ and $N_\mathrm{w} = 8000$ mm^{-1}m^{-3} have been used.*

Another major difference is in the implementation of dual polarisation techniques. Until recently dual polarisation radars have been solely for research purposes, using an alternate pulse technique where a horizontally polarised wave is transmitted and returns measured in both polarisations, followed by a pulse of vertical polarisation (Goddard *et al.*, 1994a). All European operational weather radars to date have used simultaneous transmission ('hybrid' mode) where the transmitted pulse has $45°$ polarisation. This $45°$ transmission method, which was initially proposed in the paper introducing the concept of Z_DR (Seliga and Bringi, 1976), is known as the "hybrid basis mode", explained in

Brunkow *et al.* (2000). The principal reason for this change is financial – if a network of such dual polarisation radars is to be a financially viable prospect for the future, the radars' cost must be kept low. The use of "hybrid" mode means that the fast rotating chopping disk, acting as a polariser switch, as used on the CAMRa radar (Goddard *et al.*, 1994a), is not needed (it may result in undue expense or unreasonable unreliability). This difference means that the linear depolarisation ratio, L_{DR}, is not available (although it may be possible to perform an "L_{DR}" scan where vertically polarised transmission is turned off, although the change to this mode would be slow so not available pulse to pulse). Performing an L_{DR} scan would provide Z and L_{DR}, but not Z_{DR}. This scan will have improved sensitivity in Z, so may be desirable, but will require time within the scan strategy. The simultaneous transmission also means that interpolation between pulses for differential terms is not necessary, hence improving the accuracy of the estimates in Z_{DR}, ϕ_{DP} and K_{DP}. The accuracy of an operational radar will however be worse than a research radar. Rapid scan rates are required operationally to achieve good coverage at a good time resolution, which means that dwell times are low and hence accuracy is limited by the low number of independent samples taken. Operational radars are also more likely to suffer from antenna imperfections resulting in a mismatch of the vertical and horizontal polarisations and the added radome will potentially introduce further error. Mismatched beams is the effect where the illumination pattern from the radar is not identical for rays of both polarisations, so if the beams see different volumes, the hydrometeors viewed will be different.

The different implementation of polarisation in the operational environment mean that larger errors than the research counterpart are to be expected. Figure 7.3, on page 139, shows the errors in Z_{DR} as a function of normalised (with respect to folding velocity) spectral width, σ_{vn}, with copolar correlation coefficient, $\rho_{hh,vv}$, assumed at 0.97 (reasonable for an operational radar; see later section 7.3.1.1).

7.2 THE THURNHAM RADAR

The first operational dual-polarisation radar in the UK is located in Thurnham, near Maidstone, Kent (the south-east of England). The radar (photographed in figure 7.2) is to be-

Figure 7.2 *Photograph of the Thurnham radar, taken from McKay (2006).*

come part of the UK radar network and the project is the result of collaboration of the Met Office and Environment Agency. The radar specifications are given in table 7.1.

In section 2.4.3 alternate pulse dual-polarisation radars were shown to have a fundamental noise in Z_{DR}, caused by the number of independent samples, the copolar correlation, spectral width of the targets and interpolation necessary due to the alternating pulses. In the 'hybrid mode' the interpolation is not needed as horizontal and vertical polarisations are sent and received simultaneously, so the error in Z_{DR} decreases with spectral width for all spectral widths, hence there is no optimal value for accurate Z_{DR}. When in alternating mode very high spectral widths increase the errors again as the interpolation between alternate scans became inaccurate; in 'hybrid mode' this is not a

Frequency	5.5 GHz
Wavelength	5.6 cm
Antenna diameter	8 m
Beam width	1 °
PRF	1180 Hz
range resolution	125 m
Max. digitised range	255 km
Peak power	250 kW
Noise at 1 km	-33 dB (in hybrid mode)
	-36 dB (in single polarisation mode)
Unambiguous velocity	16.6 m s^{-1}

Table 7.1 *Properties of the Thurnham operational radar system.*

problem. So the fundamental limit for a radar with the characteristics of the Thurnham radar as a function of spectral width is given in figure 7.3. The plot shows the decrease in error as the spectral width increases, a result of increasing number of independent observations. At 0.5 m/s the lowest possible error would be 0.6 dB; by 1 m/s that error limit has reduced to 0.45 dB and by 2 m/s that limit is just 0.3 dB.

To examine the spectral width of rainfall in the UK, Chilbolton will be used. Figure 7.4 shows spectral widths of data from a PPI, after ground clutter removal. The plot shows contours of the density of points plotted with spectral width against reflectivity. The plot shows that spectral widths generally increase as the reflectivity (hence rainfall) increases. High spectral widths are also seen to be more frequent than low spectral widths (shown by the vertical extension of density contours above the centre). The increase in spectral width with reflectivity is explained by turbulence being greater in heavy rain High shear across the beam is also more likely in heavier rain, as both turbulence and shear increase spectral width. It must be remembered that the Chilbolton radar has a radar beam of $\frac{1}{4}^{\circ}$ where the 1° beam of the Thurnham radar is much larger. The larger beam volume for the operational radar means that shear across the beam will be larger, increasing spectral
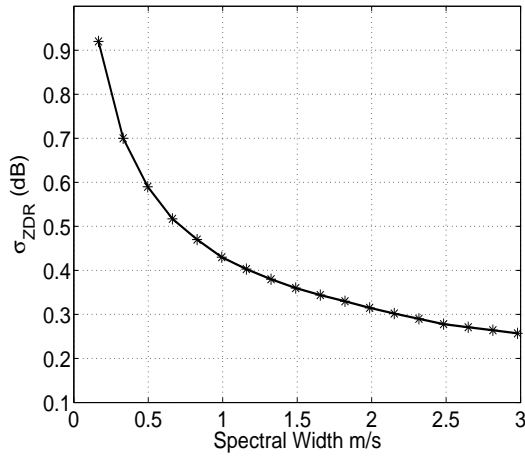
Figure 7.3 *Plot showing the theoretical standard deviation of recorded Z_{DR} as a function of spectral width for the Thurnham radar setup caused solely by the sampling problem (this plot assumed a correlation of 0.97). In the UK moderate rainfall tends to have spectral width of ~ 0.75 m/s which corresponds to a fundamental limit on the accuracy of Z_{DR} of ≈ 0.5 dB. Stormy rain has higher Doppler widths, ~ 2.2 m/s, which means that in stormy rain the fundamental limit of Z_{DR} has dropped to ≈ 0.3 dB.*
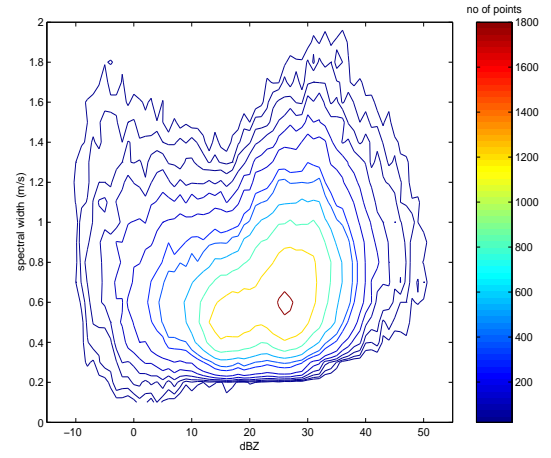
Figure 7.4 *Spectral width as a function of reflectivity. This data is taken from a single scan on 18/08/2000 with CAMRa, having used an $L_{DR} < -20$ dB threshold to remove non-rain targets. This is the passing of a vigorous cold front. Contours show the density of points. The plot also shows that spectral widths are ~ 0.6 m/s.*

width.

As spectral widths of ~ 0.75 m/s are expected in moderate rain (see figure 7.4 and adding a small amount for increased shear across the beam) the Thurnham radar cannot be expected to have Z_{DR} more accurate than 0.5 dB. The addition of radar imperfections increase this number further. Figure 7.5 shows a histogram of observed Z_{DR} at low reflectivity (23dBZ), demonstrating the spread in Z_{DR} from the instrument (at this reflectivity the natural variability will have a very small effect). The data shows Z_{DR} has a standard deviation of 0.7 dB, 0.2 dB above the estimate from the sampling expectation. This is

a result of imperfections in the radar meaning the copolar correlation, ρ_{HV}, drops below the 0.97 assumed.
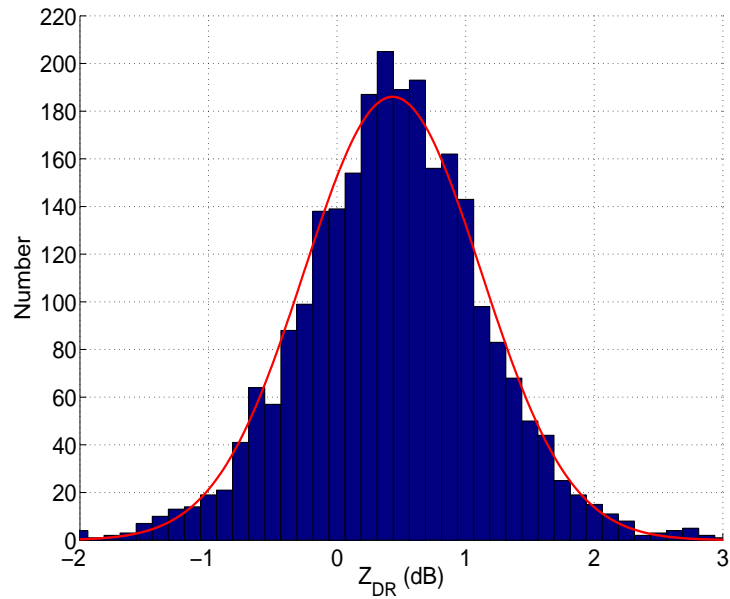
Figure 7.5 *Histogram of Z_{DR} data (250m resolution) with $22 < dBZ < 24$ from a single scan of Thurnham radar data. Overlaid is a normal distribution, with mean $0.43dB$ and standard deviation $0.69dB$. At these low values of reflectivity the natural variability of the rainfall will be small as drop spectra changes have little impact on drop shapes.*

Given that the noise found is 0.7 dB in Z_{DR}, it is clear that rainfall rates derived using Z_{DR} on a point by point basis will have large errors (standard deviations will be of order of a factor of three) and frequently observe negative Z_{DR} where rain calculation is either impossible or unphysical (depending on method); clearly no improvement over a simple $Z - R$ method. However, the Z_{DR} data remains useful, despite the signal being swamped by the noise; clearly averaging or integrated techniques will be needed to utilise the information available from Z_{DR} in the operational environment. To achieve a Z_{DR} accuracy good enough to gain improvement over a traditional $Z - R$ simple averaging would require so many points as to have an unacceptably poor spatial resolution. The integrated Z/Z_{DR} technique is well suited to the operational radar. It utilises the high resolution and accurate Z data available point by point to calculate high resolution rainfall rates, using the noisy Z_{DR} for best fit, so considering each Z_{DR} pixel independently

to find the average drop concentration. This method infers the signal from within the underlying noise.

7.3 OPERATIONAL DIFFICULTIES

In this section three possible problems for operational polarisation radar will be considered and the potential for overcoming these problems will be studied. Those problems are calibrating Z_{DR}, the greater attenuation, but first that of ground clutter.

7.3.1 GROUND CLUTTER/ANAPROP

Because the Thurnham radar operates in simultaneous transmit mode ('hybrid mode') to collect Z_{DR} data, simultaneous L_{DR} is not available (an "L_{DR} scan" is performed regularly as part of the scan strategy but this will be time offset from available Z_{DR} data, so it may not be relevant). This means that L_{DR} cannot be used for clutter rejection and another option must be considered.

7.3.1.1 ρ_{HV} FOR CLUTTER REMOVAL

Previous sections of this thesis (2.4.3 or 7.1.1) discussed the copolar cross-correlation, ρ_{HV}. ρ_{HV} is the correlation of the vertically and horizontally polarised reflectivities. This is a measurement of variety in shapes and fall modes of the targets. The value of ρ_{HV} depends on the target type: for instance in rain one would expect a value approaching unity, (in truth imperfections in radars mean that unity cannot be recorded so values of $\approx 0.97 - 0.99$ are expected with operational radar) for an operation radar such as Thurnham, where mis-matched beams may be an issue, but higher (≈ 0.997) at Chilbolton (Illingworth and Caylor, 1991).

Ground clutter has lower correlation as the scattering will be non-Rayleigh, so a threshold in ρ_{HV} could be used to remove ground clutter.

The problem with using ρ_{HV} is that measurements may be rather noisy and hence

"miss" some clutter infected points. So, although ρ_{HV} appears a natural replacement for L_{DR} in removing ground targets the noise makes this very problematic.

7.3.1.2 Z_{DR} SPREAD FOR CLUTTER REMOVAL

The next option to consider is the spread in Z_{DR} data. For this we calculate the standard deviation of a 3×3 pixel area (this is the same as the texture described by Gourley *et al.*, 2005). For rainfall the variations in Z_{DR} between pixels will be small as rainfall variations will be small on such small spatial scales. In ground clutter or anomalous-propagation the Z_{DR} returns a near random value so has a much higher spread (because of the scattering characteristics of the large target the ground forms). This means that a threshold on the value of the spread may be used for classification and removal of ground echoes, and the value of this threshold should be at 1.5 dB.

The problem that arises from this method of reduction is a return to a familiar problem: the sampling noise in Z_{DR}. Assuming there is no natural variability in the rainfall of the nine pixels being considered, they would have a spread equal to the sampling noise (0.7dB). This noise is large enough to be nearing the spread expected from ground targets (see figure 7.6), so again some ground targets may be missed by any threshold.

7.3.1.3 ϕ_{DP} SPREAD FOR CLUTTER REMOVAL

The spread of ϕ_{DP} is similar to the spread of Z_{DR}, only using the differential phase. Again it is calculated as the standard deviation of a 3×3 pixel box. Again hydrometeors are expected to have a low yet finite value, with ground targets with much higher spread due to the random returns from the surface (the phase of the return from the surface can in fact be exploited to gain information of the refractivity of the air [Illingworth *et al.*, 2005], but this is beyond the scope of this thesis). The noise in ϕ_{DP} is much smaller relative to the range of expected values with the Thurnham radar (see figure 7.7), so this option may be the best suited to use for clutter removal operationally. A cut-off to remove clutter of $5°$ removes most clutter, although for use where clutter removal is vital, such as
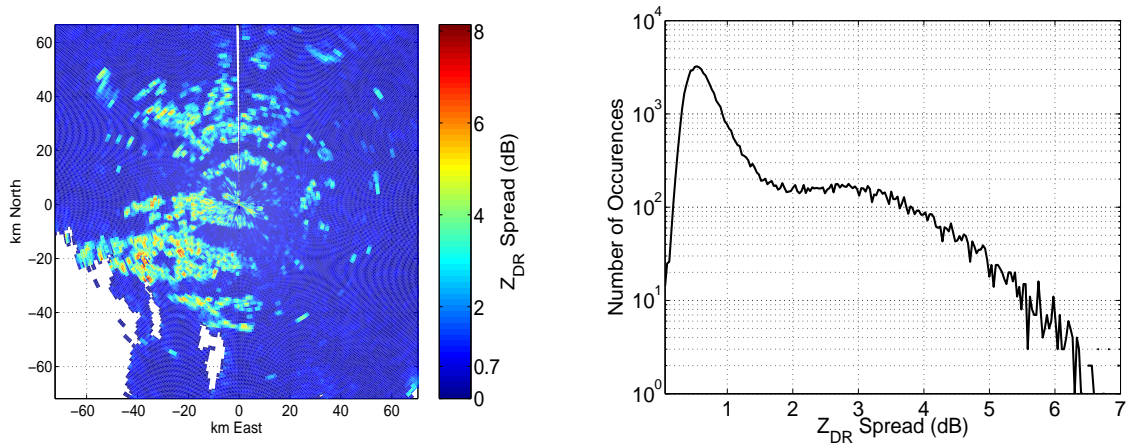
Figure 7.6 *False colour plot of spread of Z_{DR} from a PPI scan with the Thurnham radar and histogram of values found. The ground clutter can be clearly seen by eye, the hydrometeors being blue with values ≈ 0.7 dB, and clutter with higher values. It can be seen that there is significant variation of these values within the rainfall.*

for the integrated Z/Z_{DR} technique for rainfall estimation, this could be reduced to $2.5°$.
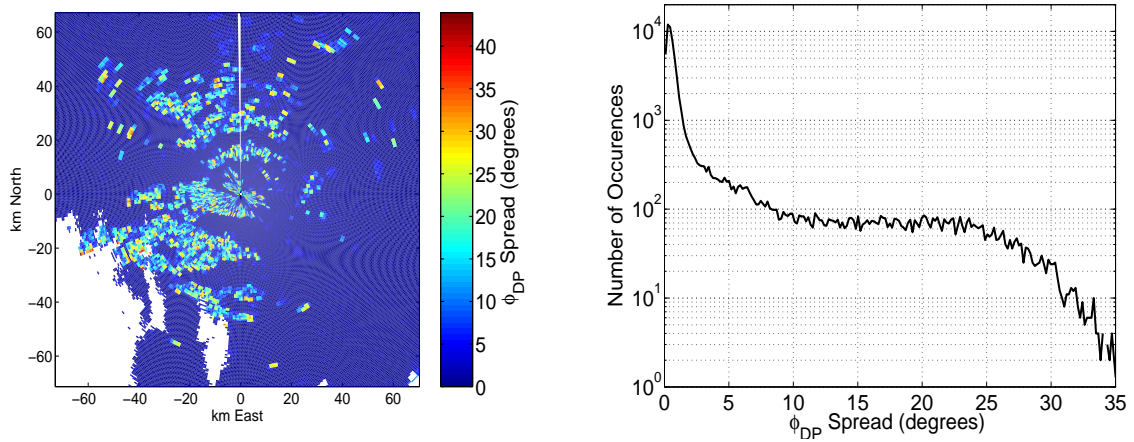
Figure 7.7 *False colour plot of spread of ϕ_{DP} from a PPI scan with the Thurnham radar and histogram of values found. The ground clutter can be clearly seen by eye, the hydrometeors being blue with values $\approx 1°$, and clutter with much higher values. It can be seen that there are only small variations within the rainfall.*

7.3.1.4 USING A DYNAMIC CLUTTER MAP

Use of a "clutter map" is common (recently for example Meischner *et al.*, 1997) for traditional single parameter radars but these do not allow for the seasonal (vegetation growth) and long term (addition/removal of objects) variations in clutter returns. A clutter map is also not able to detect temporary anaprop returns. A dynamic clutter map would involve updating the clutter map used regularly with information from a previous time period. This dynamic clutter map would predominantly remain constant with minor changes due to changes in the ground targets. The clutter map can be formulated from consistency of the appearance of echo in each pixel, but with L_{DR} scans available the consistency of high L_{DR} may give a better clutter map.

Currently the operational network radars of the Met Office use signal variability to detect clutter which rejects $45 - 95\%$ of clutter, then the marginal signal variability points are compared to a dynamic clutter map to remove those pixels classed as usually cluttered (Sugier *et al.*, 2002).

For polarisational operational radars a similar use of a dynamic clutter map could be designed. The best parameter for determining clutter pixels operationally is the spread in ϕ_{DP} values. Very high values of spread can be removed without fear of a false alarm, with the more marginal values determined using a combination with a dynamic clutter map to determine the likelihood of a given pixel being clutter. Similar fuzzy logic systems are suggested by Gourley *et al.* (2005) and Gourley *et al.* (2006).

7.3.2 CALIBRATION OF THE RADAR

Calibration of the radar will be of the utmost importance for using rainfall estimation algorithms. For the integrated Z/Z_{DR} technique to retain the desired 25% accuracy in moderate rainfall rates, reflectivity must be calibrated to 1 dB, and Z_{DR} to 0.1 dB. Although not trivial to automate, reflectivity can be calibrated to the necessary accuracy using the consistency of Z, Z_{DR} and ϕ_{DP} along rays as suggested by Goddard *et al.* (1994b). Calibrating Z_{DR} was discussed in section 3.3. Operationally a solution must

be found and potentially incorporated into the chosen scan strategy. Again, viewing the sun can be ruled out as, although it occurs every day, it tests only the receiver, not transmission. This leaves the possibilities as either considering light rain or vertical dwells. Distinguishing between lots of small drizzle drops or a small number of large raindrops will be even tougher than with CAMRa due to the increased noise. This leads to the optimal option for calibrating Z_{DR} to be vertical dwells, although these require some time in the scan strategy to be assigned; not just during the dwell, but also adjusting elevation to and from vertical. The Thurnham radar currently operates on a 10 minute cycle, which performs low level PPIs at 5 minute intervals, with a vertically pointing scan once per cycle as well as "L_{DR} scans" and high level PPIs for Doppler winds. This means that a new calibration can be calculated every 10 minutes when a target is present, which will allow for any drift in calibration to be quickly recognised.

7.3.3 ATTENUATION AND DIFFERENTIAL ATTENUATION

Attenuation is the reduction of power of the radar beam caused by absorption and scattering (not including the spreading caused by diffraction). Once the beam has reduced power, there is less power to be scattered by the targets, hence less returned power. The returned power is then attenuated again on the return trip, so the power of the signal detected by the radar is reduced during the trip in both directions. The reduced power is then converted to reflectivity, resulting in reduced reflectivity. For a graphical demonstration see figure 7.8.

Attenuation of radar beams by air is a very small effect, although hydrometeors may have a significant attenuation. The attenuation of the beam is greater at higher radar frequencies, hence the Thurnham radar will suffer more attenuation than the Chilbolton radar. At S-band (such as with the Chilbolton radar) attenuation by meteorological targets is negligible in all but the very heaviest of rains. At C-band, such as used operationally in the UK, attenuation will be a more significant problem, occurring with higher regularity. Attenuation means that any rain behind very heavy rain appears reduced. An example of attenuation observed with the Thurnham radar is shown in figure 7.9.
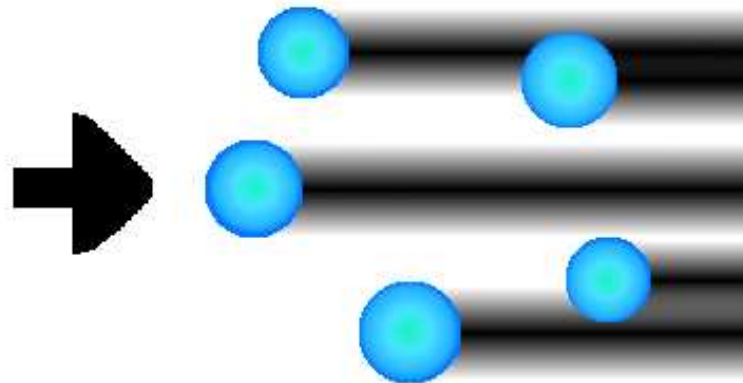
Figure 7.8 *Schematic of attenuation, with raindrops reducing the power in a radar beam. In the plot, the radar beam is entering from the left (shown by the arrow) and meeting raindrops, represented as blue circles. The beam passing through the drop reduces the power in the beam behind as is indicated by the darkening at the right of the figure. Note that in this figure the effect is vastly exaggerated.*
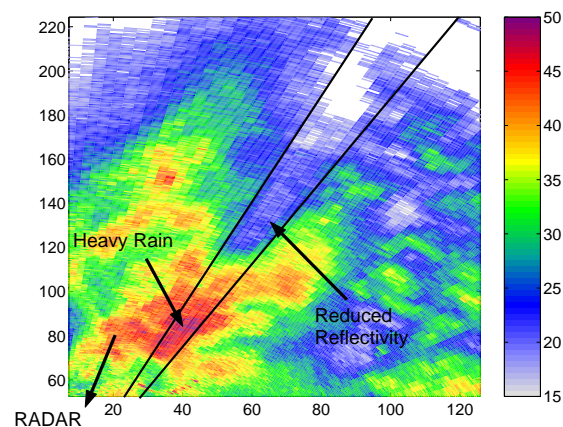
Figure 7.9 *Attenuation as observed by the Thurnham C-band radar. Indicated is the region of heavy rain, with the rain with reduced reflectivity behind. Lines to show radials from the radar are shown for clarity.*

Differential attenuation is the effect where the Z_{DR} signal is reduced by the presence of heavy rain nearer the radar. The Z_{DR} is affected by attenuation due to the horizontally polarised beam being attenuated more strongly than the vertically polarised version, because the drop shapes imply the horizontal beam must travel through more water than the vertical beam. Differential attenuation becomes significant at lower rates than attenua-

tion of Z, this is because of the scale of variation in Z_{DR}, despite the specific differential attenuation (in dB per km) being smaller than the specific attenuation (attenuation per kilometre in dB per km) because of the signal size. Differential attenuation can have a quite interesting effect on observations. When observing light rain beyond an area of very heavy rain, negative Z_{DR} can be recorded, where attenuation in the heavy rain has reduced the already low Z_{DR}. The lower attenuation for the vertically polarised waves is the prime reason for the current UK operational radar network, of which all but the Thurnham radar do not offer polarisation diversity, using a vertically polarised radar beam.

Attenuation can be corrected with reflectivity alone. Hitschfeld and Bordan (1954) suggest that attenuation, in dB, is given by

$$A = \int K R^{\alpha} dr, \tag{7.1}$$

where A is attenuation in dB per mile, r is range in miles and R is mm/hr. At C-band they suggest $K = 0.0047$ and $\alpha = 1.1$ (note that these values are for Imperial units of equation 7.1), calculating R from a standard $Z - R$ relationship. Because R is calculated just from a $Z - R$ relation, this is as error-ridden as the rainfall calculated this way for the same drop size spectrum change reasons. However, the bigger error in the method of Hitschfeld and Bordan (1954) is that caused by small changes in the calibration of Z. As the correction is applied gate-by-gate, the correction becomes unstable as shown by Hildebrand (1978). Methods using just Z or Z and Z_{DR} for attenuation corrections suffer from instability, and hail causes problems as it is relatively non-attenuating.

The introduction of dual polarisation to radar has meant improvement in attenuation correction. The cause of differential attenuation is the same as the creation of the differential phase shift observed with polarisation radar (see section 2.5.1). Bringi *et al.* (1990) show estimation of attenuation and differential attenuation as a function of K_{DP}. So

$$A_H = \beta_H K_{DP} \tag{7.2}$$

and

$$A_{DR} = \beta_{DR} K_{DP}, \tag{7.3}$$

where, this time A is in dB/km. Values of $\beta_H = 0.054$ and $\beta_{DR} = 0.0157$ are suggested for use at C-band, allowing for improved correction of Z and Z_{DR}, although retaining problems with stability. Smyth and Illingworth (1998) proposed a correction scheme for S-band radar using the negative Z_{DR} behind the heavy rain, and ϕ_{DP} measured, which remains stable, presenting results showing correction good to 1 dB. At C-band Smyth and Illingworth (1998) suggest the algorithm is simpler as the ϕ_{DP} would not be needed as A_{H} and A_{DR} can be assumed linearly related at C-band, hence the negative Z_{DR} can be used to estimate reflectivity attenuation.

The integrated Z/Z_{DR} technique presented in this thesis is untested for use where attenuation correction applies. This is because, once differential attenuation becomes significant, phase shift is strong enough for rainfall estimation via the ZPHI technique, so once attenuation is occurring, ZPHI should be used. This was shown to have improved rainfall rate by Le Bouar *et al.* (2001).

7.4   INTEGRATED Z/Z_{DR} IN THE OPERATIONAL ENVIRONMENT

Operationally the integrated Z/Z_{DR} technique will remain essentially the same as was described in chapter 5, although a few minor alterations are required. The need for a different criterion for clutter rejection to that used for Chilbolton data was considered in section 7.3.1. The lines of expected Z and Z_{DR} must be corrected for the changed radar frequency as discussed in section 7.1.1.

Use of any radar to rainfall algorithm in an operational system requires an algorithm that can be run quickly, so that all the data processing and storage necessary can be performed quicker than it is taken. Modern computing means that complex algorithms are possible, but algorithm efficiency remains an important consideration.

7.4.1 GRID SIZE FOR USE IN THE OPERATIONAL INTEGRATED Z/Z_{DR} TECHNIQUE

The increased noise and reduced resolution of the operational radar has implications on the grid size usable with the integrated Z/Z_{DR} technique. Assuming equation 5.21 from section 5.6.2.1 and the error of 0.7 dB, 49 points are required for 25% accuracy. To examine the grid size the method used in section 5.6.2.1 to generate figure 5.13 will be applied for Thurnham data. Here a 64×64 data points area is used and N_{w} calculated over various grid sizes ranging from 4096 to 4 points, with results plotted in figure 7.10. This figure shows the expected behaviour, with large noise in the smallest grid, which
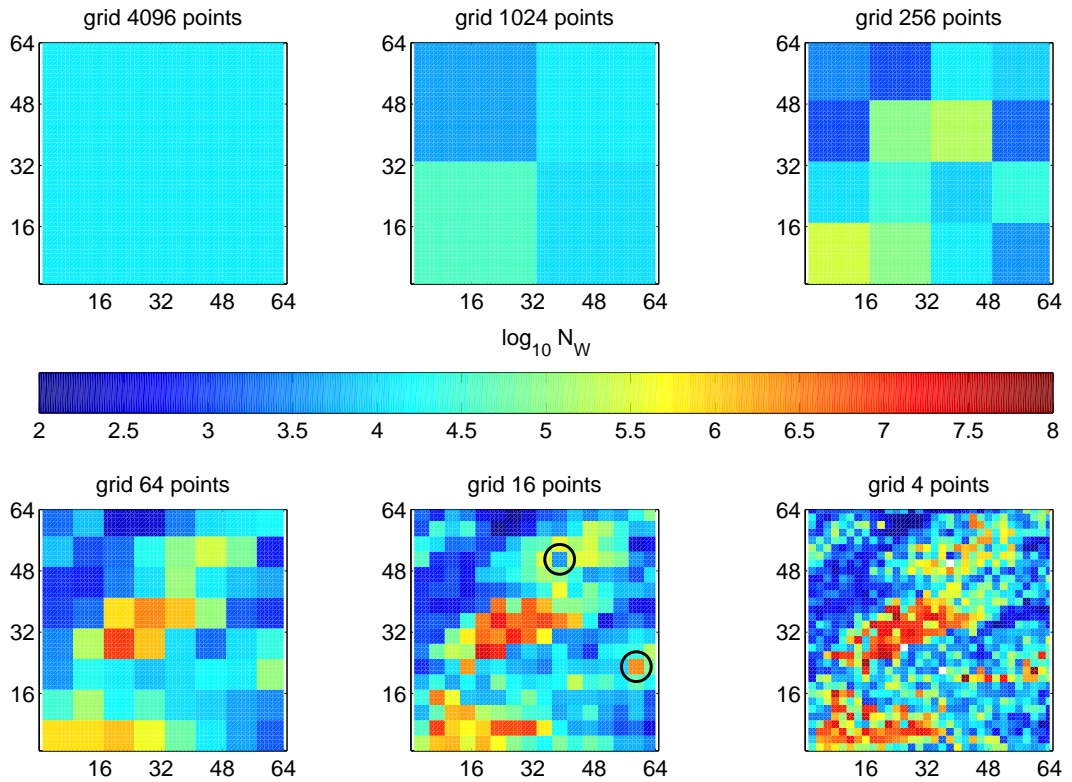
Figure 7.10 *Colour plots showing the N_{w} calculated from grids of various sizes. The data used was taken with the Thurnham radar, where each pixel has range of 500 m and has $1\,^{\circ}$ in azimuth at a range of 90 km (chosen for a large region of moderate rain). The grid scales are [top left] ~ 55 km, [top centre] ~ 30 km, [top right] ~ 15km, [lower left] ~ 7 km, [lower centre] ~ 3.5 km, [lower right] ~ 1.8 km. Some extreme points are indicated in the lower middle plot, and are explained further in the text.*

is reduced in the next grid (16 points) and indistinguishable by 64 points. Although the 16 point grid a shows generally good pattern there remains some unacceptable noise; example points showing particularly extreme values which are most probably unphysical are indicated. This means that the algorithm requires of order of 50 points as predicted above.

As the resolution of Thurnham data is lower than Chilbolton data, the grid used needs to be larger. Choice of grid size becomes a greater compromise for Thurnham than Chilbolton. Enough points for accurate calculation are required, yet if the area selected is too large natural variability will not be adequately characterised. Within 50 km a 5×5 km grid is usable, but beyond this the data volume from the $1°$ beam is too small for enough data to allow for the Z_{DR} error. To reach the ranges of the radar the grid must be increased to 10×10 km (it is worth considering at the largest ranges ~ 250 km the beam is well above the surface [~ 7 km with a $0.5°$ elevation] and also well above the bright band so use of the integrated Z/Z_{DR} technique is unlikely to be feasible).

For operational use it is preferable to use a grid based on a polar grid. The natural variations in rain do not occur on a polar grid based around the radar; a Cartesian approximation would give a better representation of the true changes. This Cartesian grid approximation is formulated to have correct range for the chosen grid scale, with number of azimuthal rays per box decreasing with range, to give the sector of an annulus closest to a square of defined length. To view the grid that results from the grid resolution and Cartesianised polar coordinates, see figure 7.11. Each grid box in the figure can be seen to be near square. The grid boxes become more square as the range from the radar increases. The central ring contains just three grid boxes each with a sector, one third of a circle. The figure also shows the resolution change, where the central grid is smaller than the outer.
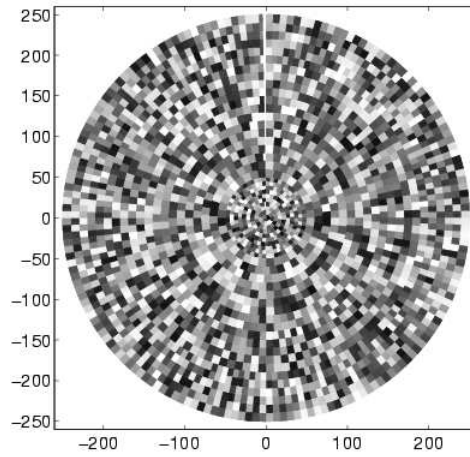
Figure 7.11 *Greyscale plot to show the near Cartesian polar grid for use with the integrated Z/Z_{DR} technique. The plot shows colour from a random number generator, which shows the grid clearly, although the darkness of the colour has no real meaning.*

7.5 OPERATIONAL EXAMPLES

In this section some examples of the integrated Z/Z_{DR} technique being used with the Thurnham operational radar will be investigated. The examples are limited due to a very small amount of reliable data from the radar at the time of writing.

7.5.1 EXAMPLE 1

This first example is for data taken during April the 7th of 2005, when the radar was in the early testing stages, during which time it was located in Alabama, USA. The weather on the occasion shows very heavy showers embedded in widespread moderate rainfall. The data chosen (figure 7.12) is a 5×5 km box of data centred on one of the embedded convective regions. The figure shows that this region has an effective (may be a μ effect) drop concentration of 2000 m^{-3} mm^{-1}. This corresponds to $a = 275$. This figure shows the very large noise level in the data of the Thurnham radar, showing a spread of more than 3 dB in Z_{DR} data with 40 dBZ. The estimated $N_{\mathrm{w}}^{\star}$ and hence a suggest the maximum rainfall rate within this embedded convection is 51 mm/hr, whereas if $N_{\mathrm{w}}^{\star}$ was assumed to be 8000 m^{-3} mm^{-1}, this would be 81 mm/hr.
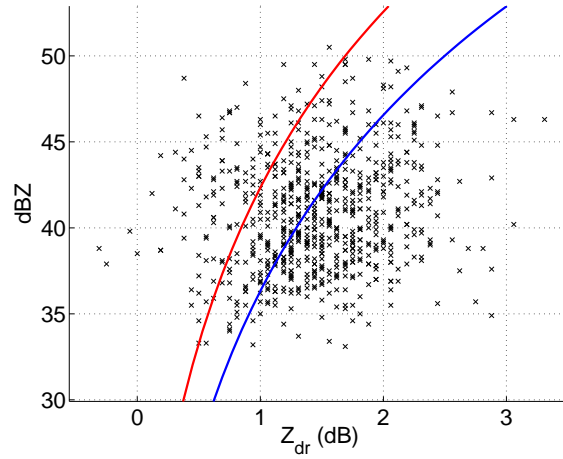
Figure 7.12 *A plot of Z and Z_{DR} for a 5×5 km area of data taken by the Thurnham radar, during testing in position in Alabama, USA. The red line shows the line corresponding to N_{w} of 8000. The blue line shows the fit from the integrated Z/Z_{DR} technique which yields $N_{\mathrm{w}} = 2000$ and $a = 275$.*

7.5.2   EXAMPLE 2

Example 2 considers the variations of a over a scan. The scan occured at $00:09$ GMT, 29th October, 2005, with the radar in its final position in Thurnham. This day rain was falling related to a front trailing from a low pressure system over the Arctic Ocean.

The left panel of figure 7.13 shows the reflectivity from the scan chosen, after removal of ground clutter using the spread of phase shift, ϕ_{DP}. Note that this scan is the one used for demonstrating clutter removal in section 7.3.1. Care has been taken to ensure the data shown does not include the bright band. The a calculated from the data is shown in the right panel of figure 7.13. It was calculated using a grid resolution of 5×5 km within 50 km range, 10×10 km outside that. The scan shows that generally this event had a low drop concentration, shown by high a. The heaviest rainfall to the north of the radar shows a low value of a, hence high drop concentration, although this pattern is not repeated to the west. To the west-most side of this heavy rain region, attenuation is found, so this data is unused for the integrated Z/Z_{DR} technique. However the ZPHI technique would be applicable here.
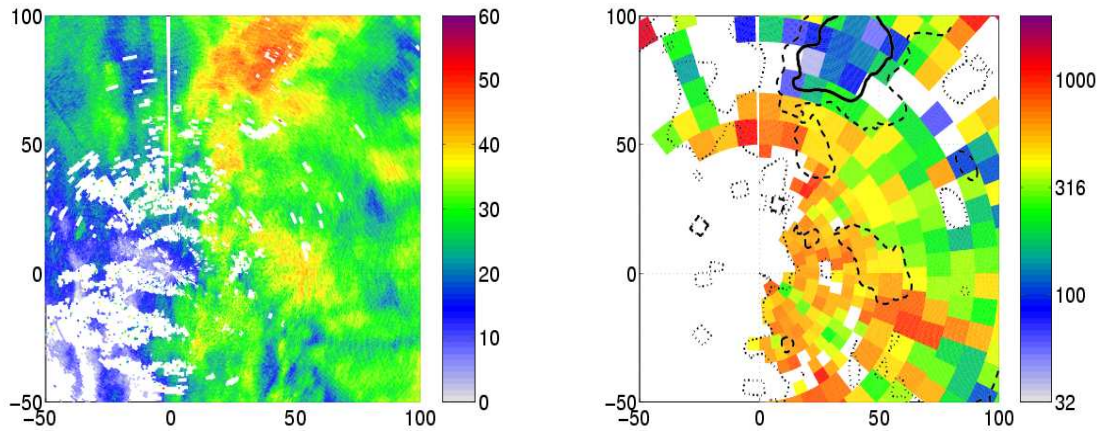
Figure 7.13 *Plots from a PPI taken at* $00 : 09$ *GMT,* 29th *October, 2005. [Left] Reflectivity in (dB), [Right]* a*. Note that the colour is based on a log scale. Overlaid are contours of reflectivity (this is averaged to make contours less noisy and hence more meaningful). The contours show the reflectivity (smoothed to avoid noise) with values; solid line* 40 *dBZ; dashed line* 35 *dBZ and dotted line* 25 *dBZ. These contours show where the rain, and especially heavy rain is occurring.*

7.5.3   FURTHER EXAMPLES

To demonstrate some of the variation of derived $Z - R$ relationships six further plots of Z against Z_{DR}, with lines showing best fit and $a = 200$ line, are shown in figure 7.14. The data used in these plots is after careful calibration of Z_{DR} using vertical dwells and removal of non-rain data points. The plots span different types of rain, including heavy showers, widespread stratiform rain and frontal rain. The grid size used varies dependent on range from the radar, but is appropriate to give an accurate retrieval as discussed in section 7.4.1, with grid sizes of 5 to 10 km.

7.6   SUMMARY

This chapter has examined the use of the integrated Z/Z_{DR} technique, as described in chapter 5, in the operational environment.

The principal difference between the CAMRa radar and radar used operationally in Europe is the wavelength that is used, affecting the occurrence frequency of non-Rayleigh scattering by meteorological targets. To reduce the cost of operational dual polarisation

(a) $a = 386$ **(b)** $a = 142$ **(c)** $a = 234$

(d) $a = 227$ **(e)** $a = 371$ **(f)** $a = 96$
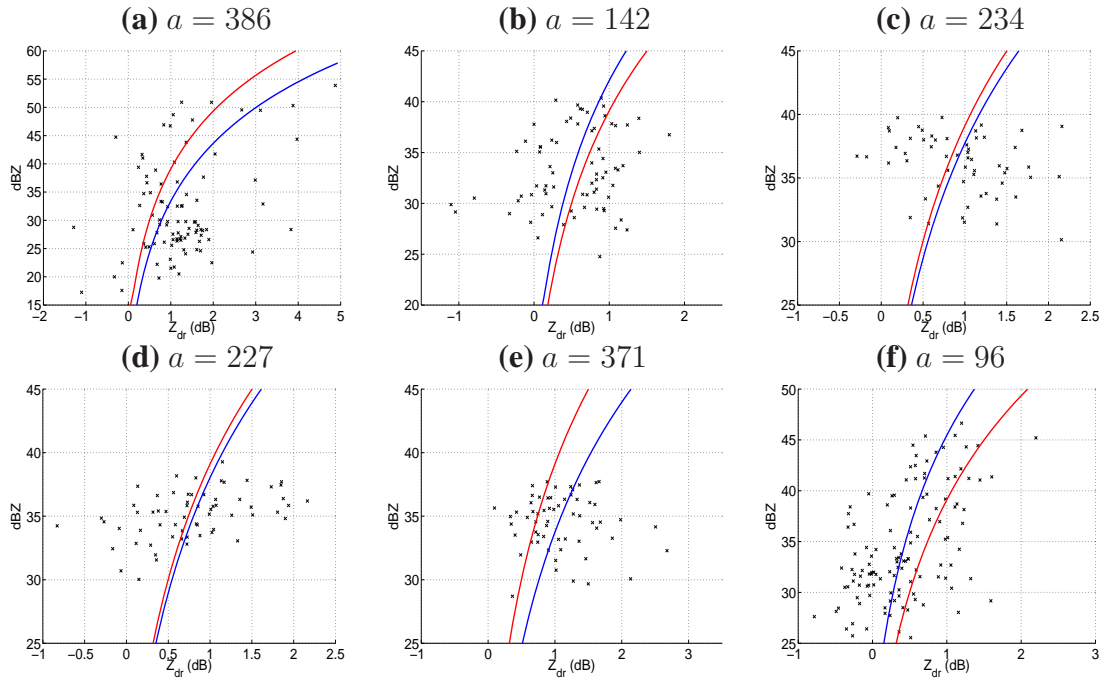
Figure 7.14 *A selection of Z/Z_{DR} plots from areas of Thurnham radar data. The data are from different scans and days, during different conditions (all are however from events during summer months). Individual data points are shown as black crosses, with the lines shown being lines of constant a (hence N_{w}): the red line is the $a = 200$; blue is the best fit line, of value shown above the plot.*

radars (to make networks of such radars a financially viable prospect) use the "hybrid" mode of dual polarisation, where the horizontal and vertical pulses are released together (transmitting at $45°$), then receiving in both channels. This has both advantages (better measurement of Z_{DR}, ϕ_{DP} and K_{DP}) and disadvantages (no simultaneous L_{DR}). The fast scan rates required operationally were explained to mean that the accuracy of measurement cannot be as good as a research radar can be. With the addition of the imperfections inevitable from the cheaper antenna on an operational radar this means that the radar parameters cannot be measured with great accuracy, and are unlikely to be better than 0.5 dB.

The Thurnham radar, the first polarisation radar to join the UK operational radar network, was introduced in section 7.2. The specifics of this radar are examined to estimate the expected errors in Z_{DR} using this radar, using spectral widths recorded by the CAMRa radar. As spectral widths of 0.75 m/s are expected during moderate rain events figure 7.3

shows that Z_{DR} in moderate rain cannot be measured more accurately than 0.5 dB (before radar imperfections are added). It was then shown that the radar actually records Z_{DR} with an accuracy of 0.7 dB with a near Gaussian distribution (figure 7.5). It was explained that this noise in Z_{DR} data from the Thurnham radar means that point by point Z and Z_{DR} will not be an improvement on a simple $Z - R$. However the data will be ideally suited for integrated techniques such as the integrated Z/Z_{DR} technique or ZPHI technique of Testud *et al.* (2000).

Clutter removal with the operational radar was discussed. Since simultaneous L_{DR} is unavailable, it was concluded that the spread (texture) of ϕ_{DP} gave the best results, but a fuzzy logic system may be implemented for more robust relations.

Section 7.3.3 describes the problems of attenuation, explaining that the lower wavelength (than the Chilbolton radar) of the Thurnham radar means that attenuation and hence differential attenuation are increased. Attenuation is then described in detail, with correction discussed.

Finally, the use of the integrated Z/Z_{DR} technique in the operational environment is examined, explaining the need for a larger grid resolution with the operational radar due to the lower grid resolution. The use of a polar, near Cartesian grid is examined and such a grid shown. The chapter ends with some examples of the use of the integrated Z/Z_{DR} technique are examined, and discussing the observed results.

CHAPTER 8:
CONCLUSIONS AND FUTURE WORK

Rainfall is of critical importance to mankind, influencing industry, property and even livelihoods. However, rain is remarkably difficult to measure because of its small scales of variation in time and space. Rain gauges provide a good measure of the rain at a point, but for a good coverage radars are needed to provide remotely sensed rainfall. This thesis has examined the potential of an integrated technique to accurately estimate the moderate rainfall rates that are common in north-western Europe using the new operational dual-polarisation radars.

8.1   THE NATURE OF RAINFALL

The introductory chapter, 1, described the normalised gamma distribution of rain drops that represents natural rainfall well. Chapter 2 then showed the drop shapes that these sizes have, explaining the polarisation parameters available from dual-polarisation radar.

In Chapter 4, 61 months of high resolution rain-gauge data is analysed. The frequency of occurrence of rainfall rates has been examined and showed that moderate rainfall rates that are considered in this thesis occur at less than 1% of the time, yet this rain accounts for $\sim 40\%$ of the accumulated rain throughout the period.

Rain was shown to have the curious property that whatever the rate, the relative changes in that rate are constant. This was shown in chapter 4. This means that very heavy rain has very large variations in intensity whereas the lighter rains have small changes, however the variations are proportional to the average rate, so in relative terms both rains are equally variant.

The decorrelation of rainfall was also examined. It was shown that as expected convective rain has much shorter decorrelation time than stratiform rain as would be expected

from the nature of the two types. The decorrelation time to a correlation of 0.5 for high accumulation convective rain is 5.1 minutes, whereas for high accumulation stratiform rain this decorrelation time is much higher, 26.8 minutes. This effect is also shown from the seasonal decorrelation, showing shorter decorrelation in the summer months. The overall decorrelation to 0.5 takes just 4.5 minutes, reaching e^{-1} in just 9.3 minutes. This is a slower decorrelation than is shown in Barcelona in the work of Burgueño, A. and Vilar, E. and Puigcerver, M. (1990), as would be expected by the increased stratiform proportion of rain in the UK. This decorrelation affects the accuracy of calculating accumulations when taking "snapshots" of the current rain rate as does a radar. The errors created by using "snapshots" are found to be 40% when sampling only every 15 minutes, dropping to 20% at 5 minutes, and just 10% if one is to sample every 2.5 minutes. This will be a concern when considering accumulations as calculated by radar.

The power spectrum of rain was formulated in chapter 4. The spectrum is compared to the model formulated by Veneziano *et al.* (1996), showing the same characteristic segmented model with turning points similar to those expected from the work of Veneziano *et al.* (1996) (the turning points at slightly higher frequencies than they found, but within two standard deviations). The third turning point of the model is not seen in the data from the Chilbolton drop counter, because the temporal resolution of the data is at a similar level to the expected frequency of the final turning point. The Chilbolton data shows the first turning point: the energy input scale (the scale of convective cell clusters), at 16.1 minutes (~ 10 km). The second turning point, from diffusion in turbulent flow, occurs at 4.8 minutes (~ 3 km). Although the Chilbolton data shows the segmented spectrum the model predicts, the gradient of each segment is flatter than the model suggests, having gradients of approximately half that of the model in each segment.

The nature of rainfall has inevitable effects on radar estimation of rainfall. The amounts and sizes of drops control the radar reflectivity; the changes in these are a significant part of the large errors with traditional $Z - R$ radar rainfall algorithms. The shapes of the raindrops allow for polarisation of radar beams to give increased information on the rainfall with Z_{DR} and ϕ_{DP}. The raingauge data shows that the moderate rainfall rates

that this thesis concerns constitute 36% of the total accumulated rain in Chilbolton. The decorrelation of rainfall has impacts on the accuracy of gauge-radar comparison, meaning that by taking a snapshot of rainfall every 5 minutes, even with perfect measurement, a 20% error in hourly accumulation is found. This situation will be worse in convective rain where decorrelation occurs more rapidly. The power spectral density of the rain shows the time variations of the rainfall, showing that convective cell clusters pass at a scale of 16 minutes.

8.2   THE USE OF DUAL-POLARISATION IN OPERATIONAL RADAR

Chapter 2 examined various methods to estimate rainfall rates from radar. The chapter began with a brief discussion of the problem associated with using reflectivity alone to estimate rainfall rates. It is explained that the huge errors observed with the traditional methods are partially caused by drop spectrum variations. Other factors such as ground clutter and calibration problems add to these problems, creating the often quoted factor of two error in radar rainfall estimation.

The use of differential reflectivity (defined as the ratio of horizontally and vertically polarised reflectivity) is discussed in terms of rain rate estimation, and its appearance due to the oblate drop shapes. Section 2.4.3 explains the sampling method of an alternate pulse radar such as the CAMRa radar, resulting in the sampling errors in Z_{DR}. A number of options for calculating rainfall from individual Z and Z_{DR} points are introduced: the physically based method of Illingworth and Blackman (2002) where Z/R is a function of Z_{DR}, and potential use of $\log(Z_{\mathrm{DR}})$ to define Z/R. Further suggestions using powers of both Z and Z_{DR} (in both logarithmic and linear terms) are considered, although it is stated that these algorithms are unjustifiable if the power for reflectivity is not one. The errors in rainfall rate that result form the sampling errors of Z_{DR} are explained and quantified, with a discussion of the problems of negative Z_{DR}, which is unphysical, but occurs as a result of the sampling noise.

In section 2.5 the differential phase, ϕ_{DP}, is considered. Its appearance due to rain drop oblateness is explained, followed by introducing the specific differential phase, K_{DP}. We saw that use of K_{DP} for estimating rain rates is an improvement over standard $Z - R$ methods as the transformation is more linear, and unaffected by hail. However, K_{DP} does not become large enough to be accurate for improvement until rain rates become heavy. The sampling errors in K_{DP} were explained, having similar source and form to those of Z_{DR}. For the moderate rainfall rates that this thesis focused upon, the specific differential phase gives no improvement over a standard $Z - R$ relation; only 40% accuracy can be achieved at rain rates as high as 50 mm hr^{-1}. We see another problem with R from K_{DP} is the effect of the drop size distribution shape parameter, μ, which adjusts the exponent in the K_{DP} to R relation. A typical $\mu = 5$ value leaves the exponent as 1.4, hence almost as non-linear as the $Z - R$ relations.

The combination of polarisation parameters to estimate rain rates is considered, starting with the combination of K_{DP} and Z_{DR}. This option can use linear Z_{DR} to avoid numerical instability from negatively observed Z_{DR}. However, the noise on both Z_{DR} and K_{DP} is large, so when combining them the noise in estimated rainfall is very large, and also the hail independence advantage of K_{DP} is lost.

Given the normalised drop size spectrum that represents natural rain well has three parameters, it would seem that excellent estimates would be available from using the three radar parameters, Z, Z_{DR} and K_{DP}. This power is however not available as the radar parameters are not independent, a fact that is taken advantage of for calibration of reflectivity by the technique of Goddard *et al.* (1994b).

Chapter 2 finishes by considering the possibility of integrated techniques to overcome the noise in the radar's polarisation parameters. The ZPHI technique of Testud *et al.* (2000), which estimates drop concentration, so as to derive rainfall from $Z = aR^{1.5}$, where a is a function of N_{w}, has been shown to give good rainfall estimation. It is considered and shown to be especially appropriate for use in an operational environment as it uses the ϕ_{DP} rather than its noisy derivative K_{DP}. The ZPHI technique shows great promise for operation rainfall estimation, but is only appropriate at heavy rain rates, or

in very widespread moderate rain. The technique estimates the drop concentration along a radar ray, so over a long yet narrow sector, longer than likely natural changes in N_{w}. The heavier rains that can be estimated with the ZPHI technique amount to 19% of the rainfall accumulated in the UK; a method for the moderate rates that accumulates 36% of UK rainfall is needed to really gain the rainfall estimation benefits dual polarisation offers to operational radar systems.

8.3   AN INTEGRATED TECHNIQUE FOR ESTIMATING MODERATE RAINFALL RATES

Chapter 5 describes the possibilities for a rainfall estimation algorithm suitable for accurate rainfall rate calculations at moderate rates. In these rains, the differential phase has not become a significant effect, so for polarisation parameters one must turn to differential reflectivity. In chapters 2 and 3; we saw that Z_{DR} is noisy, with an operational radar this noise is so large the benefit of its use is not seen when used at each gate. Even the very accurate Chilbolton radar has noise in Z_{DR} measurement which is large enough to cause problems with gate-by-gate methods (such as unphysical negative Z_{DR}). Integration of the normalised gamma distribution of rain drops, with constant concentration (N_{w}) yields a $Z - R$ relationship of $Z = aR^{1.5}$, with (assuming μ is constant) a inversely proportional to the square root of N_{w}. Changes in the exponent (1.5) relate to the functional relationship between drop concentration and median drop diameter. The aim of the technique described is to estimate a from the Z and Z_{DR} values over an area, which can be then used as a $Z - R$ over said area.

As the technique will use the rain drop shapes for calculation, any gates where the targets are not rain need to be carefully removed. The effect of hail, melting snow, ice and measuring the ground all cause Z and Z_{DR} to not give expected results when assumed to be measuring rain, but can be removed with other polarisation parameters, especially L_{DR}. Where L_{DR} is not available (as may be the case especially operationally) the spread of local K_{DP} values gives an excellent removal of ground clutter. The rainfall occurring

above the melting level (where the hydrometeors are ice) will also not have the same shape characteristics, so the technique described is only suitable for rain detected within the bright band.

Chapter 5 described a number of possible methods for calculating the $Z - R$ relationship to be used. Each subsequent method suggested solves problems with the previous; such problems are with biases being induced by non-independence of fitted variables and negative Z_{DR} being ignored. Also consistency and physical meaning of results is a consideration. Finally the optimised Z/Z_{DR} fit is arrived at, where the data is fitted in a least squares fit to lines of constant N_w and hence a. The method is described with a flow chart in figure 5.10. The rest of chapter 5 examines how the optimised Z/Z_{DR} fit is operated computationally, including the amount of data required for estimating rainfall rate to 25% (just four points for Chilbolton data, but ~ 50 for the Thurnham radar). Finishing the chapter is the possibility of reintroducing variability of b.

Chapter 6 shows examples of the use of the optimised Z/Z_{DR} fit. The chapter examines the variations detected across a scan and with time, examining the results from various different rain conditions. The results are considered in terms of the physical meanings of the derived drop concentrations. A case study where the rain derived by the integrated Z/Z_{DR} technique is compared to that of a tipping bucket rain gauge is examined. This shows the technique has excellent agreement with ground "truth".

8.4 USE OF POLARISATION RADAR IN AN OPERATIONAL ENVIRONMENT

Dual-polarisation radars are beginning to be introduced into operational weather radar networks of Europe (UK, France and Germany). Generally in Europe radars operate at smaller wavelengths than Chilbolton or the operational radars in the USA. Operational radars will inevitably not be as accurate as research radars due to financial constraints. This means that the polarisation parameters are especially noisy. Chapter 7 introduced

the Thurnham radar, a new dual-polarisation radar in the UK operational network. This radar has high levels of noise in polarisation parameters: Z_{DR} has a noise level of 0.7 dB. This level of noise is much to large for point by point rainfall using Z_{DR} data to show improvements over a standard $Z - R$ method.

A significant difference between the Chilbolton CAMRa radar and the Thurnham radar is the mode of operation. CAMRa operates with alternating pulses, whereas Thurnham operates in "hybrid mode", with simultaneous transmission. This means that the linear depolarisation ratio parameter is not available, so an alternative must be found for effective removal of ground clutter and anaprop. Four options for removal of ground clutter are considered in section 7.3.1. The copolar cross-correlation should have values near unity in rain (imperfections in the radar reduce the value from 1), but when the target is the surface the value would be much smaller. Unfortunately, ρ_{HV} is noisy (like many of the polarisation parameters), potentially causing missed clutter points (where clutter is not removed) or false alarms (where a genuine rain pixel is removed as clutter). This means that although ρ_{HV} seems a good replacement for L_{DR}, the noise loses its potential. The spread in Z_{DR} is considered next. In rainfall the noise in Z_{DR} will be approximately at the level of the sampling noise. With the Thurnham radar, however, the 0.7 dB noise in Z_{DR} from sampling is approaching the spread in Z_{DR} caused by ground targets. The spread of ϕ_{DP} has more promise, as the value in rain should again be small (the level of the sampling noise of ϕ_{DP}), with clutter having a high value. The range covered by rain in this case is small enough to distinguish the clutter from rain more effectively than with Z_{DR}. Finally a dynamic clutter map is considered. Here the likelihood of a point being clutter is considered from the frequency of a signal above a chosen threshold being measured. This way points that are often cluttered are removed and by changing the clutter map using the data of previous periods, the clutter map can allow for changes in the surface being viewed (i.e. the growth/death of trees, erection of new buildings etc.). A dynamic clutter map will be unable to detect anaprop pixels. Use of ϕ_{DP} spread in conjunction with a dynamic clutter map for marginal cases is recommended for operational use to minimise missed clutter and false alarms.

The shorter wavelength means that attenuation and differential attenuation are a more significant factor. Fortunately, once attenuation becomes large enough to cause problems with data in Z and Z_{DR}, ϕ_{DP} becomes large enough for use in the ZPHI technique. Attenuation must be recognised however, as incorporating attenuated data into algorithms using Z and Z_{DR} will lead to incorrect results.

The noisy polarisation parameters from operational radars, such as that at Thurnham, mean that the benefit to rainfall estimation will be via integrated methods (such as the integrated Z/Z_{DR} technique described in chapter 5 or the ZPHI technique). The radars provide a good measurement of Z (which can be calibrated to 1 dB using the method of Goddard *et al.*, 1994b), so the use of integrated polarisation parameters and individual reflectivity values will give good estimates of rainfall rates. The wavelength difference alters the values of Z and Z_{DR} a little, as is seen in figure 7.1, but the changes are known. The reduced resolution from the operational radar mean that the area over which the drop size distribution is characterised must be larger, increasing to 10×10 km boxes. Also for operational use, a polar grid is preferred for operation of the algorithm, so a polar grid with approximate Cartesian boxes is formulated.

The optimised fit integrated Z/Z_{DR} technique is to be tested with the Thurnham radar, to evaluate its performance in estimating rainfall in an operational environment. However one must be cautious with comparisons of radar and rain gauges, alternate methods of verification may be applied, (for instance use of profiling radar to estimate N_{w} from Doppler spectra).

Operational radar has been shown to have very high noise levels in polarisation parameters (the Thurnham radar has Z_{DR} noise of 0.7 dB). This level of noise might be expected to render the information provided by Z_{DR} useless. However, the integrated Z/Z_{DR} technique works as the noise in Z_{DR} is random, so is removed by the use of many points, drawing the information embedded within the noisy data.

8.5 FUTURE WORK

The work of this thesis can be continued in a number of ways. To further the statistics of rainfall, the drop distribution parameters such as normalised drop concentration or median drop diameter, could be considered in a manner similar to the rainfall as in chapter 4, this would give insight into the scales one must average on for algorithms such as the integrated Z/Z_{DR} technique.

A key improvement to the integrated Z/Z_{DR} technique would be the introduction of a calculated error in the derived N_{w}, a and R, giving an indication of the quality of the estimate, this would be important for data assimilation into numerical models.

The technique could also be used to investigate the development of rainfall events, for instance tracking a convective shower and using the technique could give an insight into the micro-physical makeup of the rain in such a storm.

Finally, validation of the technique with operational radar must be performed to show the benefit of the algorithm, this is likely to be performed using the Thurnham radar.

GLOSSARY

ANAPROP *Anomalous Propagation, the result of atmospheric conditions bending the radar beam back to the surface.*

ANTENNA *The device for focusing the transmitted and received signals (eg dish).*

AREAL *Of/over an area.*

AREAL RAINFALL *Average rainfall depth over an area.*

AXIAL RATIO, r *The ratio of the size of major and minor axis of drops.*

BEAM *The volume of focused microwave energy transmitted for the radar.*

CAMRa *Chilbolton Advanced Meteorological Radar. The world's largest steerable pointable meteorological radar, operating at S-band ($3GHz$ frequency, $10cm$ wavelength).*

CLUTTER *See "Ground Clutter".*

DIFFERENTIAL REFLECTIVITY, Z_{DR} *The ratio of power received in the horizontal polarisation, given horizontal transmission, and power received in the vertical polarisation, given vertical transmission. Defined as $Z_{\mathrm{DR}} = 10 \log_{10}\left(\frac{Z_H}{Z_V}\right)$; Seliga and Bringi (1976).*

DOPPLER VELOCITY, v *The radial velocity of the targets.*

DSD *Drop Size Distribution.*

DWELL TIME   *Time spent sampling a single ray of data.*

ECHO   *The returned radar transmission from the target(s).*

EFFECTIVE DROP CONCENTRATION   *The drop concentration of the normalised gamma distribution, assuming that $\mu = 5$.*

GATE   *An individual pixel in range (along the radar beam).*

(GROUND) CLUTTER   *The result of the radar beam impacting the ground surface, buildings or trees etc.*

HYDROMETEOR   *A falling precipitation particle.*

LINEAR DEPOLARISATION RATIO, L_{DR} *The ratio of power received in the vertical polarisation and the horizontal polarisation, both given horizontal transmission.*

NORMALISED GAMMA DISTRIBUTION/FUNCTION   *A widely used raindrop size distribution function; formula:*

$$N(D) = N_w f(\mu)(\frac{D}{D_o})^{\mu} \exp(-\frac{(3.67 + \mu)D}{D_o})$$
$$f(\mu) = \frac{6}{(3.67)^4} \frac{(3.67 + \mu)^{\mu+4}}{\Gamma(\mu + 4)}$$

PPI   *Plan Position Indicator scan. A scan in which elevation remains constant but azimuth changes.*

RAINFALL RATE, R *A measure of the amount of rain falling, usually given in mm/hr.*

REFLECTIVITY, Z *Also known as the 'reflectivity factor'; this is a measure of the*

reflectance of the target.

$$Z \left[mm^6 m^{-3} \right] = \int_0^\infty \frac{|K|^2}{0.93} N \left(D \right) D^6 dD$$

The magnitudes of this mean it is often expressed in the logarithmic unit, $dBZ = 10 \log_{10} \left(Z \left[mm^6 m^{-3} \right] \right)$. This is what is detected by a conventional radar.

RHI   *Range Height Indicator scan. A scan in which azimuth remains constant but elevation changes.*

SCAN RATE   *The speed to perform a scan (usually to perform a $360°$ PPI.*

SIDELOBES   *The further energy maxima located outside the main lobe of the radar beam. These have low power relative to the main beam, but may produce significant erroneous echoes in the right conditions.*

SPECIFIC DIFFERENTIAL PHASE SHIFT, K_{DP} *The change of phase difference between horizontally and vertically polarised returns with distance.*

TERMINAL VELOCITY   *The maximum speed at which a object can fall without decelerating, where gravitational and viscous forces are balanced. This is the speed at which hydrometeors fall. Proportional to $D^{0.67}$.*

$Z - R$ **RELATIONSHIP**   *The function by which one can convert from reflectivity (Z) to rainfall rate (R) or vice versa.*

SYMBOLS USED

CHAPTER 1

Z Radar reflectivity.

R Rainfall Rate.

a the coefficient of $Z - R$ relationships; $Z = \underline{a}R^b$.

b the exponent of $Z - R$ relationships; $Z = aR^{\underline{b}}$.

P_r Received power.

P_t Transmitted power.

g Antenna gain.

θ Beamwidth (horizontal).

ϕ Beamwidth (vertical).

h Pulse length.

$|K|^2$ The dielectric factor (for rain 0.93).

D_i Scatterer diameters.

λ Radar wavelength.

r Distance between sample and radar antenna.

C The radar constant.

N The number of drops.

dB Used to demonstrate something used in decibels; $\mathrm{dB}X = 10\log_{10} X$

N_0 The drop concentration for drops of zero size.

Λ Marshall and Palmer (1948) rain parameter, a function only of R.

N_{w} The drop concentration (normalised for constant liquid water content [close to R]).

D_{o} Median drop diameter.

μ Normalised gamma distribution; shape parameter.

$f(\mu)$ Normalising function in normalised gamma distribution; relates to the

shape parameter.

Z_{DR} *Differential Reflectivity.*

CHAPTER 2

Z *Radar reflectivity.*

R *Rainfall Rate.*

a *The coefficient of $Z - R$ relationships; $Z = \underline{a}R^b$.*

b *The exponent of $Z - R$ relationships; $Z = aR^{\underline{b}}$.*

N *The number of something (either drops or samples depending on context).*

D *The drop size.*

r *Drop axial ratio.*

D_{o} *Median volume drop diameter.*

μ *DSD shape parameter.*

N_{w} *Drop concentration.*

dB *Used to demonstrate something used in decibels; $\mathrm{dB}X = 10\log_{10} X$*

Z_{DR} *Differential Reflectivity.*

$Z_{\mathrm{1mm/hr}}$ *The reflectivity which would be a result of targets of 1 mm/hr rainfall rate. $Z_{\mathrm{1mm/hr}}$ is a function of Z_{DR}.*

c *The coefficient of rainrate relationships using Z_{DR}.*

$g(Z_{\mathrm{DR}})$ *A function of only Z_{DR}.*

α *Z exponent of $R = c\,Z^{\alpha}\,Z_{\mathrm{DR}}^{\beta}$.*

β *Z_{DR} exponent of $R = c\,Z^{\alpha}\,Z_{\mathrm{DR}}^{\beta}$.*

c_1 *The coefficient of rainrate relationship using linear Z_{DR}.*

α_1 *Z exponent of rainrate relationships using linear Z_{DR}.*

β_1 *Z_{DR} exponent of rainrate relationships using linear Z_{DR}.*

$SD(\hat{Z}_{DR})$ *Standard deviation of observed Z_{DR}.*

l *The of index of summation.*

ρ *Correlation.*

$\rho_{hh,vv}$ *Co-polar correlation at zero lag time.*

σ_v *Spectral width.*

n *The number of pulses.*

T_s *Time between pulses.*

λ *The radar wavelength.*

σ_{vn} *Normalised spectral width.*

PRF   *The pulse repetition frequency.*

ϕ_{DP} *Phase Shift.*

ϕ_V *Phase of vertically polarised return.*

ϕ_H *Phase of horizontally polarised return.*

K_{DP} *The specific differential phase shift.*

$\mathcal{A}$ *The coefficient of an R-K_{DP} relationship.*

$\mathcal{B}$ *The exponent of an R-K_{DP} relationship.*

c_2 *The coefficient of rainrate relationship using K_{DP} and Z_{DR}.*

α_2 *The K_{DP} exponent of rainrate relationship using K_{DP} and Z_{DR}.*

β_2 *The Z_{DR} exponent of rainrate relationship using K_{DP} and Z_{DR}.*

c_3 *The coefficient of rainrate relationship using K_{DP} and linear Z_{DR}.*

α_3 *The K_{DP} exponent of rainrate relationship using K_{DP} and linear Z_{DR}.*

β_3 *The Z_{DR} multiplier of rainrate relationship using K_{DP} and linear Z_{DR}.*

f *Constant used in the ZPHI technique.*

g *Constant used in the ZPHI technique.*

CHAPTER 3

Z *Radar reflectivity.*

Z_{DR} *Differential Reflectivity.*

dB *Used to demonstrate something used in decibels; $\mathrm{dB}X = 10\log_{10} X$*

N_{w} *Drop concentration.*

D_{o} *Median volume drop diameter.*

μ *DSD shape parameter.*

Z_H *Radar reflectivity from horizontal polarisation.*

Z_V *Radar reflectivity from vertical polarisation.*

D *The drop size.*

L_{DR} *The linear depolarization ratio.*

$\overline{Z_{\mathrm{DR}}}$ *Mean Z_{DR} measurement.*

$\sigma_{Z_{\mathrm{DR}}}$ *Standard deviation of Z_{DR} measurement.*

CHAPTER 4

Z_{DR} *Differential Reflectivity.*

Z *Radar reflectivity.*

dB *Used to demonstrate something used in decibels; $\mathrm{dB}X = 10\log_{10}X$*

v *Doppler velocity.*

R *Rainfall Rate.*

N *The number of something (either drops or samples depending on context).*

D *The drop size.*

N_{w} *Drop concentration.*

D_{o} *Median drop diameter.*

μ *Normalised gamma distribution; shape parameter.*

$f(\mu)$ *Normalising function in normalised gamma distribution; relates to the shape parameter.*

a *The coefficient of $Z - R$ relationships; $Z = \underline{a}R^{b}$.*

$F_Z(\mu)$ *A function of the shape parameter resulting from integration for reflectivity.*

$F_R(\mu)$ *A function of the shape parameter resulting from integration for rain rate.*

$H(\mu)$ *A function of the shape parameter, $H(\mu) = F_Z(\mu)F_R(\mu)^{1.5}$.*

$Z_{1\mathrm{mm/hr}}$ *The reflectivity which would be a result of targets of 1 mm/hr rainfall rate. $Z_{1\mathrm{mm/hr}}$ is a function of Z_{DR}.*

$|K|^{2}$ *The dielectric factor.*

L_{DR} *The linear depolarization ratio.*

b *The exponent of $Z - R$ relationships; $Z = aR^{\underline{b}}$.*

m The gradient of a line, $y = mx + c$.

c The constant of a line, $y = mx + c$.

$N_{\mathrm{w}}^{\star}$ Effective drop concentration.

σ_{total} Standard deviation error of combination of N_{samp} points.

σ_{point} Standard deviation error of a single sample.

N_{samp} Number of samples.

N_{req} Number of samples required.

T A number used in iterating to find $N_{\mathrm{w}}{}^{*}$; it is a function of $N_{\mathrm{w}}{}^{*}$.

CHAPTER 5

Z Radar reflectivity.

Z_{DR} Differential reflectivity.

dB Used to demonstrate something used in decibels; $\mathrm{dB}X = 10\log_{10}X$

L_{DR} The linear depolarisation ratio.

N_{w} Drop concentration.

a The coefficient of $Z - R$ relationships; $Z = \underline{a}R^{b}$.

T An algorithm value defined by equation 5.22.

RMS Root Mean Square distance of points to that N_{w}.

D_{o} Median drop diameter.

b The exponent of $Z - R$ relationships; $Z = aR^{\underline{b}}$.

$N_{\mathrm{w}}^{\star}$ Effective drop concentration.

μ Normalised gamma distribution, shape parameter.

CHAPTER 6

P_{HA} Near instantaneous (30s average) rainfall rate as a proportion of the hourly average rainfall rate.

R_{30s} / R_i Near instantaneous (30s average) rainfall rate.

R_{HA} Hourly average rainfall rate.

r	Normalised rainfall rate.
C	Used in finding a model of the rainfall PDF.
P	Probability of occurrence.
ΔR	Error in rainfall rate.
R	Rainfall rate.
N	Number of points.
RMS	Root Mean Square distance of points to that N_{w}.
σ_{option}	Standard deviation of points caused by error "option".
t	Time.
τ	Lag time.
ρ_x	Correlation between rain rate now and rate lagged by x s.
R_x	Rainfall rate at time x.
$\overline{R}$	Mean rainfall rate.
ω_1	First turning point of segmented spectrum, corresponding to the convective scale.
ω_2	Second turning point of segmented spectrum, corresponding to the introduction of microscale influence.
ω_3	Third turning point of segmented spectrum, corresponding to very small scales.

CHAPTER 7

Z	Radar reflectivity.
Z_{DR}	Differential Reflectivity.
a	The coefficient of $Z - R$ relationships; $Z = \underline{a}R^b$.
N_{w}	Drop concentration.
λ	Radar wavelength.
μ	DSD shape parameter.
L_{DR}	The linear depolarisation ratio.
ϕ_{DP}	Differential Phase Shift.
K_{DP}	Specific Differential Phase Shift.

PRF	*The pulse repetition frequency.*
dB	*Used to demonstrate something used in decibels;* $\mathrm{dB}X = 10\log_{10} X$
$\rho_{hh,vv}/\rho_{\mathrm{HV}}$	*Co-polar cross-correlation.*
A	*Attenuation.*
K	*Coefficient in attenuation equation.*
α	*Exponent in attenuation equation.*
A_{H}	*Attenuation of horizontal reflectivity.*
β_{H}	*Coefficient of horizontal reflectivity attenuation from* K_{DP}.
A_{DR}	*Differential attenuation; attenuation in* Z_{DR}.
β_{DR}	*Coefficient of differential attenuation from* K_{DP}.
$N_{\mathrm{w}}^{\star}$	*Effective drop concentration.*

CHAPTER 8

Z	*Radar reflectivity.*
Z_{DR}	*Differential Reflectivity.*
R	*Rainfall rate.*
ϕ_{DP}	*Differential Phase Shift.*
K_{DP}	*Specific Differential Phase Shift.*
μ	*DSD shape parameter.*
a	*The coefficient of* $Z - R$ *Relationships;* $Z = \underline{a}R^b$.

Bibliography

Andsager, K., Beard, K. V., and Laird, N. F. (1999). Laboratory measurements of axis ratios for large raindrops. *Journal of Atmospheric Science*, **56**, 2673–2683.

Battan, L. J. (1973). *Radar Observations of the Atmosphere*, chapter 7, pages 90–92. University of Chicago Press.

Beard, K. V. and Chuang, C. (1987). A new model for the equilibrium shape of raindrops. *Journal of Atmospheric Science*, **44**(11), 1509–1524.

Beard, K. V. and Jameson, A. R. (1983). Raindrop canting. *Journal of Atmospheric Science*, **40**, 448–454.

Beard, K. V. and Tokay, A. (1991). A field study of small raindrop oscillations. *Geophysical Research Letters*, **18**, 2257–2260.

Blanchard, D. (1953). Raindrop size distribution in Hawaiian rains. *Journal of Meteorology*, pages 457–473.

Brandes, E., Ryzhkov, A., and Zrnić, D. (2001). An evaluation of radar rainfall estimates from specific differential phase. *Journal of Atmospheric and Oceanic Technology*, **18**, 363–375.

Brandes, E., Zhang, G., and Vivekanandan, J. (2002). Experiments in rainfall estimation with a polarimetric radar in a subtropical environment. *Journal of Applied Meteorology*, **41**, 674–684.

Bringi, V. N. and Chandrasekar, V. (2001). *Polarimetric Doppler Weather Radar: Principles and Applications*. Cambridge University Press, 1st edition.

Bringi, V. N., Seliga, T., and Aydin, K. (1984). Hail detection with a differential reflectivity radar. *Science*, **225**, 1145–1147.

Bringi, V. N., Chandrasekar, V., Balakrishnan, N., and Zrnić, D. (1990). An examination of propagation effects in rainfall on radar measurements at microwave frequencies. *Journal of Atmospheric and Oceanic Technology*, **7**, 829–840.

Brunkow, D., Bringi, V. N., Kennedy, P. C., Rutledge, S. A., Chandrasekar, V., Mueller, E. A., and Bowie, R. K. (2000). A description of the CSU CHILL National Radar Facility. *Journal of Atmospheric and Oceanic Technology*, **17**, 1596–1608.

Burgueño, A. and Vilar, E. and Puigcerver, M. (1990). Spectral analysis of 49 years of rainfall rate and relation to fade dynamics. *IEEE Transactions on Communications*, **38**(9), 1359–1366.

Burt, S. (2005). Cloudburst upon Hendraburnick Down: The Boscastle storm of 16 August 2004. *Weather*, **60**(8), 219–227.

Chandrasekar, V. and Bringi, V. N. (1988). Error structure of multiparameter radar and surface measurement of rainfall. Part 1: Differential reflectivity. *Journal of Atmospheric and Oceanic Technology*, **5**, 783–795.

Chandrasekar, V., Bringi, V. N., Balakrishnan, N., and Zrnic, D. S. (1990). Error structure of multiparameter radar and surface measurement of rainfall. Part 3: Specific differential phase. *Journal of Atmospheric and Oceanic Technology*, **7**, 621–629.

Collier, C. G. (1986). Accuracy of rainfall estimates by radar, part 1: calibration by telemetering raingauges. *Journal of Hydrology (Amsterdam)*, **83**, 207–223.

Collier, C. G., editor (2001). *COST Action 75 - Advanced weather radar systems - 1993-97*. European Commision.

Crane, R. K. (1990). Space-time structure of rain rate fields. *Journal of Geophysical Research*, **95**(D3), 2011–2020.

Drufuca, D. and Zawadzki, I. I. (1975). Statistics of raingauge data. *Journal of Applied Meteorology*, **14**, 1419–1429.

Fletcher, J. O. (1990). *Radar in Meteorology*, chapter 1. (ed: D. Atlas), American Meteorological Society.

Folland, C. K., Karl, T. R., Christy, J., Clarke, R. A., Gruza, G. V., Jouzel, M., Mann, M., Oerlemans, J., Salinger, M. J., and Wang, S.-W. (2001). *Climate Change 2001: The Scientific Basis: Contribution of Working Group 1 to the Third Assesment Report of the Intergovernmental Panel on Climate Change*, chapter 2: Observed Climate Variability and Change, pages 99–181. Cambridge University Press.

Fritsch, J. M., Houze, R. A., Adler, R. Bluestein, H., Bosart, L., Brown, J., Carr, F., Davis, C., Johnson, R. H., Junker, N., Kuo, Y.-H., Rutledge, S., Smith, J., Toth, Z., Wilson, J. W., Zipser, E., and Zrnić, D. (1998). Quantitative precipitation forecasting: Report of the eight prospectus development team, U.S. weather research program. *Bulletin of the American Meteorological Society*, **79**(2), 285–299.

Frost, I., Goddard, J. W. F., and Illingworth, A. (1991). Hydrometeor identification using cross polar radar measurement and aircraft verification. In *25th Int. Conf. on Radar Met.*, pages 658–661. American Meteorological Society.

Goddard, J. W. F., Cherry, S., and Bringi, V. (1982). Comparison of dual-polarization radar measurements of rain with ground based disdrometer measurements. *Journal of Applied Meteorology*, **21**, 252–256.

Goddard, J. W. F., Eastment, J. D., and Thurai, M. (1994a). The Chilbolton Advanced Meteorological Radar: A tool for multidisciplinary atmospheric research. *Electronics and Communication Engineering Journal*, **6**(2), 77–86.

Goddard, J. W. F., Tan, J., and Thurai, M. (1994b). Technique for calibration of meteorological radars using differential phase. *Electronics Letters*, **30**(2), 166–167.

Goddard, J. W. F., Morgan, K. L., Illingworth, A. J., and Sauvageot, H. (1995). Dual-wavelength polarisation measurements in precipitation using the CAMRa and Rabelis radar. In *27th Conf. on Radar meteorology*. American Meteorological Society.

Golding, B., Clark, P., and May, B. (2005). The Boscastle flood: Meteorological analysis of the conditions leading to flooding on 16 August 2004. *Weather*, **60**, 230–235.

Golding, B. W. (1998). Nimrod: A system for generating automated very short range forecasts. *Meteorological Applications*, **5**, 1–16.

Gorgucci, E. and Scarchilli, G. (1997). Intercomparison of multiparameter radar algorithms for esimating of rainfall rate. In *Preprints: 28th Conf. on Radar meteorology*. American Meteorological Society.

Gorgucci, E., Scarchilli, G., and Chandrasekar, V. (1994). A robust estimator of rainfall rate using differential reflectivity. *Journal of Atmospheric and Oceanic Technology*, **11**, 586–592.

Gourley, J., Tabary, P., and du Chatelet, J. (2006). A fuzzy logic algorithm for the separation of precipitating from non-precipitating echoes using polarimetric radar observations. *Submitted to: Journal of Atmospheric and Oceanic Technology*.

Gourley, J. J., Tabary, P., and du Chatelet, J. (2005). Classification of hydrometeors and non-hydrometeors using polarimetric C-band radar. In *32nd Conference on Radar Meteorology*. American Meteorological Society.

Hagen, M. (1997). Identification of ground clutter by polarimetric radar. In *28th Conference on Radar Meteorology*, pages 67–68. American Meteorological Society.

Harrold, T. W., English, E. J., and Nicholass, C. A. (1974). The accuracy of radar-derived rainfall measurements in hilly terrain. *Quarterly Journal of the Royal Meteorological Society*, **100**, 331–350.

Hildebrand, P. H. (1978). Iterative correction for attenuation of 5 cm radar in rain. *Journal of Applied Meteorology*, **17**, 508–514.

Hitschfeld, W. and Bordan, J. (1954). Errors inherent in the radar measurement of rainfall at attenuating wavelengths. *Journal of Meteorology*, **11**, 58–67.

Illingworth, A. J. (2004). Improved precipitation rates and data quality by using polarimetric measurements. In P. Meischner, editor, *Weather Radar: Principles and Advanced Applications*. Springer.

Illingworth, A. J. and Blackman, T. M. (2002). The need to represent raindrop size spectra as normalized gamma distributions for the interpretation of polarization radar observations. *Journal of Applied Meteorology*, **41**, 286–297.

Illingworth, A. J. and Caylor, I. J. (1991). Co-polar correlation measurements of precipitation. In *25th Conference on Radar Meteorology*, pages 650–653.

Illingworth, A. J. and Johnson, M. P. (1999). The role of raindrop shape and size spectra in deriving rainfall rates using polarisation radar. In *29th Conference on Radar Meteorology*, pages 301–304.

Illingworth, A. J., Nicol, J., and Pavelin, E. (2005). A radar technique for mapping the humidity structure in the boundary layer. In *Royal Meteorological Society Conference 2005: Book of Abstracts: Measurements, observations and analysis - Joint weather and climate*, page 55.

Jones, D. M. A. (1956). Rainfall drop-size distribution and radar reflectivity. *Res. Rept. no. 6. Urbana: Meteor. Lab., Illinois State Water Survey*.

Jones, D. M. A. and Sims, A. L. (1978). Climatology of instantaneous rainfall rates. *Journal of Applied Meteorology*, pages 1135–1140.

Joss, J. and Waldvogel, A. (1990). *Radar in Meteorology*, chapter 29a, pages 577–606. (ed: D. Atlas), American Meteorological Society.

Kozu, T. and Nakamura, K. (1991). Rainfall parameter estimation from dual-radar measurements combining reflectivity profile and path-integrated attenuation. *Journal of Atmospheric and Oceanic Technology*, **8**(2), 259–270.

Le Bouar, E., Testud, J., and Keenan, T. D. (2001). Validation of the rain profiling algorithm 'ZPHI' from the C-band polarimetric weather radar in Darwin. *Journal of Atmospheric and Oceanic Technology*, pages 1819–1837.

Lee, G. W. (2003). *Effects in Rain Measurement by Radar: Effect of Variability of Drop Size Distributions*. Ph.D. thesis, Dept. Atmospheric and Oceanic Sciences, McGill University.

List, R. (1988). A linear radar reflectivity-rainrate relationship for steady tropical rain. *Journal of Atmospheric Science*, **45**, 3564–3572.

Marshall, J. and Palmer, W. (1948). The distribution of raindrops with size. *Journal of Meteorology*, **5**, 165–166.

Marshall, J., Langille, R., and Palmer, W. (1947). Measurement of rainfall by radar. *Journal of Meteorology*, pages 186–192.

Matrosov, S. Y., Kropfli, R. A., Reinking, R. F., and Martner, B. E. (1999). Prospects for measuring rainfall using propagation differential phase in X- and Ka- radar bands. *Journal of Applied Meteorology*, **38**, 766–776.

May, P., Keenan, T., Zrnic, D., Carey, L., and Rutledge, S. (1999). Polarimetric radar measurements of of tropical rain at 5-cm wavelength. *Journal of Applied Meteorology*, **38**, 750–765.

McKay, R. e. (2006). Royal Meteorological Society: Meteorological observing systems special interest group: Newsletter issue 22: Spring 2006.

Meischner, P., Collier, C., Illingworth, A., Joss, J., and Randeu, W. (1997). Advanced weather radar systems in Europe: The cost 75 action. *Bulletin of the American Meteorological Society*, **78**(7).

Nastrom, G. D. (1997). Doppler radar spectral width broadening due to beamwidth and wind shear. *Annales Geophysicae - Atmospheres Hydrospheres and Space Sciences*, **15**(6), 786–796.

Norbury, J. R. and White, W. J. (1971). A rapid-response rain gauge. *Journal of Physics E: Scientific Instruments*, **4**, 601–602.

Pamment, J. and Conway, B. (1998). Objective identification of echoes due to anomalous propagation in weather radar data. *Journal of Atmospheric and Oceanic Technology*, **15**(1), 98–113.

Petersen, W., Carey, L., Rutledge, S., Knievel, J., Doesken, N., McKee, T., Volder Haar, T., and Weaver, J. (1999). Mesoscale and radar observations of the Fort Collins flash flood of 28th July 1997. *Bulletin of the American Meteorological Society*, **80**, 191–216.

Probert-Jones, J. R. (1962). The radar equation in meteorology. *Quarterly Journal of the Royal Meteorological Society*, **88**, 485–495.

Pruppacher, H. and Pitter, R. (1971). A semi-empirical determination of the shape of cloud and raindrops. *Journal of Atmospheric Science*, **28**, 86–94.

Ryzhkov, A. and Zrnić, D. (1995). Comparison of dual-polarisation radar estimators of rain. *Journal of Atmospheric and Oceanic Technology*, **12**, 249–256.

Ryzhkov, A. and Zrnić, D. (1996). Assessment of rainfall measurement that uses specific differential phase. *Journal of Applied Meteorology*, **35**, 2080–2090.

Ryzhkov, A. V., Schuur, T. J., Burgess, D. W., Heinselman, P. L., Giangrande, S., and Zrnić, D. (2005a). The joint polarization experiment polarimetric rainfall measurements and hydrometeor classification. *Bulletin of the American Meteorological Society*, pages 809–824.

Ryzhkov, A. V., Gaingrande, S. E., and Schuur, T. J. (2005b). Rainfall estimation with a polarimetric prototype of wsr-88d. *Journal of Applied Meteorology*, **44**, 502–515.

Sachidananda, M. and Zrnić, D. S. (1986). Differential propagation phase shift and rainfall estimation. *Radio Science*, **21**, 235–247.

Sachidananda, M. and Zrnić, D. S. (1987). Rain rate estimates form differential polarization measurements. *Journal of Atmospheric and Oceanic Technology*, **4**, 588–598.

Sekelsky, S. M. (2001). Near-field corrections for meteorological radars. In *30th Conference on Radar Meteorology*, number P1.5. American Meteorological Society.

Seliga, T. A. and Bringi, V. N. (1976). Potential use of radar differential reflectivity measurements at orthogonal polarizations for measuring precipitation. *Journal of Applied Meteorology*, pages 69–75.

Smyth, T. J. and Blackman, T. M. Illingworth, A. J. (1999). Observations of oblate hail using dual polarization radar and implications for hail-detection schemes. *Quarterly Journal of the Royal Meteorological Society*, **125**, 993–1016.

Smyth, T. J. and Illingworth, A. (1998). Correction for attenuation of radar reflectivity using polarization data. *Quarterly Journal of the Royal Meteorological Society*, **124**, 2393–2415.

Straka, J. M., Zrnić, D. S., and Ryzhkov, A. V. (2000). Bulk hydrometer classification and quantification using polarimetric radar data: Synthesis of relations. *Journal of Applied Meteorology*, pages 1341–1372.

Sugier, J., Parent du Châtelet, J., Roquain, P., and Smith, A. (2002). Detection and removal of clutter and anaprop in radar data using a statistical scheme based on echo fluctuation. In *Proceedings of ERAD (2002)*, pages 17–24.

Testud, J., Bouar, E., Obligis, E., and Ali-Mehenni, M. (2000). The rain profiling algorithm applied to polarimetric weather radar. *Journal of Atmospheric and Oceanic Technology*, **17**, 332–356.

Ulbrich, C. W. (1983). Natural variations in the analytical form of the rain size distribution. *Journal of Climate and Applied Meteorology*, **22**, 1764–1775.

Veneziano, D., Bras, R. L., and Niemann, J. D. (1996). Nonlinearity and self-similarity of rainfall in time and a stochastic model. *Journal of Geophysical Research*, **101**(D21), 26371–26392.

Wilson, D. R., Illingworth, A. J., and Blackman, T. M. (1997). Differential Doppler velocity: a radar parameter for characterizing hydrometeor size distributions. *Journal of Applied Meteorology*, **36**(6), 649–663.

Wilson, J. W. and Brandes, E. A. (1979). Radar measurement of rainfall - a summary. *Bulletin of the American Meteorological Society*, **60**(9), 1048–1058.

Zawadzki, I. (1973). Statistical properties of precipitation patterns. *Journal of Applied Meteorology*, **12**(3), 459–472.

Zawadzki, I. (1987). Fractal structure and exponential decorrelation in rain. *Journal of Geophysical Research*, **92**(D8), 9586–9590.